# Bilag 2 til hovedrapport

# Opsys 2.0 Projektet

EUDP-journal nr.: 64108-0581

Dette bilag indeholder de vigtigste artikler og notater fra projektet

# Transient analysis of individual return temperatures in hydronic floor heating systems

*Simon* Thorsteinsson [a], *Henrik Lund* Stærmose [b], *Jan Dimon* Bendtsen [a]

[a] Section of Automation and Control, Department of Electronic Systems, Aalborg University, Denmark, sith@es.aau.dk.

[b] Neogrid Technologies ApS, Niels Jernes Vej 10 - 9220 Aalborg east, Denmark, hls@neogrid.dk.

**Abstract.** In this work, we investigate some potential benefits and opportunities gained from monitoring the return temperature of all the circuits in a *hydronic floor heating* (FH) system. It is for example possible to obtain information on the flow distribution in the FH system. Since flow sensors are relatively expensive, most currently installed FH systems do not provide any information on the flow entering the forward manifold, let alone flows in the individual circuits. This lack of information inhibits analysis of performance and prevents commissioning of more advanced control methods. The approach proposed here, based on temperature sensors mounted on the exterior of the pipes, provides a possible cheap alternative to measuring the flows directly. Further, we argue that this retrofitted solution can be applied to most already installed floor heating systems. The paper contains a description of the retrofit kit and a dynamic model, which is shown to be able to replicate the behaviour of measurements acquired from an actual FH system installed in a single-family house, as well as a method for calculating the relative flows. The results show that flow-related parameters such as circulation time are, under the right circumstances, directly observable in the data. Overall, we conclude that measuring the individual return temperatures provides valuable information when monitoring the health and performance of a floor heating system.

**Keywords.** Floor Heating, Flow, Retro-fit, Estimation, Simulation
**DOI**: https://doi.org/10.34641/clima.2022.140

## 1. Introduction

In this paper we discuss the potential benefits of continuously measuring the return temperatures of the individual circuits in a *hydronic floor heating* (FH) system placed in a single family house, and propose a method to roughly estimate the *flow distribution* (FD) and thereby the distribution of energy consumption in the different FH pipes. The word *distribution* signals that only a relative, and not an absolute, measure of the heat consumption of the individual circuits is obtained.

On the topic of energy efficiency, single family houses are interesting and problematic. Interesting because they cover a significant amount of heated area (about 55 % in Denmark) [1]. Problematic since this large share is distributed over many small units, which means the potential for energy savings in each unit is relatively small. Further, a majority of these units are owned by the residents themselves [2], meaning that any investment into energy efficiency has to be understood from a perspective of a relative low budget. The consequence is that, without any active incentive programs, energy efficiency solutions for single family houses have to be highly cost effective. Solutions for retrofitting existing buildings are, in this text, characterized into two main groups, passive, where changes are made to the physics of the building, and active, which covers changes in the operation under the existing conditions. The active solutions to a large extent cover exchanging existing controllers, together with updating the set of sensors and actuators, in order to operate the overall system more efficiently.

Returning to the theme of this paper, a question arises: why is the FD, in a FH system, interesting and useful information? To answer this, it is helpful to visit a class of controllers called Model Based Controllers. Among controllers classified as model based, *Model Predictive Control* (MPC) is the most widely known. The method combines a model with an objective function, which assign costs to states and inputs over a control window. To obtain the specific model it has to be constructed and identified. In [3] the authors used a grey-model method called *Maximum Likelihood* (ML) to estimate the dynamics of an arctic low-energy house heated by FH. For the

identification of the parameters, the heat flow, based on forward/return temperature and mass flow of the water, is used as input for each circuit. A *Least Squares* (LS) method is used by [4] to fit the parameters in a grey-box model. In [5] the authors use an *Unscented Kalman Filter* (UKF) to online estimate the parameters of a five room building. Common for the mentioned texts is that they assume the heat flows from the HVAC systems to be known. This is rarely the case in single family houses. The text in [5] touches upon this problem and discusses numerical instabilities, related to not providing a scaled input for the different rooms. Although, the scale here refers to the difference of actual heat flows between individual rooms, we argue that on room level a relative scale based on e.g. FD is enough, since it is possible to further scale the relative estimates, if a central measure of the heat consumption is available. This is e.g. the case if the house is provided by district heating, since the overall heat consumption is needed to settle the energy bill. The authors of [3] do something similar when they correct the individual estimated heat flows according to the measured total heat consumption obtained centrally. Further, being able to scale FH circuits is useful in MPC. If all circuits are considered equal the MPC cannot ration the energy appropriately. If the actual heat consumption of the rooms are not obtainable, then it is at least useful to know whether one circuit is twice as expensive as the other. The notion of flow distribution and relative heat distribution is not new, [6] defines it as *relative heating coefficient* (RHC). The authors derive and compare an array of RHCs, which are used to rate the heat efficiency of the rooms of an office building. The work carried out in [6] lays the foundation for the work of this paper. Having established the importance of knowing the flow distribution and relative heating distribution, we pose the hypothesis: *It is possible to obtain a relative flow and heating distribution, based on measuring the forward/return temperature and control-valve state for all circuits. This approach outperforms scaling circuits using only floor area distribution.*

The rest of the paper contains an introduction to the system and retrofit-kit. Sec. 2. describes a simulation, which is used to investigate the method under ideal circumstances, followed the experiment conducted in the test house. Section 3. contains results from the simulation and test house before Sec. 4. concludes.

## 2. Method

This section presents the retrofit kit, simulation and derivation for the relative heating coefficient.

### *2.1 System*

Figure 1 presents the system which is considered in this paper. The system reflects a common installation seen in many single family houses. The heat source provides a common forward temperature for the FH circuits. Each floor heating circuit is ON/OFF controlled with hysteresis based on temperature difference between measured room temperature and reference. The actuators are wax-motor valves [7]. The mass flow in circuit $j$, $q_j$ combined with the total flow entering the forward manifold $q$ are considered unknown.

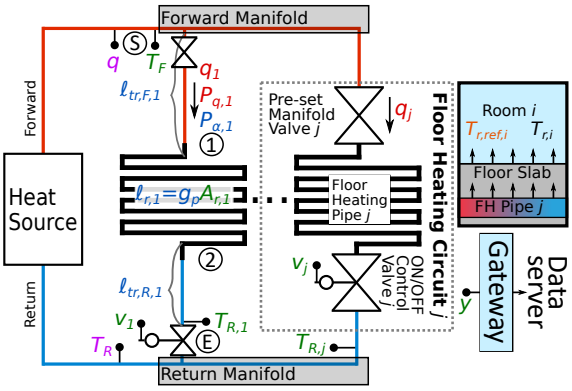


**Fig. 1** – The system diagram containing the important signals. The signals are color coded: (green) measured signals or known inputs, (blue) estimated parameters, (magenta) measured for validation and (red) unknown but desired variables.

The FH system is placed in a test house, where data is gathered using the retrofit kit presented in the upcoming section. The house is built according to the BR2020 standard and heated using an air-to-water heat pump. There are 15 FH circuits distributed on two manifolds. The FH circuits are controlled using temperature feedback from the rooms. Each room has one thermostat. Rooms with more than one FH circuit are controlled using the same thermostat. Two rooms have two circuits, one has three, and the remaining have one each.

**Assumption 1** (Constant flow)**.** The flow in an open circuit is constant, regardless of the state of the other FH circuits.

**Assumption 2** (Common cross-area)**.** The cross area of the pipe $A_\mathrm{p}$ is the same for all FH circuits.

**Assumption 3** (Measured return temperatures)**.** The return temperature for each FH circuit is measured.

**Assumption 4** (Common pipe length per $\mathrm{m}^2$ floor)**.** Pipe length per square meter floor, $g_\mathrm{p}$, is the same for all rooms. This is shown in Fig. 1.

**Assumption 5** (Floor area)**.** The area covered by the floor heating pipe is assumed known.

We are aware that Assumptions 1, 2 and 4 are not always satisfied, but they are considered

acceptable in a retrofit situation. In the next section, we shall address a way to satisfy Assumption 3.

### 2.2 The retrofit kit

The retrofit kit, used to measure the return temperatures, consists of three components. Firstly, surface mounted temperature sensors are placed on each pipe before the collector manifold. The sensors, circled in red in Figure 2, are covered by insulation to lower effects from air temperature and heat radiation. The common forward temperature are measured in the same way. Second, the inputs to the ON/OFF control valves are monitored. The data samples are, in our case, sent via a gateway to an the online data server, provided by Neogrid Technologies ApS, but any sample-based data acquisition method may of course be employed. Third, the gateway supports overwriting control signals. Therefore, if the natural fluctuation of return temperatures is insufficient for estimation, reference manipulation is used to force control valves to open and close on demand.

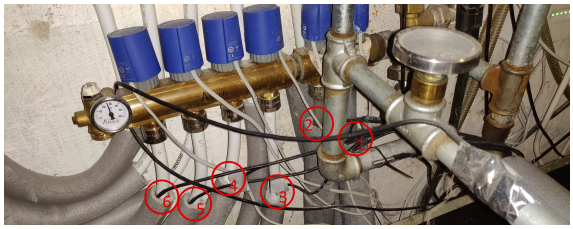

**Fig. 2** – Shows temperature sensors placed under the insulation of each return pipe. Although the retrofit solution is the same, the picture is not from the test house discussed in this text.

### 2.3 Relative heat consumption

The heat consumption at time $t$ for FH pipe $j$ is in this text, defined as the instantaneous heat transferred from the water in the pipe to the floor. We denote this function as $\dot{Q}_{\mathrm{FH},j}(t)$. This heat transfer is dependent on multiple factors such as flow rate, temperature profile along the pipe and floor temperature, making it difficult to use in practice. To simplify the measure, the heat transferred is assumed well approximated by the difference between energy entering and exiting the pipe as seen in Eq. (1):

$$\dot{Q}_{\mathrm{FH},j}(t) \approx c_{\mathrm{w}} q_j(t) \left(T_{\mathrm{F}}(t) - T_{\mathrm{R},j}(t)\right) \tag{1}$$

With $c_{\mathrm{w}}$ being the heat capacity of water, $T_{\mathrm{F}}$ the forward temperature and $T_{\mathrm{R},j}$, $q_j$, the return temperature and mass flow of circuit $j$, respectively. The total heat consumption of the FH is given as the sum of the consumption of each circuit or as the total flow times temperature difference.

$$\dot{Q}_{\mathrm{FH}} = \sum_{j=1}^{N} \dot{Q}_{\mathrm{FH},j}(t) = c_{\mathrm{w}} q(t) \left(T_{\mathrm{F}}(t) - T_{\mathrm{R}}(t)\right) \tag{2}$$

The return temperature, $T_{\mathrm{R}}$, and total flow, $q$, are given as sums of contributions as well.

$$T_{\mathrm{R}}(t) = \sum_{j=1}^{N} \frac{q_j(t)}{q(t)} T_{\mathrm{R},j}(t) \quad q(t) = \sum_{j=1}^{N} q_j(t) \tag{3}$$

As mentioned, both the total flow $q$ and the circuit flows $q_j$ are considered unknown, meaning that Eq. (2) cannot be computed in practice. Alternatively, as suggested in [6], one can introduce a *relative heating coefficient* (RHC) denoted $\beta$, which describes the relative consumption between the circuits. Instead of using the absolute flow a nominal distribution of flows is used. The term nominal distribution is used to indicate that the flow is a percentage share of the total and that the flows are independent of each other as stated in Assumption 1. The RHC derived in this test is seen in Eq. (4), and it is based on the advective heat flow of the circuit.

$$\beta_{q,j}(t) = v_j(t) \alpha_j \left(T_{\mathrm{F}}(t) - T_{\mathrm{R},j}(t)\right) \tag{4}$$

Here, $\alpha_j$ is the flow distribution scalar and $v_j$ binary valve state. The total relative consumption is given by Eq. (5).

$$\beta(t) = \sum_{j=1}^{N} \beta_j(t) \tag{5}$$

Eq. (4) is equivalent to Eq. (2) if Assumption 1 holds. The factor is $q_{\max} c_{\mathrm{w}}$.

$$\dot{Q}_{\mathrm{FH}} = q_{\max} c_{\mathrm{w}} \beta_q \tag{6}$$

To get the by room percentage share of consumed heat, normalize the total heat transferred:

$$\mathcal{P}_{\beta,j}(\beta_j(t)) = \frac{\int_0^T \beta_j(t) \mathrm{d}t}{\int_0^T \beta(t) \mathrm{d}t} \tag{7}$$

The next section shows the derivation of the scalar $\alpha_j$ presented in Eq. (4)

### 2.4 Nominal flow distribution

We start by stating the two common flow equations for pipe with constant flow and pipe area.

$$q_j = v_j A_{\mathrm{p}} \rho \tag{8}$$

$$v_j = \frac{\ell_{\mathrm{r},j}}{\Delta t_{\mathrm{r},j}} \tag{9}$$

where $v$ is the velocity of the water, $A_{\mathrm{p}}$ is the area of the cross section of the pipe and $\rho$ is the mass density of water, $\ell_{\mathrm{r}}$ is the length of the pipe under the floor and $\Delta t_{\mathrm{r}}$ is the time water spends under the floor in the circuit. Since the pipe is buried in

the floor, the length is unknown, but if Assumption 4 is true, the length is given by

$$\ell_{\mathrm{r},j} = g_{\mathrm{p}} A_{\mathrm{r},j} \tag{10}$$

where $g_{\mathrm{p}}$ is the common pipe length per area floor. Inserting Eq. (9) and (10) into (8) gives

$$q_j = A_{\mathrm{p}} g_{\mathrm{p}} \rho \frac{A_{\mathrm{r},j}}{\Delta t_{\mathrm{r},j}}. \tag{11}$$

According to Assumptions 4 and 2 the pipe area $A_{\mathrm{p}}$, mass density of water $\rho$ and pipe length factor $g_{\mathrm{p}}$ are common for all circuits, meaning that the flow in circuit $q_j$ is proportional to the ratio $A_{\mathrm{r},j}/\Delta t_{\mathrm{r},j}$.

$$q_j \propto \frac{A_{\mathrm{r},j}}{\Delta t_{\mathrm{r},j}} = \alpha_j \tag{12}$$

### 2.5 Measuring the round trip time $\Delta t_j$

According to assumption 5, the room areas are assumed known, but the circulation time $\Delta t_{\mathrm{r},j}$ for circuit $j$ is not, meaning it has to be measured. To measure the round trip time $\Delta t_j$ of circuit $j$, time series measurements from the forward temperature $T_{\mathrm{F}}$ and individual return temperatures $T_{\mathrm{R},j}$ are used.

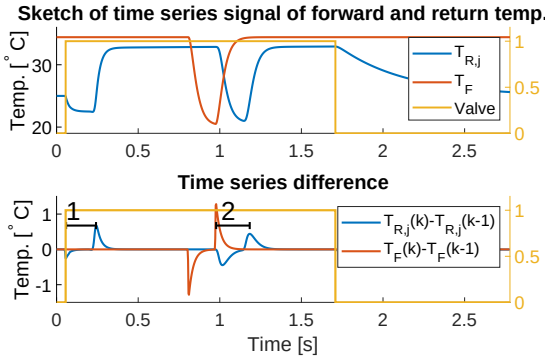


**Fig. 3** – Shows a sketch of the measured forward and return temperature of a circuit. The figure presents two events that can be used for measuring the round trip time. The first (marked 1) is the time after a circuit opens. In this period old cooled water is replaced by fresh warm. The second event (marked 2) is caused by a large step on the forward temperature. Note that $k$ indicates sample number.

Events, shown in Figure 3, with rapid changes in the forward temperature can be observed on both the forward and return temperature sensor. First on the forward temperature sensor, then later in a low pass filtered version on the return sensor. The challenge lies in figuring out when to start and stop the timer. It has been observed from measurements that the steepest gradient on the signal marks a sufficient and often clear point in the data; this claim is explained in more detail in Section *3.1*. By taking the time series difference, the slope graph is obtained, and the round trip time is easily measured as the time distance between the two peaks.

### 2.6 Considerations on circulation time $\Delta t_r$

Having shown that the flow is proportional to room area over room circulation time, this section deals with the estimate of the circulation time. The simple expression in Eq. (11) is derived under the assumption that the circulation time under floor, denoted $\Delta t_{\mathrm{r},j}$, is measured. This is equivalent to measure from (1) to (2) in Fig. 1. In practice, however, it is the time from point (S) to (E), denoted $\Delta t_j$, which is measured. Eq. (13) shows the relation between the measured, $\Delta t_j$, and desired time, $\Delta t_{\mathrm{r},j}$:

$$\Delta t_j = \Delta t_{\mathrm{r},j} + 2\Delta t_{\mathrm{tr},j} \tag{13}$$

where $\Delta t_{\mathrm{tr}}$ is the transport time from the manifold to the floor. The time $\Delta t_{\mathrm{tr}}$ is scaled by two because the water has to be transported to and back from the floor. If the transport time is not considered, a significant bias is introduced. It is a weakness of the method that it is the round trip time, and not the time spent under the floor, that is measured. This said, it is possible to compensate for this bias by using information from the system. To obtain the corrected circulation time one has to obtain an estimate of the percentage share of the full pipe length placed under the floor, $\mathcal{P}_{\mathrm{r}}$. The percentage share $\mathcal{P}_{\mathrm{r}}$, seen in Eq. (14), is calculated using estimates on the length of the transport pipe $\hat{\ell}_{\mathrm{tr}}$ and the length of pipe per square meter floor $\bar{g}_{\mathrm{p}}$.

$$\begin{aligned}\hat{\Delta} t_{\mathrm{r},j} &= \Delta t_j \frac{\ell_{\mathrm{r},j}}{\ell_{\mathrm{r},j} + 2\ell_{\mathrm{tr},j}} \\ &= \Delta t_j \frac{\bar{g}_{\mathrm{p}} A_{\mathrm{r},j}}{\bar{g}_{\mathrm{p}} A_{\mathrm{r},j} + 2\hat{\ell}_{\mathrm{tr}}} = \Delta t_j \mathcal{P}_{\mathrm{r},j}\end{aligned} \tag{14}$$

This means that the estimate of the pipe length under the floor $\ell_{\mathrm{r}}$, is based on an assumption of a linear relationship between floor area and pipe length. The pipe density $g_{\mathrm{p}}$ is often between 3 and 6 $m/m^2$. The transport length $\ell_{\mathrm{tr},j}$ can be estimated with some uncertainty, based on distance from room to manifold. Inserting Eq. (14) into (12) gives the corrected proportionality constant:

$$q_j \propto \frac{A_{\mathrm{r},j}}{\Delta t_j \frac{\bar{g}_{\mathrm{p}} A_{\mathrm{r},j}}{\bar{g}_{\mathrm{p}} A_{\mathrm{r},j} + 2\hat{\ell}_{\mathrm{tr}}}} = \frac{A_{\mathrm{r},j} + \frac{2\hat{\ell}_{\mathrm{tr}}}{\bar{g}_{\mathrm{p}}}}{\Delta t_j} = \alpha_j \tag{15}$$

The updated expression seen in (15) is used to calculate the RHC coefficient $\alpha_j$.

### 2.7 Simulation

To investigate the claim that the maximum slope measures the complete circulation time, a simulation of a simple floor heating system is implemented. As seen in Figure 4, the model consists of six parts. A room modelled as a first order system, a floor, a water pipe (under floor

and two transport sections), a piece of pipe placed in the heating room and a simple sensor model attached to this pipe. Note that indexes such as $i$ and $j$ refer to partitions of one pipe and not circuits, since the model is representative for all circuits.

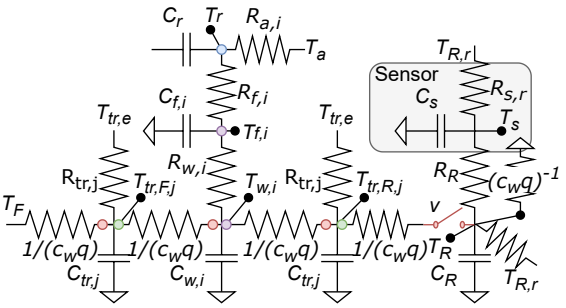


**Fig. 4** – Shows the resistor-capacitor equivalent of the simulation model. The green dot indicates that this model section is repeated $M_{\text{part}}$ times. The purple dot indicates that the section is repeated $N_{\text{part}}$ times. The blue dot describes a summation point, where the heat contribution from all the floor parts are collected. The red dots indicate circuit breakers. If the binary valve indicator is 1 the circuit is closed and the water is flowing, and 0 stops the flow.

The model of the transport pipe (tr), for both directions are shown in Eq. (16a).

$$C_{\text{tr},\{\cdot\},j}\dot{T}_{\text{tr},\{\cdot\},j} = c_{\text{w}} q \left(T_{\text{tr},\{\cdot\},j-1} - T_{\text{tr},\{\cdot\},j}\right) v + \frac{1}{R_{\text{tr},i}} \left(T_{\text{tr},e} - T_{\text{tr},\{\cdot\},j}\right) \quad (16a)$$

with $C$ being the heat capacity, $T$ the temperature, $q$ the nominal mass flow, $v \in \{0, 1\}$ the valve indicator variable and $R$ the heat resistance. The placeholder $\{\cdot\}$ indicates that the equation is valid for both the *forward* (F) and *return* (R) pipe. This is the case since they are modelled as being equally long. The pipes have $M_{\text{part}}$ partitions each, with $j \in \{1, ..., M_{\text{part}}\}$. The equation consists of a term describing the water being transported within the pipe and one describing transport loss. Eq. (16b) describes the water in the pipe under the floor:

$$C_{\text{w},i}\dot{T}_{\text{w},i} = \frac{1}{R_{\text{w},i}} \left(T_{\text{f},i} - T_{\text{w},i}\right) + c_{\text{w}} q \left(T_{\text{w},i-1} - T_{\text{w},i}\right) v \quad (16b)$$

Again a term describes the water transport and one describes the transfer of energy to the *floor* (f) slab. Note that losses to the ground or other rooms are not considered. There are $N_{\text{part}}$ partitions, with $i \in \{1, .., N_{\text{part}}\}$. Eq. (16c) shows the equation for floor partition $i$. There is an equal number of floor and water pipe partitions, since they are paired together.

$$C_{\text{f},i}\dot{T}_{\text{f},i} = \frac{1}{R_{\text{w},i}} \left(T_{\text{w},i} - T_{\text{f},i}\right) + \frac{1}{R_{\text{f},i}} \left(T_{\text{f},i} - T_{\text{r}}\right) \quad (16c)$$

The floor partition is nothing more than a capacitance and two resistances placed between the the pipe and room. Eq. (16d) describes a *room* (r) with an equal distributed air temperature.

$$C_{\text{r}}\dot{T}_{\text{r}} = \sum_{i=1}^{N} \frac{1}{R_{\text{f},i}} \left(T_{\text{f},i} - T_{\text{r}}\right) + \frac{1}{R_{\text{a},i}} \left(T_{\text{a}} - T_{\text{r},i}\right) \quad (16d)$$

The energy flow from the floor is the sum of the flow from each floor partition. The other term describes the heat loss to the environment. Eq. (16e) describes the part of the return pipe (R) placed in the heating room.

$$C_{\text{R}}\dot{T}_{\text{R}} = c_{\text{w}} q \left(T_{\text{tr,R},N_{\text{part}}} - T_{\text{R}}\right) v + \frac{1}{R_{\text{R,r}}} \left(T_{\text{R,r}} - T_{\text{R}}\right) + \frac{1}{R_{\text{R}}} \left(T_{\text{s}} - T_{\text{R}}\right) \quad (16e)$$

Eg. (16e) has three terms, the water flow, a small heat loss to the sensor and the loss to the heating room. Eq. (16f) describes the temperature sensor as a small first order capacity. The state $T_{\text{s}}$ describes the measured value.

$$C_{\text{s}}\dot{T}_{\text{s}} = \frac{1}{R_{\text{s,r}}} \left(T_{\text{R,r}} - T_{\text{s}}\right) + \frac{1}{R_{\text{R}}} \left(T_{\text{R}} - T_{\text{s}}\right) \quad (16f)$$

$$T_{\text{tr,F},1} = T_{\text{F}} \quad T_{\text{r}} \in \mathbb{R} \quad \mathbf{T}_{\text{f}} \in \mathbb{R}^{N_{\text{part}}} \quad \mathbf{T}_{\text{w}} \in \mathbb{R}^{N_{\text{part}}}$$

The water pipe is divided into two *transport* (tr) sections and the part embedded in the floor. The floor and pipes are discretized along the length, which makes the model a high order system. The length of each partition $\ell_{\text{part}}$ in the floor and transport pipe is decided by a exchange percentage $\alpha_{\text{p}}$, meaning a certain percentage of water needs to be exchanged at each sample.

$$\ell_{\text{part}} = \frac{q dt}{\rho_{\text{w}} \pi r_{\text{p}}^2 \alpha_{\text{p}}} \implies \ell_{dt} = \alpha_{\text{p}} \ell_{\text{part}} \quad (17)$$

where $\ell_{dt}$ is the distance the water travel each simulation sample period $dt$. To create a correlation between coefficients in the simulation, a number of relations can be formulated for heat capacities, $C_{\{\cdot\}}$, and resistances $R_{\{\cdot\}}$.

$$C_{\text{w},i} = C_{\text{tr},\{\cdot\},j} = c_{\text{w}} \rho_{\text{w}} A_{\text{p}} \ell_{\text{part}} \quad (18)$$

$$C_{\text{R}} = c_{\text{w}} \rho_{\text{w}} A_{\text{p}} \ell_{\text{R}} \quad (19)$$

$$C_{\text{f},i} = \frac{A_{\text{r}} g_{\text{f}}}{N_{\text{part}}} \qquad C_{\text{r}} = V_{\text{r}} c_{\text{a}} \rho_{\text{a}} + A_{\text{r}} g_{\text{e}} \quad (20)$$

$$R_{\text{w},i} = \frac{N_{\text{part}}}{2\pi r_{\text{p}} u_{\text{w}} g_{\text{p}} A_{\text{r}}} \quad R_{\text{tr},i} = \frac{1}{2\pi r_{\text{p}} u_{\text{tr}} \ell_{\text{part}}} \quad (21)$$

$$R_{\text{R,r}} = \frac{1}{2\pi r_{\text{p}} u_{\text{R,r}} \ell_{\text{R}}} \quad (22)$$

$$R_{\text{a},i} = \frac{N_{\text{part}}}{u_{\text{a}} A_{\text{r}}} \qquad R_{\text{f},i} = \frac{N_{\text{part}}}{u_{\text{f}} A_{\text{r}}} \quad (23)$$

$$R_{\text{R}} = \frac{1}{U_{\text{R}}} \qquad R_{\text{s,r}} = \frac{1}{U_{\text{s,r}}} \quad (24)$$

$$q = g_q A_{\text{r}} \quad (25)$$

with $A_\mathrm{p}$ being the cross area of the pipe and $\rho$, $c$ the density and specific heat capacity, respectively. Volumes are denoted as $V$. The heat capacity per square meter floor is given as $g_\mathrm{f}$. The heat conduction per square meter is $u$ and heat conduction is $U$. The ratio between floor area and wall capacity and flow is given by $g_\mathrm{e}$ and $g_q$, respectively. The model can then be summed up as an switched-input linear model. The state space version is seen in (26):

$$\mathbf{C}\dot{\mathbf{T}} = v\mathbf{A}_\mathrm{on}\mathbf{T} + (v-1)\mathbf{A}_\mathrm{off}\mathbf{T} + v\mathbf{B}T_\mathrm{F} + \mathbf{E}d \tag{26}$$

where $\mathbf{A}$, $\mathbf{B}$, $\mathbf{C}$ and $\mathbf{E}$ are matrices and $\mathbf{T}$ a vector of temperatures. The model is simulated with a time period of $dt$ using first order Euler integration.

$$\mathbf{T}(k+1) = [\mathbf{I} + v(k)\mathbf{A}_\mathrm{on}dt + (v(k)-1)\mathbf{A}_\mathrm{off}dt]$$
$$\mathbf{T}(k) + v(k)dt\mathbf{B}T_\mathrm{F}(k) + dt\mathbf{E}d(k) \tag{27}$$

### *2.8 Experiment in test house*

The test house used in this project has a flow-meter on the common circuit of the FH system. This flow-meter is used to establish a baseline flow distribution. To obtain the distribution, the flow is measured with only one circuit open. This is done for all circuits. Note, the distribution obtained from this approach does not account for any saturation effects on the circulation pump occurring at high flow rates.

To obtain the round trip times $\Delta t_j$ used for Eq. (15), all circuits are opened. Then a step in the forward temperature is performed by turning of the heat source while circulating the water. In this particular case the heat pump turned off periodically. This is illustrated as event two in Fig. 3 and seen in Fig 5.b. The data from the return sensors is sampled with a period of 20 seconds and low-pass filtered to reduce noise and quantization effects. Multiple samples are carried out and averaged. In practice the experiment can be carried out without forcing the circuits open.

## 3. Results

This section presents the results from the simulation based sensitivity analysis and the experiment on the inhabited test house.

### *3.1 Simulation results*

In Sec. *2.5* it is claimed that round-trip time can be measured using the return sensors. In this section, the simulation from Sec. *2.7* is used to investigate whether this is consistent under varying conditions and configurations.

**Tab. 1** – The distribution of random parameters

| Parameter | Distribution | Unit |
|---|---|---|
| $A_\mathrm{r}$ | $\mathcal{U}(5, 30)$ | $[m^2]$ |
| $g_q$ | $\mathcal{U}(0.002, 0.005)$ | $[kg/(m^2 s)]$ |
| $g_\mathrm{f}$ | $\mathcal{U}(24000, 36000)$ | $[J/(m^2 K)]$ |
| $g_\mathrm{e}$ | $\mathcal{U}(12000, 17000)$ | $[J/(m^2 K)]$ |
| $g_\mathrm{a}$ | $\mathcal{U}(0.3, 1)$ | $[\cdot]$ |
| $r_\mathrm{p}$ | $\mathcal{U}(0.01, 0.02)$ | $[m]$ |
| $u_\mathrm{a}$ | $\mathcal{U}(0.45, 0.55)$ | $[W/(m^2 K)]$ |
| $u_\mathrm{f}$ | $\mathcal{U}(3.5, 4.5)$ | $[W/(m^2 K)]$ |
| $u_\mathrm{w}$ | $\mathcal{U}(6, 12)$ | $[W/(m^2 K)]$ |
| $u_\mathrm{tr}$ | $\mathcal{U}(2, 4)$ | $[W/(m^2 K)]$ |
| $u_\mathrm{R,r}$ | $\mathcal{U}(0.05, 0.15)$ | $[W/(m^2 K)]$ |
| $U_\mathrm{R}$ | $\mathcal{U}(0.5, 0.5)$ | $[W/K]$ |
| $U_\mathrm{s,r}$ | $\mathcal{U}(0.05, 0.15)$ | $[W/K]$ |
| $\ell_\mathrm{tr}$ | $\mathcal{U}(3, 25)$ | $[m]$ |
| $C_\mathrm{s}$ | $\mathcal{U}(80, 120)$ | $[J/K]$ |
| $\mathcal{P}_\mathrm{p}$ | $\mathcal{U}(0.5, 0.5)$ | $[\cdot]$ |

The analysis is performed by repeating a 10 room simulation, supplied with randomly drawn coefficients, 100 times. The coefficients are distributed according to Tab. 1 where $\mathcal{U}$ denotes the uniform distribution. The pipe distribution $g_\mathrm{p}$, follows Assumption 4. Fig. 5 shows the transient response from the simulation compared with the measured one.

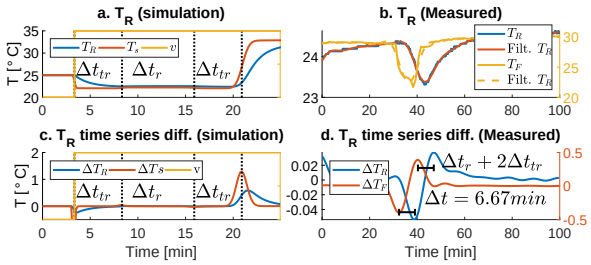


**Fig. 5** – Column one: shows an example of the simulated transient response and time series diff. for the simulation. Column two: shows one the measured values. Note that $\Delta T_R = T_R(k) - T_R(k-1)$.

The simulation allows us to investigate otherwise inaccessible states such as transport time $\Delta t_\mathrm{tr}$ and the actual water temperature $T_\mathrm{R}$. As mentioned in Sec. *2.5*, the peak for $\Delta T_\mathrm{R}$, seen in Fig. 5.c, exactly measures the total round trip time. We think this is the case, since this is the time where the new front of warm water arrives at the sensor. Further, it can be seen that the measured value $T_\mathrm{s}$ has a slower time constant, since the heat needs to propagate through the pipe. To measure the performance the root mean square error seen in (28), is computed for the difference between the actual flow distribution $\mathcal{P}_q \in \mathbb{R}^N$ and the particular flow distribution estimates $\mathcal{P}_{x,j}$ with $x \in \alpha, A_\mathrm{r}$. The subscript $\alpha$ indicates that the distribution is based on Eq. (15), and $A_\mathrm{r}$ that it is

based purely on area distribution.

$$RMSE_x = \frac{1}{N}\sum_{j=1}^{N}\left(\mathcal{P}_{q,j} - \hat{\mathcal{P}}_{x,j}\right) \tag{28}$$

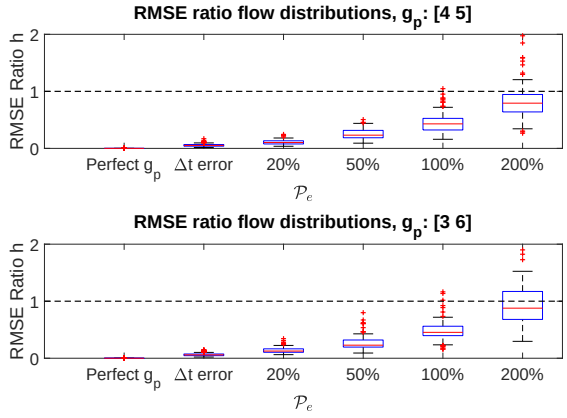


**Fig. 6** – Upper and lower show the RMSE ratio of the test performed with the pipe density $g_\mathrm{p}$ drawn uniformly between 4 and 5 and 3 to 6 $m/m^2$, respectively The x-axis shows the results with increased error on the transport pipe estimate. The first entry contains the results using perfect information. The second shows the results where only the error from measuring the round-trip time affects the result. $\mathcal{P}_e$ is the percentage error.

To quantify the results, the root mean square error calculated from the simulations are formulated as a ratio $h$ seen in Eq. (29).

$$h = \frac{RMSE_\alpha}{RMSE_{A_\mathrm{r}}} \tag{29}$$

This ratio allows us to evaluate whether the overall distribution improved. If $h$ is zero, it means that the fit is perfect, and if it is greater than one, it would be better to distribute based on area alone. The estimates for the flow distribution, $\mathcal{P}_{\alpha,j}$, is calculated using the normalized version of (15) with $\bar{g}_\mathrm{p} = 4.5$ and $\hat{\ell}_\mathrm{tr}$ as the real transport length plus estimation error:

$$\hat{\ell}_\mathrm{tr} = \ell_\mathrm{tr} + e_\mathrm{tr} \tag{30}$$

The error is correlated with the actual length of the transport pipe and normally distributed according to the following $3\sigma$ rule.

$$e_\mathrm{tr} \sim \mathcal{N}(0, (1/3\mathcal{P}_e\ell_\mathrm{tr})^2) \tag{31}$$

where $1/3\mathcal{P}_e\ell_\mathrm{tr}$ is the standard deviation of the error of the one-way transport distance, meaning that 99% of the errors are within plus/minus this range. Figure 6 and 7 show the results of the simulations. As can be seen in Figure 6, it is important to have a good estimate of the length of the transport pipe, since it has a large effect on the quality of the estimate. The outliers, seen with red crosses, have been related to bad measurements where the wrong peak is obtained.

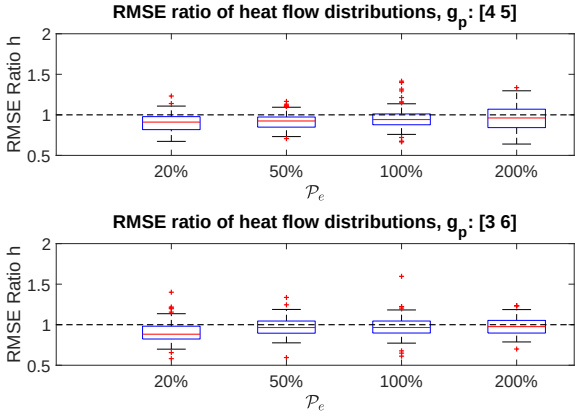


**Fig. 7** – Sums up the results for the calculated heat distributions. The figure has the same structure as Fig. 6. The RMSE resulting from using the RHC in Eq. (4) is divided by the RMSE from Eq. (32).

The heat distributions, defined as the percentage share of accumulated heat consumption, are also calculated from the simulations. The heat distribution is based on the RHC in Eq. (4) and compared with Eq. (32) taken from [6].

$$\beta_{A_\mathrm{r},j}(t) = A_{\mathrm{r},j}\frac{T_\mathrm{F}(t) - T_{\mathrm{R},j}(t)}{\ln\left(\frac{T_\mathrm{F}(t)-T_{\mathrm{r},j}(t)}{T_{\mathrm{R},j}(t)-T_{\mathrm{r},j}(t)}\right)} \tag{32}$$

This RHC also uses the return temperature together with the room temperature $T_{\mathrm{r},j}$ and floor area over the circuit. The RHC in Eq. (32) assumes that the specific heat conduction from water to room is the same for all rooms. The final heat distribution is obtained by integrating the RHC using Eq. (7). As in the case with pipe density, the specific heat conductance's in the floor are varied with each simulation, but kept constant between rooms in any given simulation. This is done to avoid punishing the method based on Eq. (32) unnecessarily. Considering the heat distribution the improvement is not that clear. It has to be mentioned that real floors do not have equal resistance, due to varying floor types and the effects caused by the interior of the room.

### *3.2 Demo house comparison*

To collect evidence for or against the ability of the method to estimate the flow distribution in real houses, the method was carried out on a test house having a flow meter on the common pipe of the FH system. The measurement results of round-trip time $\Delta t_\mathrm{r}$ are seen in Tab. 3. Two measurements are made and the average value is used. Note that the times differ quite significantly between the two tests, and the reason for this is unexplained. It is worth noting, though, that if the values are plotted, the pattern is preserved. Besides the measured times, the actual measured flow for each circuit is shown in liters per hour. The areas and assumed transport lengths are presented too. Figure 8 shows the results of the estimated flow distribution. As can be seen, 12

out of 15 circuits improved when compared to the measured distribution.

**Tab. 2** – Shows the RMSE and *mean absolute error* (MAE) of the estimates for the nominal flow distribution based on floor area and Eq. 15

| Measure | $A_\mathrm{r}$ | $\frac{A_\mathrm{r}}{\Delta t}$ | Ratio h |
|---|---|---|---|
| RMSE | 0.014 | 0.0093 | 0.62 |
| MAE | 0.012 | 0.0077 | 0.63 |

**Tab. 3** – Results for room 1-15

| Room | 1 | 2 | 3 | 4 | 5 | 6 | 7 | 8 |
|---|---|---|---|---|---|---|---|---|
| $q[l/h]$ | 173 | 135 | 87 | 154 | 158 | 184 | 119 | 132 |
| $\Delta t^1_{\mathrm{r},j}[s]$ | 460 | 500 | 440 | 480 | 420 | 420 | 280 | 480 |
| $\Delta t^2_{\mathrm{r},j}[s]$ | 420 | 440 | 380 | 480 | 340 | 340 | 240 | 440 |
| $A_\mathrm{r}j[m^2]$ | 12.7 | 9.2 | 3.6 | 9.5 | 9.3 | 9.6 | 4.8 | 9.5 |
| $\hat{\ell}_{\mathrm{tr},j}[m]$ | 8 | 5.5 | 7 | 1.5 | 3 | 3 | 1.5 | 5.5 |
| Room | 9 | 10 | 11 | 12 | 13 | 14 | 15 | |
| $q[l/h]$ | 126 | 184 | 150 | 140 | 165 | 156 | 95 | |
| $\Delta t^1_{\mathrm{r},j}[s]$ | 440 | 520 | 520 | 480 | 360 | 460 | 300 | |
| $\Delta t^2_{\mathrm{r},j}[s]$ | 340 | 500 | 460 | 400 | 300 | 360 | 280 | |
| $A_{\mathrm{r},j}[m^2]$ | 9.5 | 15 | 14.6 | 7.7 | 9.6 | 13 | 5.5 | |
| $\hat{\ell}_{\mathrm{tr},j}[m]$ | 5.5 | 11.5 | 2.5 | 8.5 | 3 | 2 | 2 | |

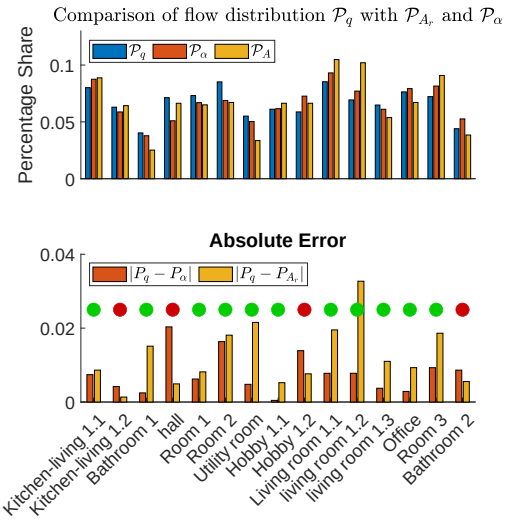


**Fig. 8** – Upper: Comparison of real percentage share of flow with estimate based on $\alpha$ and $A_\mathrm{r}$. Lower: difference for each room plus improvement indicator.

## 4. Conclusion

In this work we investigated the use of retrofitted sensors on the return pipes to estimate the flow distribution in a FH system. Simulation and experimental results suggest that it is possible to observe round-trip time in the data, and the flow distribution resulting therefrom is better than the one merely based on floor area distribution. The method improved the estimate in a test house by 38%. Work to be done, is to carry out a statistic, which either supports or disproves the result presented in this text. The results also suggest that measuring the temperature in the pipe could improve the results substantially.

The datasets generated during and/or analysed during the current study are available in the git repository, `https://gitlab.com/Thorsteinsson/clima-2022.git`.

## References


[1] Danish Energy Agency, "Data, tabeller, statistikker og kort Energistatistik 2019," da, Danish Energy Agency, Tech. Rep., ISSN: 0906-4699 year: 2019, p. 60. [Online]. Available: `https://ens.dk/sites/ens.dk/files/Statistik/energistatistik2019_dk-webtilg.pdf` (visited on 05/07/2021).

[2] Statistics Denmark, *Boligbestanden*, da, 2021. [Online]. Available: `https://www.dst.dk/da/Statistik/emner/borgere/boligforhold/boligbestanden` (visited on 11/25/2021).

[3] P. D. Andersen, M. J. Jiménez, H. Madsen, and C. Rode, "Characterization of heat dynamics of an arctic low-energy house with floor heating," en, *Building Simulation*, vol. 7, no. 6, pp. 595–614, Dec. 2014, ISSN: 1996-8744. DOI: 10.1007/s12273-014-0185-4.

[4] I. Hazyuk, C. Ghiaus, and D. Penhouet, "Optimal temperature control of intermittently heated buildings using Model Predictive Control: Part I – Building modeling," en, *Building and Environment*, vol. 51, pp. 379–387, May 2012, ISSN: 0360-1323. DOI: 10.1016/j.buildenv.2011.11.009.

[5] P. Radecki and B. Hencey, "Online Model Estimation for Predictive Thermal Control of Buildings," *IEEE Transactions on Control Systems Technology*, vol. 25, no. 4, pp. 1414–1422, Jul. 2017, Conference Name: IEEE Transactions on Control Systems Technology, ISSN: 1558-0865. DOI: 10.1109/TCST.2016.2587737.

[6] J. Ploennigs, A. Ahmed, B. Hensel, P. Stack, and K. Menzel, "Virtual sensors for estimation of energy consumption and thermal comfort in buildings with underfloor heating," en, *Advanced Engineering Informatics*, Special Section: Advances and Challenges in Computing in Civil and Building Engineering, vol. 25, no. 4, pp. 688–698, Oct. 2011, ISSN: 1474-0346. DOI: 10.1016/j.aei.2011.07.004.

[7] T. M. Kull, M. Thalfeldt, and J. Kurnitski, "Modelling of Wax Actuators in Underfloor Heating Manifolds," en, *E3S Web of Conferences*, vol. 246, p. 11 009, 2021, Publisher: EDP Sciences, ISSN: 2267-1242. DOI: 10.1051/e3sconf/202124611009.

# Long-term experimental study of price responsive predictive control in a real occupied single-family house with heat pump ⋆

Simon Thorsteinsson [a], Alex Arash Sand Kalaee [b], Pierre Vogler-Finck [b], Henrik Lund Stærmose [b], Ivan Katic [c], Jan Dimon Bendtsen [a]

[a] *Section for Automation and Control, Aalborg University, Aalborg, Denmark*

[b] *Neogrid Technologies ApS, Aalborg, Denmark*

[c] *Danish Technological Institute, Taastrup, Denmark*

**Abstract**

The continuous introduction of renewable electricity and increased consumption through electrification of the transport and heating sector challenges grid stability. This study investigates load shifting through demand side management as a solution. We present a four-month experimental study of a low-complexity, hierarchical Model Predictive Control approach for demand side management in a near-zero emission occupied single-family house in Denmark. The control algorithm uses a price signal, weather forecast, a single-zone building model, and a non-linear heat pump efficiency model to generate a space-heating schedule. The weather-compensated, commercial heat pump is made to act smart grid-ready through outdoor temperature input override to enable heat boosting and forced stops to accommodate the heating schedule. The cost reduction from the controller ranged from 2-33% depending on the chosen comfort level. The experiment demonstrates that load shifting is feasible and cost-effective, even without energy storage, and that the current price scheme provides an incentive for Danish end-consumers to shift heating loads. However, issues related to controlling the heat pump through input-manipulation were identified, and the authors propose a more promising path forward involving coordination with manufacturers and regulators to make commercial heat pumps truly smart grid-ready.

*Key words:* Hierarchical model predictive control; Heat pump; Retrofit building control; Real experiment; Load shifting; Demand side management.

## 1 Introduction

A fast and determined transition to a carbon neutral economy is more urgent than ever. The summary for policy makers associated with the $6^{th}$ annual report from The Intergovernmental Panel on Climate Change reads: *"All global modelled pathways that limit warming to* $1.5°C(> 50\%)$ *with no or limited overshoot, and those that limit warming to* $2°C(> 67\%)$ *involve rapid and deep and in most cases immediate [Green house gas] emission reductions in all sectors"* [25]. This means that not only long term solutions, but also existing solutions need to be implemented, immediately. Space heating is major energy consumer with potential for large reductions both short and long term. The focus here is on single-family houses, since they pose a particular grand challenge for the overall savings potential in the space heating sector. Single-family houses are small but many in numbers, meaning that they make up a large share of the sector. Estimates indicate that about 55% of Danish heated area belongs to single-family houses [8]. Further complicating the issue is that a majority of the single-family houses are owned by the residents themselves 26. This is not bad in itself—self-ownership has many socioeconomic benefits—but it does mean that any solution introduced to a single-family house has to be highly cost-beneficial in order to get the individual owners to invest in energy upgrades. A popular investment, seen across the European Union, is to acquire a heat pump (HP). In the period 2005 to 2020, sales increased from about 0.5 mill. to 1.62 mill units sold with air-sourced

⋆ This work is funded the Danish Energy Agency through the EUDP project OPSYS 2.0 (Case num.: 64018-0581) and the Department of Electronic Systems at Aalborg University.

*Email addresses:* sith@es.aau.dk (Simon Thorsteinsson), ask@neogrid.dk (Alex Arash Sand Kalaee), pvf@neogrid.dk (Pierre Vogler-Finck), hls@neogrid.dk (Henrik Lund Stærmose), ik@teknologisk.dk (Ivan Katic), dimon@es.aau.dk (Jan Dimon Bendtsen).

being the most popular type [29]. The rise in heat pumps is only one factor in an increasingly electrified economy, which starts to put strain on the electric grid with peak loads threatening stability and capacity. In Denmark the response is a new network tariff model for electricity, *tarifmodel 3.0*, which was introduced on the 1st of January, 2023 [9]. This model allows the DSO(grid)-operators to differentiate the end-user tariffs substantially over the course of the day in order to nudge the end-user into changing their consumption away from peak load periods and increase demand at night. This situation also impacts households heated by an electric heat pump who, although having some tax-benefits, still have to pay the full grid-tariffs. In other words, the owners need to change their heating habits or face the cost of heating in expensive periods. Many danish households are already on a time-varying price which is based on the Nord Pool hourly spot-market and time-of-use distribution prices. Adding the two price schemes together means that the difference between high and low prices within a day can be several times larger than the lower price, as seen in Fig. 1. This can create some very costly situations, but also opportunities for cost savings. One such opportunity is to utilize a price-aware controller to load shift by boosting heat production (charge) in low cost periods and decrease (discharge) in high cost periods either with help of an energy storage [14, 6] or directly using the thermal mass of the building itself [4, 28, 13]. A variable-speed heat pump can be used to boost heat by increasing the compressor speed, but this comes with a significant loss of efficiency (*coefficient of performance*, COP). Further, the COP of an air-to-water HP is highly dependent on ambient temperature, which means that not only price but also weather factors need to be considered as well.

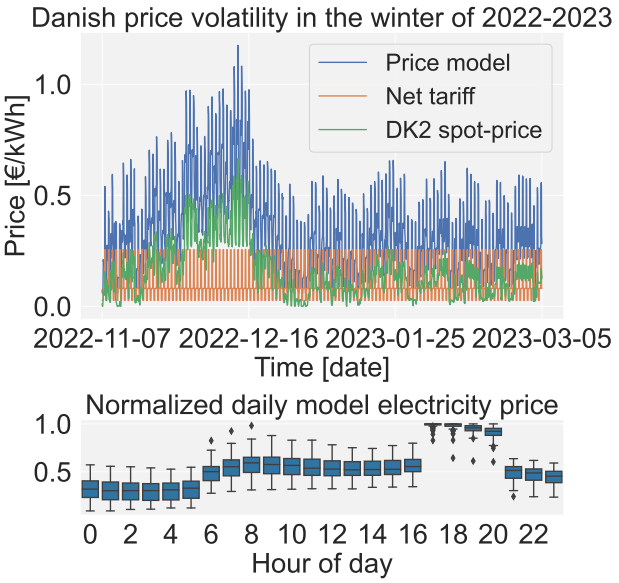


Fig. 1. Upper: The Nord Pool market spot price plotted together with the Danish tariff Model 3.0. The price model is used for the economical evaluation of the experiment. Lower: The normalized ($x_i / \max(x)$) daily price development of the price model.

A method suitable for automating heat load shifting is Model Predictive Control (MPC) [4]. During the last 30 years, MPC has been studied extensively in the context of building control due to its structural ability to integrate building dynamics, heating system and environmental aspects into an optimal control problem (OCP) formulation capable of handling both constraints and discrete states. A range of different versions of MPC have been suggested: Deterministic MPC, Stochastic MPC, Robust MPC, Learning MPC, Offset-free MPC, Implicit MPC and Explicit MPC [11]. While the studies are numerous, the method has so far failed to make a broad impact on the space heating sector. The reported reasons are installation costs of sensor and actuators, model development costs [27] and user-acceptance.

Although the number of long term (beyond 30 days) building scale demonstrations are few compared to simulation studies, a selection of noteworthy examples do exist. In [27] a 6000 $m^2$, occupied office building in Switzerland both in periods during winter and summer which combined into about 30 weeks of testing. While reporting that the control itself was a success, the author questions whether the method is mature enough to be implemented in similar buildings. In [10] two heat pumps and a gas boiler were controlled in a 960 $m^2$ occupied office building in Brussels during the winter of 2014-2015 reporting cost savings of 30% while improving comfort. In Halifax, Canada, a 10000 $m^2$ university building was controlled using MPC for four months with reported savings of 29% electricity and 63% heat [12]. In the category single-family houses, [23] controlled four houses for 5 months and reported an average cost reduction of 9% when compared to 7 benchmark houses and in [21] HPs in 300 homes were ON/OFF throttled to reduce peak loads. The low number of residential experiments is likely due to the low potential for savings, which disqualifies large implementation costs. The requirement for simple solutions have spurred a branch of low-cost MPC e.g. with only one central heat meter as in [4]. Recent studies [4, 30] have demonstrated the basic feasibility of such schemes, but both studies point out that longer evaluation periods are needed to reliably verify their practical usefulness. Furthermore, occupancy in single-family houses is a fundamentally different condition from office buildings due to the invasive nature of sensor feedback on the occupants´ behavior, which must also be addressed.

Our contribution in this paper is a *97 day long* study demonstrating a price responsive, low cost, hierarchical Mixed-Integer MPC control scheme on an *occupied* single-family house featuring an air-to-water heat pump and floor heating (FH). The controller is designed to minimize costs by shifting heating loads according to the electricity price signal together with other predictable

and/or measurable factors. The controller is developed as a comparably low cost solution which only makes use of an internet connected control unit, a central heat meter, electricity meters, and room thermostats. Further, the weather forecast is provided by a weather service and the model is a single zone model which is based on a weighted average room temperature for the entire house. The controller is deliberately designed not to make use of explicit occupancy information, in order to protect the occupants´ right to privacy. The main findings from the experiment are: the near zero emission house demonstrated a high level of flexibility with respect to time-of-heating. Further, it is possible to boost the floors with heat during intensive sun radiation periods (when there is plenty of own-produced PV electricity) without further deteriorating the comfort. Controlling the upper layer using an area weighted average building temperature has shown to be unproblematic with respect to comfort in the test house.

The layout for the rest of the paper is as follows. Section 2 presents the case, an overview of the heating side and the electrical side viewed from a control perspective. Section 3 presents the hierarchical control strategy, starting with the supervisory controller and followed by the mid-level controllers. Section 4 contains the models used in the paper. Section 5 describes the experiment before the results are presented in Section 6. As the results are based on real data, Section 7 is dedicated to the authors' interpretation of the results. Finally, a common discussion section followed by conclusion in Sections 8 and 9, respectively.

## 2 System

This section starts with an introduction to the case followed by an overview of the heating system and electrics before delving into the control retro-fit. The relevant signals are listed in Table 1.

### *2.1 Case study*

The case is a 230 $m^2$, two-story single-family house from 2018; see Fig. 2.1. According to the Danish building regulation, it is classified as a low energy class building (BR2020), which, among other requirements, implies a maximum annual heat demand of 20 kWh/$m^2$ [1]. It is located on Sjælland (Zealand) in Denmark, with a south view over the sea. A south facing photovoltaic system is placed on the roof with a measured peak output of 4 kW in end of December and 5.5 kW in June. Space heating and domestic hot water is provided by a *Bosch Compress 7000i* AW (air-to-water) heat pump. Domestic hot water takes priority over space heating. Based on measured data the nominal electric consumption ranges from 200 W to 2500 W. Floor heating, embedded in concrete, is installed throughout the house. The floor heating system is controlled by a Wavin controller and consists of 15 circuits delivering heat to 11 heating zones. Each zone has one thermostat assigned, meaning that if more circuits are supplying the same zone all valves in the particular zone opens when heat is requested. The circuits are ON/OFF controlled based on deviations from the temperature reference provided for each zone. The heat pump is controlled by an ambient temperature compensated heat curve. The household has a variable electricity price contract, which is based on the Nord Pool market spot-price.

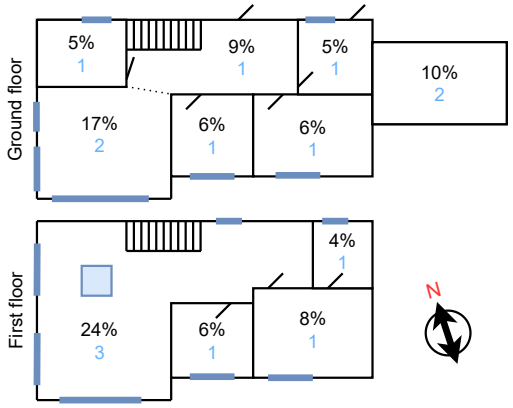


Fig. 2. Blueprint of the floor plan with area distribution. Blue numbers indicate the number of FH circuits in each zone

Table 1
Relevant signals

| Variable | Unit | Description |
|---|---|---|
| $\dot{Q}_{\mathrm{HP}}$ | [W] | Heat flow output from HP |
| $Q_{\mathrm{HP}}$ | [kW h] | Heat output from HP |
| $P_{\mathrm{HP}}$ | [W] | Electric power input to HP |
| $E_{\mathrm{HP}}$ | [kW h] | Electric energy input to HP |
| $P_{\mathrm{PV}}$ | [W] | Electric power output from photovoltaic |
| $P_{\mathrm{G}}$ | [W] | Electric power bought from grid |
| $P_{\mathrm{APP}}$ | [W] | Household electric power consumption |
| $T_{\mathrm{R}}$ | [°C] | Return temperature to HP |
| $T_{\mathrm{R},i}$ | [°C] | Return Temperature from FH circuit $i$ |
| $T_{\mathrm{r},j}$ | [°C] | Air temperature in room $j$ |
| $T_{\mathrm{r,ref},j}$ | [°C] | Reference temperature in room $j$ |
| $T_{\mathrm{f},j}$ | [°C] | Estimated floor temperature in room $j$ |
| $v_i$ | [°C] | ON/OFF Valve setting for circuit $i$ |
| $\mathcal{U}_{\mathrm{a}}$ | [V] | Output voltage from ambient temperature sensor |

### 2.2 *Heating system*

Fig. 3 shows the heating system with associated signals. Note that heat flow to the floor heating system, $\dot{Q}_{\mathrm{HP}}$, and electric power consumption of the heat pump, $P_{\mathrm{HP}}$, are measured.

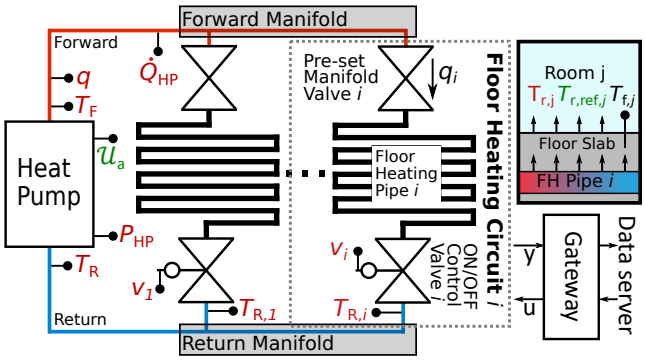


Fig. 3. The diagram of the heating system in the house. The colors represent the kind of signal: red for measured variables, green for control inputs and black for estimated variables. Pipes on warm side are red and cold side blue.

The HP feeds the floor heating system with water, which in turn deliver the heat to the heating zones.

### 2.3 *Electricity*

The household electric grid is shown in Figure 4. The main units are photovoltaic panels and the heat pump which have separate electricity meters. The other household appliances are aggregated into an unknown disturbance.

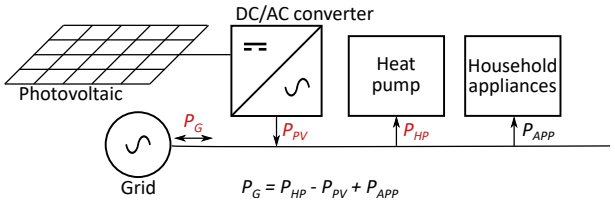


Fig. 4. The internal electricity grid of the house expressed in power. Red variables are measured quantities.

### 2.4 *Retrofit architecture*

The retrofit architecture, which is built and implemented by Neogrid Technologies, is seen in Fig. 5. The infrastructure consists of an onsite part and a backend with the control box acting as gateway between them. The backend is responsible for refining, organizing, downloading data from weather and price services, and storing data, which is used for analysis and model fitting. The control box is responsible for providing control signals and collecting measurements from all units.

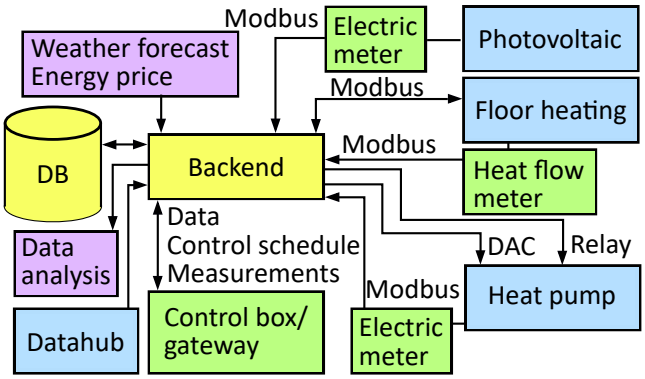


Fig. 5. Shows the overview of the hardware and communication protocols. Blue color is for preinstalled hardware, green for installed sensors, yellow is the off-site infrastructure and purple are data services.

In this case, it means to provide the artificial ambient temperature overwrite, via a digital to analog converter (DAC) and blocking the compressor using a relay. We use the BACnet and Modbus protocols to communicate with the floor heating controller for collecting room temperatures and other data from the floor heating system, and sending set-points to the valves.

### 2.5 *Object oriented description of commercial domestic heat pump*

In this section common properties for commercial air-to-water HP's are listed together with references to how they are modelled in the literature.

(1) **ON/OFF indicator**: the HP turns off when heat demand is absent. In this work the indicator variable $\delta_{\mathrm{HP}} \in \{0, 1\}$ is one when the HP is on and zero if off [17, 20].
(2) **Minimum load:** the minimum load and operation range of a variable speed HP is often considered and modelled as a set $P_{\mathrm{HP}} \in \{0\} \cup [\underline{P_{\mathrm{HP}}}, \overline{P_{\mathrm{HP}}}]$ [16, 17, 19].
(3) **Coefficient of performance:** the coefficient of performance (COP) is the ratio between consumed input energy (here electricity) and the produced heat. It is often modelled as a static function, $f_{\mathrm{HP}} : \mathbb{R} \to \mathbb{R}$.
(4) **Down-time:** to avoid start-up cycling some HPs feature a (sometimes adaptive) down-time period measured in hours. To incorporate this a model for minimum up- and down-time can be included [20, 18].
(5) **Limit on rate off change:** the internal controllers of a domestic HP sometimes prevent it from changing state too rapidly.
(6) **Domestic hot water production:** the HP switches between providing space heat and domestic hot water. Domestic hot water is often prioritized.

(7) **Discrete compressor speed steps:** the compressor speed is often operated at certain steps rather than continuous action. Some speeds are excluded as resonance with the casing can cause noise.
(8) **Low pass filter on ambient temperature signal:** it is common practice that commercial HPs apply a low pass filter to the ambient temperature signal before it is provided to the internal controllers.
(9) **Defrosting:** an air-to-water HP needs to defrost the evaporator regularly in order to function properly. This event is treated as a random process which takes priority.

It is desirable that any MPC operating an HP can handle the listed properties.

## 3 Control

The control objective is to provide the required comfort level at the lowest cost feasible. To accomplish this, the controller needs to make two high-level control actions. First, it must choose the heat pump heat flow $\dot{Q}_{\mathrm{HP}}(t) \in \mathbb{R}$ and the FH water flow $q(t) \in \mathbb{R}$. Second, it must guide the water to the most suitable rooms. It is not possible to control the heat and water flow directly, but it is possible to influence them indirectly. The heat production can be indirectly controlled using ambient temperature $T_{\mathrm{a}}$, and valve positions $v$ affect flow:

$$\dot{Q}_{\mathrm{HP}}(t) = f(T_{\mathrm{a}}, \cdot), \quad q = g(v, \cdot), \quad v \in \mathbb{R}^N, \quad T_{\mathrm{a}} \in \mathbb{R} \quad (1)$$

The $(\cdot, \cdot)$ notation indicates that heat and water flow are not only functions of ambient temperature and valve positions, but other factors too.

### *3.1 Control hierarchy*

The control concept comprises three control levels, see Fig. 6. The upper layer contains the supervisory controller that is aware of energy assets connected to the system as well as important externalities such as weather and electricity prices. It treats the energy assets as objects with properties which can be utilized for optimal control. A key feature of the supervisory controller is that it knows what the energy assets can do, and why they should do it, but not how to make them do it. The middle layer is tasked with tracking the heat reference, delivered by the supervisory controller, and distributing the heat to appropriate rooms. This layer knows how to deliver the demanded energy, but not why it does it. Based on the heat reference and room temperatures, the valve controller selects the valves to be opened in order to provide a flow, which works as an operating point for the heat controller, and to transport the heat to the rooms that need it the most. The heat controller follows the heat reference by providing an artificial ambient temperature to the HP to indirectly control the compressor speed.

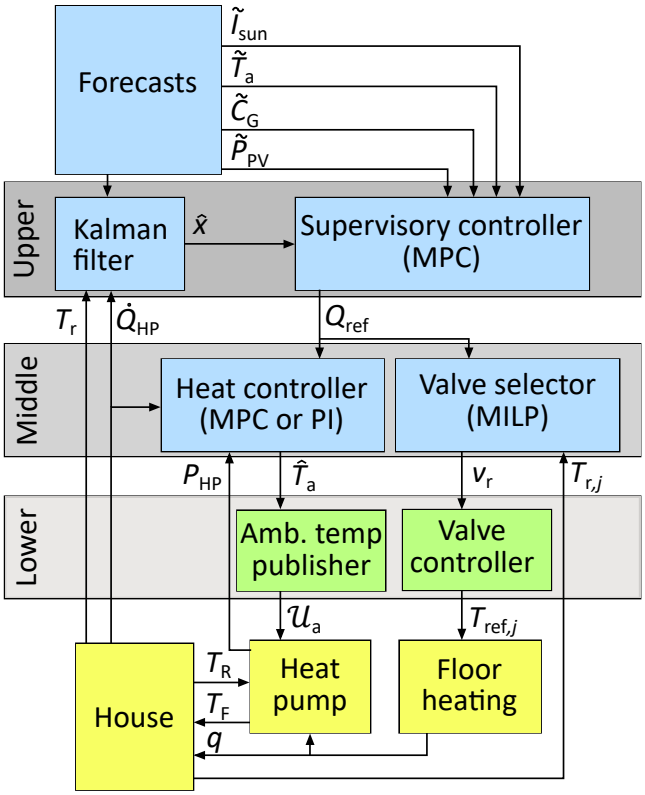


Fig. 6. Shows the control diagram with signals. Blue indicates computations conducted remotely and green indicates onsite units and yellow the physical components. The grey boxes contain the control layers in the hierarchical control structure

The lowest layer handles the interface between the control signal and the actual hardware. The Heat publisher translates the artificial ambient temperature provided by the heat controller to a voltage which emulates the outdoor temperature sensors output at given temperature. The valve publisher translates the valve selection into room temperature references designed to force circuits open or closed.

### *3.2 Supervisory controller*

Fig. 7 presents the concept for the supervisory controller in the upper layer.

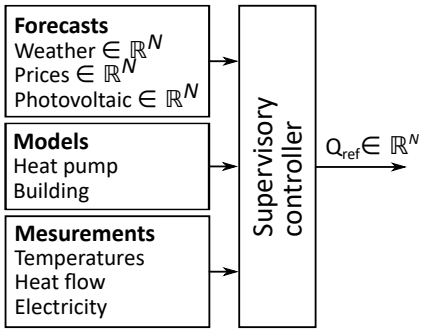


Fig. 7. Overview of the top layer supervisory controller.

The controller relies on three main components, forecasts, models and measurements. Based on these, the controller computes a heat reference (or "budget"), $Q_{\text{ref}}$, which is dispatched to the lower level controllers. The hierarchical structure makes the supervisory controller more flexible than a monolithic structure, since it can calculate the heat reference without concern for how the heat is delivered—it just needs to know at which efficiency and rate the heat can be delivered. The biggest drawback of using heat for the interface is that it needs to be measured, and adding a heat flow sensor to the hydraulic network is costly.

### *3.2.1 Design of supervisory controller*

The conceptualized version of the *Mixed Integer Optimal Control Problem* (MIOCP) at the core of the *Mixed Integer Model Predictive Control* (MIMPC) is seen in equation system (2) on a form which describes the functionality of the cost and various constraints rather than the implementation. Note that (2) contains two subversions decided by the indicator variable $\delta_{\text{OP}}$. It must be stressed that the value of $\delta_{\text{OP}}$ is chosen before implementing the problem, it is not an optimization variable. The difference between the two versions is the HP efficiency model.

$$J(u^*_{\text{OP}}) = \min_{u_{\text{OP}}} f_{\text{G}}(P_{\text{G}}) + f_{\text{CO}_2}(P_{\text{G}}) + f_{\text{cmf}}(T_{\text{r}}, T_{\text{r,ref}}) \tag{2a}$$

$$u_{\text{OP}} = \begin{cases} (P_{\text{HP}}, \delta_{\text{HP}}, S) & \delta_{\text{OP}} = 1 \\ (\dot{Q}_{\text{HP}}, \delta_{\text{HP}}, S) & \delta_{\text{OP}} = 0 \end{cases} \tag{2b}$$

$$u_{\text{OP}} \in \mathbb{R}^N \times \{0,1\}^N \times \mathbb{R}_+^{N_{\text{s}}} \tag{2c}$$

s.t.

$$P_{\text{G}} = P_{\text{HP}} - \tilde{P}_{\text{PV}} + P_{\text{APP}} \tag{2d}$$

$$\mathbf{x}_{i+1} = \mathbf{A}\mathbf{x}_i + \mathbf{B}\dot{Q}_{\text{HP},i} + \mathbf{E}d_i, \quad T_{\text{r},i} = \mathbf{C}\mathbf{x}_i \tag{2e}$$

$$\text{if } \delta_{\text{OP}} = 1 \text{ then } \dot{Q}_{\text{HP},i} = f_{\text{HP},\dot{Q}}(P_{\text{HP},i}, T_{\text{a},i})\delta_{\text{HP},i} \tag{2f}$$

$$\text{if } \delta_{\text{OP}} = 0 \text{ then } P_{\text{HP},i} = f_{\text{HP},P}(\dot{Q}_{\text{HP},i}, T_{\text{a},i})\delta_{\text{HP},i} \tag{2g}$$

$$P_{\text{HP},i} \in \begin{cases} [\underline{P_{\text{HP}}}, \overline{P_{\text{HP}}}] & \delta_{\text{HP},i} = 1 \\ 0 & \delta_{\text{HP},i} = 0 \end{cases} \tag{2h}$$

$$\Delta\delta_{\text{HP},i} = \delta_{\text{HP},i} - \delta_{\text{HP},i-1} \quad \Delta P_{\text{HP},i} = P_{\text{HP},i} - P_{\text{HP},i-1} \tag{2i}$$

$$\Delta P_{\text{HP},i} \in \begin{cases} [\Delta\underline{P_{\text{HP}}}, \Delta\overline{P_{\text{HP}}}] & \delta_{\text{HP},i} = 1 \\ (-\infty, \Delta\overline{P_{\text{HP}}}] & \delta_{\text{HP},i} = 0 \end{cases} \tag{2j}$$

$$\Delta\delta_{\text{HP},i} = -1 \implies \delta_{\text{HP},i+1}, \ldots, \delta_{\text{HP},i+M-1} = 0 \tag{2k}$$

The cost function is the sum of three functions. First, a linear term, $f_{\text{G}}(P_{\text{G}})$, describing the differentiated cost of either importing from or exporting to the electricity grid. The input is consumed electricity from the grid, $P_{\text{G}}$, with positive values indicating import. The prices for buying and selling to the grid are given as $c_{\text{E}}^+ > 0$ and $c_{\text{E}}^- > 0$, respectively. The second term is a self-imposed $CO_2$-tax. The third is the comfort term which punishes deviations from the desired temperature. Slack variables are used to ensure feasibility. Together the terms make out a convex cost-function.

The constraint (2d) describes the electricity balance were the amount of electricity bought from the grid (G) is calculated. Constraint (2e) describes the linear dynamics of the house. Constraints (2f)-(2k) models the properties of the HP presented in Section 2.5. Constraints (2f) and (2g) both describes the HP efficiency, but only one is active dependent on the initial choice of $\delta_{\text{OP}}$. Constraint (2h) describes the piece-wise function where the compressor either is off, or operating in the range $[\underline{P_{\text{HP}}}, \overline{P_{\text{HP}}}]$. The constraint (2j) limits the rate off change between control periods. To meet the requirement that the HP can be turned off from any operational state, the down rate is set to $-\infty$ when $\delta_{\text{HP},i} = 0$. Last (2k) forces the HP to stay turned off for minimum $M$ sample times. Having described the functionality of the optimization problem the next part focuses on implementation aspects.

The guiding principle for the implementation is that the structure of the problem is convex if the problem is relaxed, meaning that if integer variables are replaced with continuous ones, the problem is convex. The cost function from equation system(2) is implemented as:

$$J(u_{\text{OP}}) = c_{\text{E}}^{-\text{T}} P_{\text{G}} + \Delta c_{\text{E}}^{+\text{T}} P_{\text{G}}^+ + z_{\text{cmf}} + c_{\text{s}}^T S \tag{3}$$

Here the auxiliary variables $P_{\text{G}}^+, z_{\text{cmf}} \in \mathbb{R}_+^N$ are introduced. The variable $P_{\text{G}}^+$ is defined as entry-wise $\max(0, P_{\text{G}})$ and $z_{\text{cmf}}$ has to be larger than any competing comfort constraints. The vector $\Delta c_{\text{E}}^+ = c_{\text{E}}^+ - c_{\text{E}}^- > 0$ describes the positive difference between buying price and selling price. Note that the buying price needs to be higher than the selling price, otherwise the solution to the optimization problem entails buying excessive amounts of electricity just to sell it again in the same instance. The auxiliary variable $z_{\text{cmf}}$ encodes the expression $\max(f_{\text{cmf},1}(T_{\text{r}}, T_{\text{r,ref}}), \cdots, f_{\text{cmf},N_{\text{cmf}}}(T_{\text{r}}, T_{\text{r,ref}}))$ where $f_{\text{cmf},i}(T_{\text{r}}, T_{\text{r,ref}})$ with $i \in \{1, ..., N_{\text{cmf}}\}$ is either an affine or quadratic positive definite function. This formulation gives room for skewed functions which can for instance penalize either over- or underheating. Note that the artificial $CO_2$-tax term is not missing, it is merely incorporated into the buying price as described in Section 4.5.

The HP efficiency model in either (2g) or (2f) is implemented using the known Mixed Logic Dynamics

technique from [7] where an auxiliary variable is introduced $z_{\mathrm{HP},i}$ to either be zero of mirror the value of the function dependent on $\delta_{\mathrm{HP},i}$. To preserve convexity of the input set, only an inequality is used instead of the original equality seen in (2g). if $\delta_{\mathrm{OP}} = 0$ then $P_{\mathrm{HP},i} \geq f_{\mathrm{HP},P}(\dot{Q}_{\mathrm{HP},i}, T_{\mathrm{a},i})$ and if $\delta_{\mathrm{OP}} = 0$ then $\dot{Q}_{\mathrm{HP},i} \leq f_{\mathrm{HP},\dot{Q}}(P_{\mathrm{HP},i}, T_{\mathrm{a},i})\delta_{\mathrm{HP},i}$. The structure of the problem forces the solution onto the curve emulating the equality constraint. When $\delta_{\mathrm{OP}} = 1$, there are a few cases where $\dot{Q}_{\mathrm{HP}}$ deviates from the curve to avoid the cost of overheating. To avoid this an equality constraint can be implemented with the added computational cost. The constraint in (2h) is implemented as e.g. in [16, 17, 22], so is the constraint in (2j). The down-time model constraint in (2k) can be implemented as shown in [22]. The problem can be summed up to

$$\min_{\mathbf{u}\in\mathbb{R}^N,} \; J(\mathbf{x}_0, \mathbf{u}) \tag{4a}$$

$$\text{s.t.} \tag{4b}$$

$$\mathbf{x}_{k+1} = \mathbf{A}\mathbf{x}_k + \mathbf{B}\mathbf{u}_k + \mathbf{E}\mathbf{d}_k \tag{4c}$$

$$\mathbf{y}_1 = \mathbf{C}\mathbf{x} + \mathbf{D}\mathbf{u} \tag{4d}$$

$$\mathbf{x}_k \in \mathcal{X} \qquad \mathbf{x}_0 = \mathbf{x}(t) \tag{4e}$$

$$\mathbf{y}_2 \geq \mathbf{f}_{\mathrm{convex}}(\mathbf{x}, \mathbf{u}) \tag{4f}$$

$$\mathbf{y}_3 \leq \mathbf{f}_{\mathrm{concave}}(\mathbf{x}, \mathbf{u}) \tag{4g}$$

where $J$ is the convex cost function. Section 4 details the models that specify the MPC formulation given here.

### *3.3 Valve selector*

The valve selector, or dispatcher, is a mixed integer linear programming problem tasked with providing the flow, $q$, as requested, $q_{\mathrm{ref}}$, and distribute the water to the most suitable rooms. Note that the Valve selector is only reactive control. The optimization problem is

$$\min_{v\in\{0,1\}^M} J(v) = \min_{v\in\{0,1\}^M} c_q \|q_{\mathrm{ref}} - q\|_2^2 + c_{\mathrm{cmf}}^{\mathrm{T}} v \tag{5a}$$

$$\text{s.t.} \tag{5b}$$

$$\overline{q} = \sum_{i=1}^{M} v_i \overline{q}_i, \tag{5c}$$

$$q = c_0 + c_1\overline{q} + c_2\overline{q}^2 \tag{5d}$$

$$q \geq q_{\min}, \tag{5e}$$

$$r_m \geq \sum_{i=1}^{M} \max(v_{0,i} - v_i, 0), \tag{5f}$$

$$v_j = 1, \qquad \forall j \in \mathcal{J}. \tag{5g}$$

The cost function is a trade-off between following the flow reference and delivering the heat to the right rooms. The two terms are weighted by $c_q \in \mathbb{R}_+$ and $c_{\mathrm{cmf}} \in \mathbb{R}^{N_{\mathrm{r}}}$. The comfort cost is pre-calculated as $c_{\mathrm{cmf},i} = a(T_{\mathrm{r},i} - T_{\mathrm{r,ref},i})$ with $a > 0$ such that cold rooms get priority. The expressions (5c) and (5d) describe the flow as a function of valve configuration. In (5c) the flow is a sum of contributions, but since the flow saturates as more valves open a second order polynomial is used in (5d) to model this effect. The term $\overline{q}^2$ seems to deliver a range of square and bilinear terms, which is inconsistent with MILP. Luckily, $v_i$ is binary, meaning that $v_i v_j$ is an AND statement $(v_i \wedge v_j)$ can be encoded by Mixed Logic Dynamics(MLD) as a linear inequality [7]. The squared terms are unproblematic since $v_i^2 = v_i$. Encoding the binary polynomial has a cost in form of added binary auxiliary variables. The added number of binary variables is $\binom{M}{2}$, which in this case is 55, making a total of 66 variables. Constraint (5e) forces a minimum flow, (5f) limits the number of valves that can be closed in one iteration and (5g) forces circuits open which belong to too cold rooms.

### *3.4 Heat controller*

The heat controller, placed in the middle layer, is required to deliver heat, $Q_{\mathrm{HP}}$, according to the heat reference. Further, it suppresses the compressor in periods with no demand and is responsible for timing the HP start. The diagram is seen in Fig. 8. The signals are: ref-

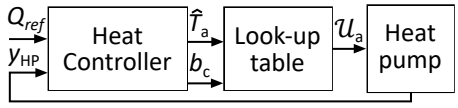


Fig. 8. Shows the heat controller with feedback

erence vector $Q_{\mathrm{ref}} \in \mathbb{R}^N$, artificial ambient temperature, $\hat{T}_{\mathrm{a}}$, the voltage representing the said ambient temperature, $\mathcal{U}_{\mathrm{a}}$, the measurement vector, $y_{\mathrm{HP}} = \begin{bmatrix}\dot{Q}_{\mathrm{HP}} & P_{\mathrm{HP}}\end{bmatrix}$, and the binary compressor blocking signal, $b_{\mathrm{c}}$. During the test period a PID-controller and a short horizon MPC were tested. The PID-controller uses the measured heat flow and the reference in regular feedback. The MPC accumulates the delivered heat flow over the hour to match the heat reference given for that hour. Beyond heat control, the two controllers need to handle defrosting periods, DHW production and start delays as mentioned in Section 2.5. Defrost periods and DHW production are handled by detecting the event and setting the controller to standby-mode. After releasing the compressor block, it takes about 1.5 hour before the heat pump starts, therefore the reference vector is used to remove the blockage a defined time-span before the actual control takes place. More detail is given in a parallel paper in progress.

## 4 Models and parameter identification

This section presents the model and the subsequent parameter identification for each module that is included

in the MIOCP. Subsections 4.1-4.4 presents models used directly for control while subsection 4.5 contains the price model which is used both for guiding the price-aware controller and evaluation. Finally, subsection 4.6 describes how benchmark data from previous heating season, where the baseline controller was running, is used to evaluate the proposed controller.

### *4.1 Single-zone lumped parameter house model*

The single-zone house model, seen in (6), has, as argued in [15], two dynamic states which describe an averaged room ($T_\mathrm{r}$) and floor temperature ($T_\mathrm{f}$). The reason for modelling using only a single zone is given in [30]. Here the affects caused by position of doors and air stratification led the authors to conclude that a single-zone model is as useful as multi-zone model for MPC. In [4] a volume weighted average temperature is used since only the central heat meter is available. The purpose of the model is to make the MPC responsive to the impact of high sun intensity, ambient temperature and heat created by household appliances. These three aspects should be included if a forecast is available, otherwise they can be omitted at the cost of increased uncertainty. In this work the forecast for heat produced by household appliances and occupation is left out. The reason is partly technical, but also driven by privacy concerns.

$$C_\mathrm{r}\dot{T}_\mathrm{r} = U_\mathrm{r}\left(T_\mathrm{f} - T_\mathrm{r}\right) + U_\mathrm{r}\left(T_\mathrm{f} - T_\mathrm{r}\right) + \dot{Q}_\mathrm{s} \tag{6a}$$

$$C_\mathrm{f}\dot{T}_\mathrm{f} = U_\mathrm{r}\left(T_\mathrm{f} - T_\mathrm{r}\right) + \dot{Q}_\mathrm{HP} \tag{6b}$$

The control input to the model is heat flow $\dot{Q}_\mathrm{HP}$ measured over the floor heating system. The two-state formulation allows for estimating the overall heat capacity of the building through $C_\mathrm{f}$ and to capture the rapid air temperature changes, caused by sun radiation, in $C_\mathrm{r}$. The state space formulation is given as,

$$\dot{\mathbf{x}}(t) = \mathbf{A}\mathbf{x}(t) + \mathbf{B}\mathbf{u}(t) + \mathbf{E}\mathbf{d}(t) \tag{7a}$$

$$\mathbf{y}(t) = \mathbf{C}\mathbf{x}(t) \qquad \mathbf{C} = \begin{bmatrix}1 & 0\end{bmatrix} \tag{7b}$$

$$\mathbf{A} = \mathcal{C}^{-1}\mathcal{U} \qquad \mathbf{B} = \mathcal{C}^{-1}\mathcal{B} \qquad \mathbf{E} = \mathcal{C}^{-1}\mathcal{E} \tag{7c}$$

$$\mathcal{C} = \begin{bmatrix}C_\mathrm{r} & 0\\ 0 & C_\mathrm{f}\end{bmatrix} \quad \mathcal{U} = \begin{bmatrix}-\left(U_\mathrm{r} + U_\mathrm{A}\right) & U_\mathrm{r}\\ U_\mathrm{r} & -U_\mathrm{r}\end{bmatrix} \quad \mathcal{B} = \begin{bmatrix}0\\1\end{bmatrix} \tag{7d}$$

$$\mathcal{E} = \begin{bmatrix}U_\mathrm{A} & g_{\mathrm{s},1} & g_{\mathrm{s},2}\\ 0 & 0 & 0\end{bmatrix} \quad \mathbf{x} = \begin{bmatrix}T_\mathrm{r}\\T_\mathrm{f}\end{bmatrix} \quad \mathbf{u} = \begin{bmatrix}\dot{Q}_\mathrm{HP}\end{bmatrix} \quad \mathbf{d} = \begin{bmatrix}T_\mathrm{a}\\ \tilde{I}_\mathrm{s}\\ \tilde{I}_{\mathrm{s,dir}}\end{bmatrix} \tag{7e}$$

The input is total heat flow, $\dot{Q}_\mathrm{HP}$, and the disturbances are ambient temperature, direct sun irradiation. The common indoor temperature is an area weighted average of all room temperatures,

$$T_\mathrm{r} = \frac{A_{\mathrm{r},1}T_{\mathrm{r},1} + \cdots + A_{\mathrm{r},N_r}T_{\mathrm{r},N_r}}{A_{\mathrm{r},1} + \cdots + A_{\mathrm{r},N_r}} \tag{8}$$

The power from sun radiation can be estimated in many ways, but is here chosen to be:

$$\dot{Q}_\mathrm{s} = g_{\mathrm{s},1}\tilde{I}_\mathrm{s} + g_{\mathrm{s},2}\tilde{I}_{\mathrm{s,dir}} \tag{9}$$

$$\tilde{I}_\mathrm{s} = \tilde{I}_{\mathrm{s,dir}}(1 - \tilde{\alpha}_\mathrm{cloud}) \tag{10}$$

where $\tilde{I}_{\mathrm{s,dir}}$ [W m$^{-2}$] is direct sun and $\tilde{\alpha}_\mathrm{cloud}$ is the fraction of cloud cover. This particular formulation gives short but intense bursts of sunlight.

The model is discretized using Zero Order Hold (ZOH) discretization. Figures of the parameter fits are shown in Appendix B.2.

### *4.2 State estimation of $T_r$ and $T_f$*

Since the virtual average floor temperature, used in the MPC, is not measured a Linear Kalman Filter (LKF) is used to estimate the state at sample time $k$. The LKF is updated each 5 min. The model in (7) is observable for any $U_\mathrm{r}, U_\mathrm{A} > 0$.

$$\mathcal{O} = \begin{bmatrix}\mathbf{C}\\ \mathbf{CA}\end{bmatrix} = \begin{bmatrix}1 & 0\\ -\left(U_\mathrm{r} + U_\mathrm{A}\right) & U_\mathrm{r}\end{bmatrix} \tag{11}$$

This is the case even if the matrices $\mathbf{A}$, $\mathbf{B}$ and $\mathbf{E}$ have been found using a black box method, since the parameter in eq. system (7) can be solved for, if $\dot{Q}_\mathrm{HP}$ is known.

### *4.3 Air-to-water heat pump efficiency model*

In order to inform the supervisory controller on the efficiency of the HP a relation between electricity consumption and heat production is formulated. It is based on the formulation provided in [31], where the HP efficiency is provided by the Carnot coefficient of performance, $\mathrm{COP}_\mathrm{CARNOT} = \frac{T_\mathrm{H}}{T_\mathrm{H} - T_\mathrm{C}}$, and the efficiency of the compressor, $\eta_\mathrm{HP}$:

$$\begin{aligned}\dot{Q}_\mathrm{HP} &= \eta_\mathrm{HP}(P_\mathrm{HP})\mathrm{COP}_\mathrm{CARNOT}P_\mathrm{HP}\\ &= \mathrm{COP}_\mathrm{HP}P_\mathrm{HP}\end{aligned} \tag{12}$$

with $\mathrm{COP}_\mathrm{HP}$ being the overall efficiency for a given HP. The expression for heat as a function of electricity (direct way) is denoted as $f_{\mathrm{HP},\dot{Q}}$ and the reverse way where electricity is calculated from heat is $f_{\mathrm{HP},P}$.

#### 4.3.1 Heat as a function of electricity: $f_{HP,\dot{Q}}$

The expression chosen for the $\mathrm{COP_{HP}}$ is:

$$\mathrm{COP_{HP}} = \frac{k}{P_{\mathrm{HP}}} + \left(\frac{k_0}{P_{\mathrm{HP}}} + k_1 + k_2 P_{\mathrm{HP}}\right)\mathrm{COP_{CARNOT}} \tag{13}$$

with

$$\mathrm{COP_{CARNOT}} \equiv \frac{T_{\mathrm{F}} + 273.15\,^{\circ}\mathrm{C}}{T_{\mathrm{F}} - T_{\mathrm{a}}} \tag{14}$$

and the requirement that the coefficient $k_2$ is negative and the forward temperature is constant $\hat{T}_{\mathrm{F}}$. The reason for this choice is that the heat function $f_{\mathrm{HP}}(P_{\mathrm{HP}})$ contains a second order polynomial when the power $P_{\mathrm{HP}}$ is multiplied onto (13):

$$\dot{Q}_{\mathrm{HP}} = k + (k_0 + k_1 P_{\mathrm{HP}} + k_2 P_{\mathrm{HP}}^2)\mathrm{COP_{CARNOT}} \tag{15}$$

and taking the second order partial derivative of (15) with respect to $P_{\mathrm{HP}}$ shows that

$$\frac{\partial^2 Q_{\mathrm{FH}}}{\partial^2 P_{\mathrm{HP}}} = k_2 \mathrm{COP_{CARNOT}} < 0 \tag{16}$$

implying that if all other variables are constants then (15) is concave.

#### 4.3.2 Electricity as a function of heat: $f_{HP,P}$

The inverse formulation, seen in (17), where electricity is the dependent variable, is concave if the coefficient $k_2 > 0$.

$$P_{\mathrm{HP}} = k + (k_0 + k_1 \dot{Q}_{\mathrm{HP}} + k_2 \dot{Q}_{\mathrm{HP}}^2)\frac{1}{\mathrm{COP_{CARNOT}}} \tag{17}$$

### 4.4 Photovoltaic power forecast

The forecast model for the power output of the photovoltaic panels (PV) is based on the data from the weather forecast service Yr.no [3] and measured historical time series of the power output from the PV. In this work it is chosen to be a regression expression, although the model for the predicted PV output could in principle be any suitable non-linear model (neural network, decision tree, etc.) since the produced electricity is not dependent on any influenceable variables.

### 4.5 Price model

The hourly price models for buying and selling electricity from/to the grid is given in (18) and (19), respectively. The models are used in the supervisory controller and for evaluation. The price for buying electricity is

$$\begin{aligned} c^{+}_{\text{excl. vat}} &= c_{\mathrm{spot}} + c_{\mathrm{tariff}} + w_{\mathrm{CO_2}} c_{\mathrm{CO_2}} + c_{\mathrm{tso}} \\ c^{+}_{\mathrm{E}} &= c^{+}_{\text{excl. VAT}} + 0.25 c^{+}_{\text{excl. vat}} \end{aligned} \tag{18}$$

where the spot price, $c_{\mathrm{spot}}$, distribution tariff, $c_{\mathrm{tariff}}$, transport tariff, $c_{\mathrm{tso}}$, and are given in [€/kWh]. The self-imposed artificial $CO_2$-tax, $c_{\mathrm{CO_2}}$, is given in [€/kg]. Hence, the variable $w_{\mathrm{CO_2}}$ is the hourly estimated $CO_2$ emission in kg per kWh electricity. The Danish VAT rate is 25% of the full price and the Transport Service Operator (TSO) tariff is a fixed rate of €0.02. The selling price model is

$$c^{-}_{\mathrm{E}} = c_{\mathrm{spot}} \tag{19}$$

The distribution tariffs, $c_{\mathrm{tariff}}$, chosen for the test are based on future signaled prices for January 1st, 2023 in Denmark. The exact tariffs vary between Distribution Systems Operators (DSOs), but the pattern is low prices at night, a higher daily price with a sharp increase in the cooking peak. The chosen model is inspired by [2].

$$c_{\mathrm{tariff}} = \begin{cases} 0.027€ & t \in [00.00, 06.00) \\ 0.081€ & t \in [06.00, 17.00), [21.00, 00.00) \\ 0.26€ & t \in [17.00, 21.00) \end{cases} \tag{20}$$

It is worth noting that the tariffs need to be realistic, since the choice of values has a large impact on savings potential. If an unrealistic price of €10 is used for the evening peakinstead of €0.26, the price-aware controller shuts the HP off in this period and gains and unfair advantage over the price-unaware.

The second part of the price model regards PV produced electricity and the impact the HP has on self-consumption. In the test house the electricity is phase-metered, but the exact per phase import and export is unknown since the numbers are aggregated and stored on hourly basis. Since the data is aggregated, the meter is instead treated as a summation meter with one-hour reporting. The netting interval is unknown even though it is important for the measure of import and export, as shown in [32]. The available signals are hourly import, $E_{\mathrm{IM}}(k)$, hourly export, $E_{\mathrm{EX}}(k)$, hourly production from the PV, $E_{\mathrm{PV}}$ and consumption from HP, $E_{\mathrm{HP}}$(k). The difference between export and import, seen in (21), is the net import, $\Delta E_{\mathrm{G}}(k)$, which is the billable amount. For notational purposes the hour indicator $k$ is implied hence on.

$$\Delta E_{\mathrm{G}} = E_{\mathrm{IM}} - E_{\mathrm{EX}} \tag{21}$$

The sun power corrected cost associated with running the HP is then:

$$E^*_{\mathrm{HP}} = \begin{cases} 0 & \Delta E_{\mathrm{G}} \leq 0 \\ \min\left(E_{\mathrm{HP}}, \Delta E_{\mathrm{G}}\right) & \Delta E_{\mathrm{G}} > 0 \end{cases} \tag{22}$$

The same amount of available PV produced solar power and consumption is imposed on similar/comparable days (definition in section 4.6), which are used in the controller evaluation. The consumption of similar days is corrected using the difference in HP consumption:

$$\Delta E_{\mathrm{HP}} = E_{\mathrm{HP,cmp}} - E_{\mathrm{HP,exp}} \tag{23}$$

with $E_{\mathrm{HP,exp}}$ being the HP consumption for the experiment and $E_{\mathrm{HP,cmp}}$the similar day. The virtual net import increases when the HP consumes more in hour $k$ and vice versa, as seen in (24).

$$\Delta E^*_{\mathrm{G}}(k) = \Delta E_{\mathrm{G}} + \Delta E_{\mathrm{HP}}(k) \tag{24}$$

The corrected net import for similar/comparison days is:

$$E^*_{\mathrm{HP}} = \begin{cases} 0 & \Delta E^*_{\mathrm{G}} \leq 0 \\ \min\left(E_{\mathrm{HP,cmp}}, \Delta E^*_{\mathrm{G}}\right) & \Delta E^*_{\mathrm{G}} > 0 \end{cases} \tag{25}$$

The idea behind this mode of calculating the HP consumption is that other appliances use the self-produced electricity too, and the HP should ideally consume less than the excess capacity.

### *4.6 Evaluation procedure*

The objective of the evaluation procedure is to answer whether the new price- and forecast-aware controller saves money when compared to the existing benchmark controller described in Section 2.1. The key performance indicator is daily cost given the weather conditions. It is inherently difficult to benchmark and validate the performance of a controller operating in a complex environment with many uncontrollable external factors such as weather and occupant activities. Further, the long time-constants play a significant role by demanding long test periods. Ideally, the benchmark and MPC-controller should be run in parallel on exact copies of the same building placed at the same location, with occupants doing the same activities. Although, some buildings support such circumstances, this can obviously not be asked of the occupants. Instead, a benchmark data-set from the same house is used for the evaluation. The benchmark data-set is based on data collected from the former heating period (2021-2022) where the original benchmark controller was operating. The data is sorted into full days creating a collection of comparison days $\mathcal{D}_{\mathrm{cmp}}$, seen in (26), from which appropriate subsets can be selected. The daily generated data on set form is:

$$\mathcal{D}_{\mathrm{cmp}} = \left\{ day^n = \left(E^n_{\mathrm{G}}, T^n_{\mathrm{a}}, c^{+,n}_{\mathrm{E}}, E^n_{\mathrm{PV}}\right) \right\} \tag{26}$$

$$n = 1, \ldots, N_{\mathrm{cmp}}, \quad E^n_{\mathrm{G}}, T^n_{\mathrm{a}}, c^{+,n}_{\mathrm{E}}, E^n_{\mathrm{PV}} \in \mathbb{R}^{N_{\mathrm{day}}} \tag{27}$$

with $E^i_{\mathrm{G}}$ and $E^i_{\mathrm{PV}}$ being the electricity consumption from grid and production from PV in kWh during day $i$, respectively, $T^i_{\mathrm{a}}$ the ambient temperature, $c^{+,i}_{\mathrm{E}}$ the hourly electricity price for day $i$, and $N_{\mathrm{day}} = 24$. Note that benchmark days where the system has been manipulated or a significant amount of data is missing are dropped to minimise pollution of the results. A similar data collection, $\mathcal{D}_{\mathrm{exp}}$, is generated from the experiment period. The MPC-controller is evaluated daily by comparing the operation cost of day $i$ to a subset of benchmark days, $\mathcal{D}^i_{\mathrm{cmp}} \subset \mathcal{D}_{\mathrm{cmp}}$, drawn from the full benchmark data-set. The subset, $\mathcal{D}^i_{\mathrm{cmp}}$, is drawn according to the following rule:

$$\begin{aligned} \mathcal{D}^i_{\mathrm{cmp}} = \{ day \mid & \\ & - \Delta\overline{T}_{\mathrm{a,dn}} \leq \overline{T}_{\mathrm{a,cmp}} - \overline{T}^i_{\mathrm{a,exp}} \leq \Delta\overline{T}_{\mathrm{a,up}}, \\ & - \Delta E_{\mathrm{PV,dn}} \leq \Sigma E_{\mathrm{PV,cmp}} - \Sigma E^i_{\mathrm{PV,exp}} \leq \Delta E_{\mathrm{PV,up}}, \\ & \overline{T}_{\mathrm{a,cmp}}, \Sigma E_{\mathrm{PV,cmp}} \in day \in \mathcal{D}_{\mathrm{cmp}} \} \end{aligned} \tag{28}$$

with $\overline{T}_{\mathrm{a}}$, $\Sigma E_{\mathrm{PV}}$ being average ambient temperature and accumulated electricity production from PV, respectively. The constants $\Delta\overline{T}_{\mathrm{a,dn}}$ and $\Delta\overline{T}_{\mathrm{a,up}}$ are the down- and up-search range for ambient temperature, respectively. Similar, $\Delta E_{\mathrm{PV,dn}}$, $\Delta E_{\mathrm{PV,up}}$ makes out the search-range for accumulated electricity produced by the PV. Here the PV is used as an indicator for sun radiation. This is not a perfect indicator, since the sun altitude and intensity vary with the seasons, thereby creating a bias. However, it is found to be a good indicator for dealing with cloud conditions on-site, since it directly measures the level of shadow on the building. With ambient temperature and sun irradiation accounted for, factors such as occupant behavior and previous day heating patterns are left out. This undeniably causes noise, making the electricity consumption of the HP distribute randomly for any given day. To decrease the influence of the noise, the controller is run over a long period to obtain more consistent results.

We calculate a virtual cost for benchmark day $j$, with respect to experiment day $i$,

$$\begin{aligned} \mathrm{cost}^j_{\mathrm{cmp}} &= \sum_{k=0}^{N_{\mathrm{day}}} c^{+,i}_{\mathrm{E}}(k) E^j_{\mathrm{G}}(k) \\ & c^{+,i}_{\mathrm{E}} \in \mathrm{day}^i_{\mathrm{exp}}, \quad E^j_{\mathrm{G}} \in \mathrm{day}^j_{\mathrm{cmp}} \in \mathcal{D}^i_{\mathrm{cmp}} \end{aligned} \tag{29}$$

It simply means that electricity consumption from similar benchmark days are imposed onto the price of the experiment day to calculate the virtual cost. This provides a plausible alternate outcome for the case where the benchmark controller had been running instead. This is done since the benchmark controller is price ignorant and thereby acts independently of the price. This manoeuvre would not be possible if the comparison was

between two price-aware controllers. In that case price curves would have to be accounted for as well. The cost of the experiment day $i$, $\text{cost}^i_{\text{exp}}$, is of course calculated using the actual electricity consumption for the day.

## 5 Experiment description

The experiment was conducted over 97 days in the period 2022-11-07 to 2023-03-05. During the experiment four combinations of hourly discomfort cost, $c_{\text{cmf}} \in \mathbb{R}^{24}$, and average room temperature reference levels, $T_{\text{r,ref}} \in \mathbb{R}^{24}$, were applied, see Fig. 9. A pair consisting of a temperature reference and a discomfort cost makes out a comfort level. The cost and reference are used in the quadratic cost term $\sum_{i=0}^{23} c_{\text{cmf},i} \left(T_{\text{r},i} - T_{\text{r,ref},i}\right)$, where $i$ is the hour. Having four comfort levels is a result of gradually adjusting the overall average indoor temperature to be similar to the one from the benchmark data in order to reduce a variable with respect to the cost analysis. Consistency of indoor temperature was achieved at comfort level 4 as seen in the upper graph in Fig. 11 where the average temperature distributions are plotted. The benchmark and experiment periods are shown in Fig. 10. The benchmark dataset used for comparison consists of 193 days with daily mean ambient temperatures in the range −2.5 to 15 °C and daily PV production in the range 0 to 39 kW h. The search bound for finding similar benchmark days are 0.5 °C for ambient temperature making it 5% of the full range and 2.0 kW h for daily PV electricity production which is 10% of the full range.

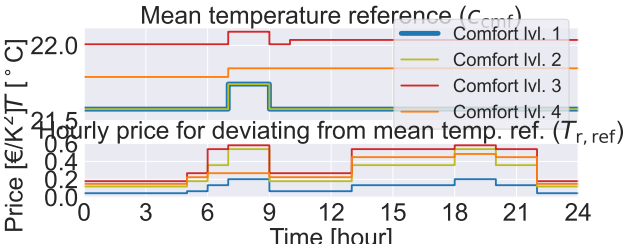


Fig. 9. Upper: Hourly mean temperature reference calculated from the collection of zone references. Lower: Hourly virtual discomfort price. Both vectors are used in equation system (2). Each comfort-cost combination has assigned a colored triangle (▲, ▲, ▲, ▲) and denoted a comfort level.

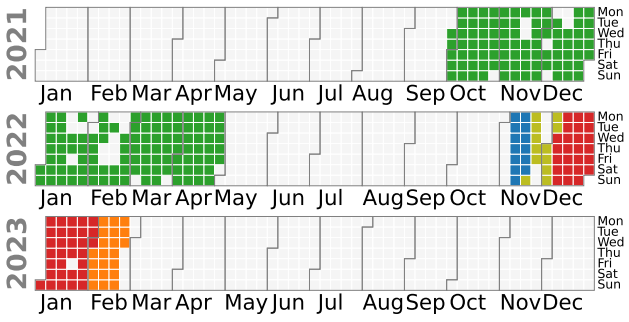


Fig. 10. Calendar overview of benchmark data and experiment periods. Green color is benchmark days and other colors are the comfort levels during the experiment.

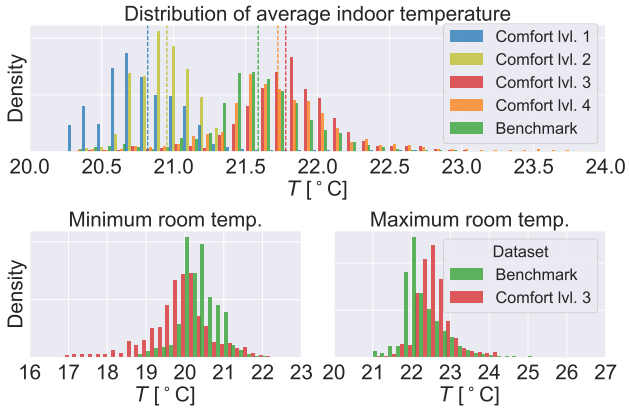


Fig. 11. Upper: Distribution of mean indoor temperature compared to the benchmark period. Lower left: Histogram of the lowest measured temperature in the rooms. Dashed line shows the mean temperature. Lower right: Highest measured temperature in the rooms.

The HP model was re-calibrated twice during the experiment. First time was after a few weeks of running MPC and second the 27th of January. The building model was changed and refitted on the 27th of January.

The optimization problems are implemented using Casadi [5] and solved with the mixed integer non-linear programming solver Bonmin [24].

## 6 Results

### 6.1 *Temperature comfort*

The temperature distributions in Fig. 11 show that the indoor temperature has not been impacted by the MPC controller providing price-led load shifting. This is particularly clear in the lower left and right plot which shows the distribution of minimum and maximum room temperatures, respectively. The min./max. room temperature are defined as $\min / \max \left(T_{\text{r},1}(t), \ldots, T_{\text{r},N_r}(t)\right)$. The lower minimum temperature is caused by one room where the reference was set to 19 °C.

Since the house was occupied throughout the test, the residents were sent a questionnaire about the experienced indoor climate on the 11th Jan. 2023. The questions and answers can be read in Appendix A.

Although each room has an assigned temperature reference, not much attention has been given to individual rooms besides responding to complaints, which was only necessary once, at comfort level 1. Two rooms,

hobby and bedroom, had reference settings at 19 and 21 °C, respectively, and the rest had 22.5 °C. The hobby room is partly detached from the rest of the house, and it was thus easy to keep the temperature low. The bedroom could not be kept at 21 °C, even though the floor heating circuit was seldom on. This shows, as pointed out by [30], that it is difficult to maintain large discrepancies between room temperatures within a NZEB.

### *6.2 Heating costs and energy consumption*

This section is dedicated to the investigation of the savings potential. The section consists of Table 2, which sums up the savings accumulated during the test periods and Fig. 13 presents costs with respect to individual days.

Table 2
Shows the accumulated economical savings estimate for space heating over the test periods.

| Comfort lvl. | Avg. compare cost [€] | Exp. cost [€] | Reduction [€] | Saving rate [%] |
|---|---|---|---|---|
| 1 (▲) | 10.92 | 7.33 | 3.59 | 32.8 |
| 2 (▲) | 49.84 | 35.34 | 14.50 | 29.1 |
| 3 (▲) | 126.42 | 123.49 | 2.93 | 2.3 |
| 4 (▲) | 43.98 | 37.68 | 6.30 | 14.3 |
| Total | 231.16 | 203.84 | 27.32 | 11.8 |

Table 2 shows a significant 11 percentage point saving on the heating bill, but looking at the absolute savings of €27.3, derived from 97 operation days, the results are more modest. Further, it can be seen that the comfort level has a significant impact on savings. Fig. 12 shows the development of the estimated saving rate for each comfort level. The large variance in daily savings means that the long-term expected saving rate has not settled after 10 days.

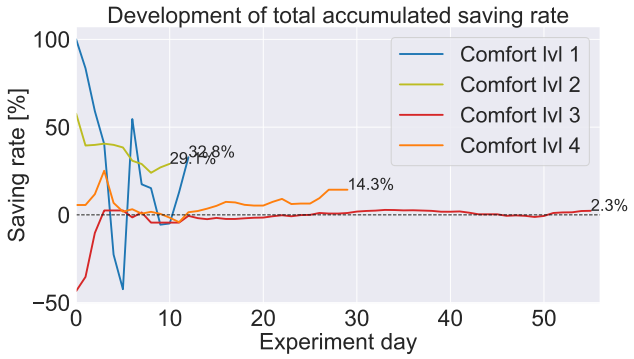


Fig. 12. Day-to-day development of the total accumulated saving rate for each comfort level.

Fig. 13 contains the cost results broken down into individual test days (One test day per column), which are analysed with respect to average ambient temperature and sun intensity. Dots are similar benchmark days derived according to description of section 4.6 and the black lines in each column represents the average cost of similar benchmark days. The results reveal three main ambient temperature regions: the warm (6 to 13 °C), the medium (0 to 6 °C) and the cold (-5 to 0 °C). In the warm region, the heating demand is so low that percentage losses or gains amounts to very small differences in savings or losses. The medium region shows the highest potential for savings. The results from cold, sunny days are difficult to assess due to a sparse amount of similar days present in the benchmark data, but the immediate results point at consistent loses. Further, it can be seen that sunny days (reddish dots and crosses) reduce costs since they drop lower than their more cloudy counterparts. This is of course related to overheating events, which might be uncomfortable. The plot also shows that the costs increase as temperature decreases.

Table 3 shows the electricity consumption. It is common that studies experience an increase in primary energy consumption when applying price responsive control (15.8% more electricity in [13], 10.3% more heat in [4]), as is the case for comfort level 1 and 4, albeit the values observed here are significantly higher. Comfort level 2 and 4 show a reduction, which is likely to be connected to the lower indoor temperature in comfort level one and a sequence of sunny days which the MPC controller could capitalize on.

Table 3
Accumulated electricity consumption from the experiment and benchmark data

| Comfort lvl. | Acc. Electricity (Exp.) [kW h] | Accumulated avg. electricity (Cmp.) [kW h] | Percentage increase [%] |
|---|---|---|---|
| 1 (▲) | 45.9 | 41.4 | 11.0 |
| 2 (▲) | 96.3 | 110.5 | -12.8 |
| 3 (▲) | 492.9 | 398.9 | 23.6 |
| 4 (▲) | 178.0 | 191.8 | -7.2 |
| Total | 813 | 743 | 9.5 |

As with electricity, the heat production (Table 4) has increased, but percentage-wise, not as much. This can be explained by the lower COP causing less heat to be produced for the electricity.

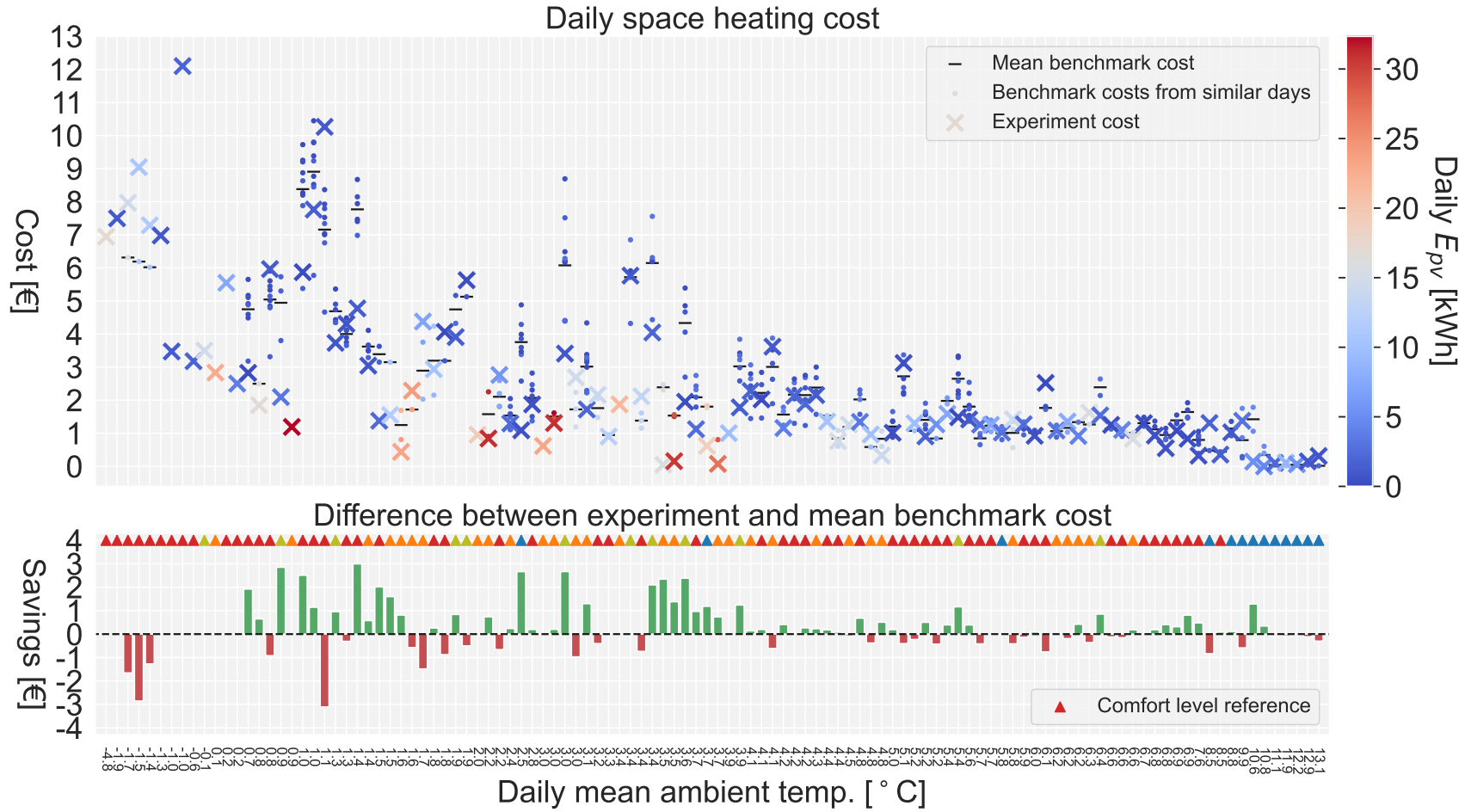


Fig. 13. Upper: Daily space heating cost during the experiment period (crosses) compared with the virtual costs, calculated based on Section 4.6, from similar days (dots). Each experiment day is assigned one column and are sorted according to daily mean temperature. The black horizontal line (-) marks the mean benchmark cost. Lower: Savings between mean benchmark cost and experiment cost. The colors of the triangles refer to the comfort level at given experiment day.

Table 4
Accumulated heat produced by the HP.

| Comfort lvl. | Acc. heat (Exp.) [kW h] | Acc. Avg. heat (Cmp.) [kW h] | Percentage Increase [%] |
|---|---|---|---|
| 1 (▲) | 218.3 | 192.6 | 13.4 |
| 2 (▲) | 385.7 | 455.1 | -15.2 |
| 3 (▲) | 1919.0 | 1667.2 | 15.1 |
| 4 (▲) | 707.5 | 799.9 | -11.5 |
| Total | 3231 | 3115 | 3.7 |

Fig. 13 gives a sense of monetary savings potential, but it hides some important factors leading to significant savings larger than €1. Fig. 14 explores these factors.

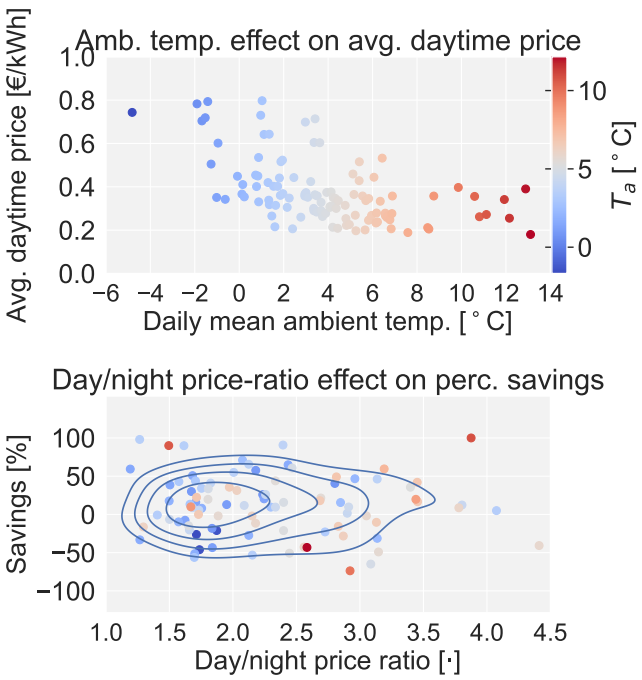


Fig. 14. Upper: Average daytime price as a function of the average temperature. Lower: Daily savings formulated in percentage as a function of the day over night price ratio. Colors indicate the daily average ambient temperature and the contours the density.

The upper figure clearly shows an inverse correlation between daily average ambient temperature and the average daytime electricity price during this heating season. This partly explains the larger savings potential between 1 and 5 °C seen in Fig. 13. The price is in the high end while the house still maintains flexibility. The next influential factor is volatility in prices which is explored in the lower graph of Fig. 14. Here the daily relative savings are plotted against the day over night average price ratio. Nighttime price is defined as the average price between 00:00 and 06:00, and daytime is given as the average over the remaining period. Although the dots are more scattered here, some important trends can be seen. First, the price ratio decreases with colder temperatures. Second, most days with a price ratio above three resulted in savings and, third, cold days gave significant loses.

### *6.3 Heat pump efficiency model*

As the HP efficiency model informs the MPC on the trade-off between heat boosting and efficiency loss, it is highly important that it is accurate. Figure 15 shows that the general COP fell when the HP was operated according to the new controller, leading to inaccurate estimates.

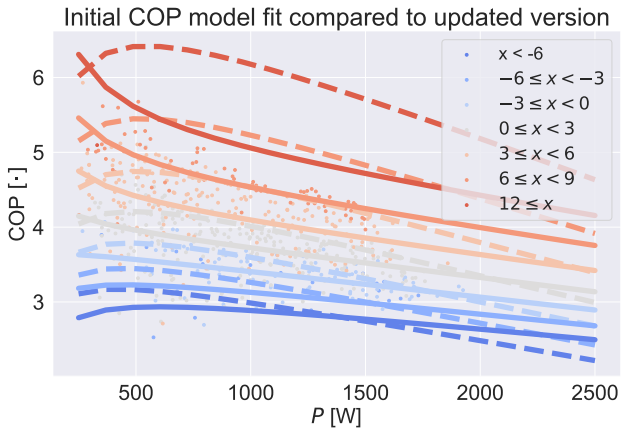


Fig. 15. The two parameter fits for the HP efficiency model during the experiment. The dashed lines describe the COP as a function of electricity consumption at varies fixed ambient temperatures. The solid lines show the updated fit, which matches the data (scatter dots), obtained during the experiment, better than the original. The coloring indicates the ambient temperature level with blue signaling cold and red warm.

The dashed lines represents the original fit, which is based on data from the benchmark controller at various fixed ambient temperatures, the scattered dots represents data points obtained in the test period and the solid lines are from an updated parameter fit. The original fit has an $R^2$ value of 0.92, but since it performed poorly during operation—often overestimating the efficiency—the fit was updated (solid lines), which resulted in lower predicted efficiencies. The main take away is that it is necessary to update the model repeatedly when the operational style changes, otherwise severe miscalculations are introduced. Fig. 16 present the results of the updated fit.

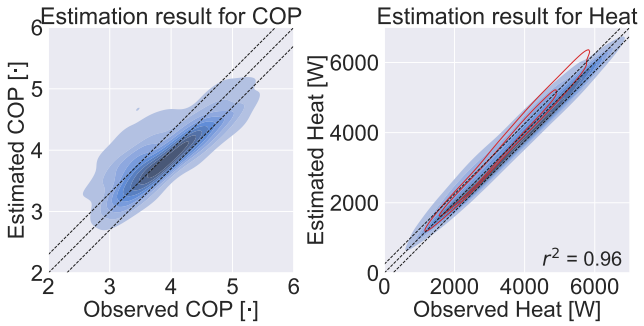


Fig. 16. The red contour lines shows the distribution of the new data calculated using the pre-experiment fit.

### *6.4 Space-heating production patterns*

In this section the daily heat production patterns are presented and compared to the benchmark data. The upper graph in Fig. 17 shows the daily heat production curves normalized with respect to part of the full day. Lower shows the actual hourly production in kWh.

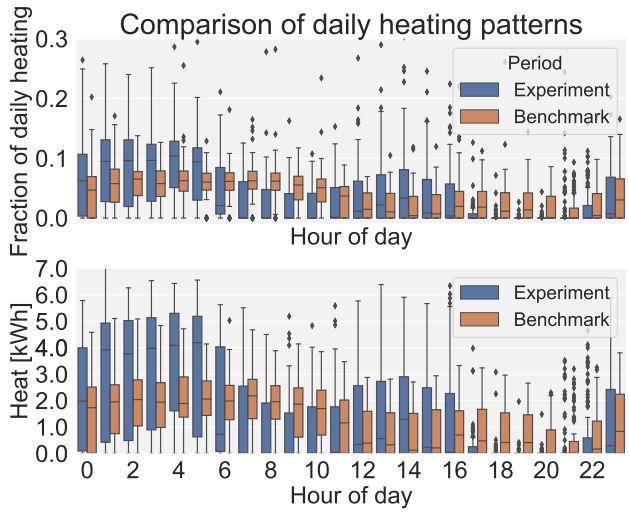


Fig. 17. Upper: Distribution of daily production patterns from the benchmark controller compared with the MPC controller. The y-axis is the hourly fraction of total production for a given day. Lower: Actual hourly heat production

The heat production has increased remarkably at night meaning that the controller bets against the classic night setback strategy despite it generally being colder at night causing the HP to be less efficient. The midday production has increased, but most notably is the complete lack of heating in the evening peak period between 17:00 and 21:00.

## 7 Interpretation of the results

In this section the authors provide their interpretation of the data and results presented in the former section. Starting with Table 2, where comfort levels 1 and 2 (▲ and ▲, respectively) show a clear percentage-vise savings potential. At comfort level 1, the indoor temperature was uncomfortably low, so this result is ignored. Test period 2 (▲) is more interesting since the residents experienced a comfortable indoor climate while saving on heating costs. This raises the question: *Did the price responsiveness cause the economical savings?* The answer is unknown since the lower average indoor temperature, and thereby lower heat demand, could have been the main reason. The main take-away from comfort level 2 is that even a NZEB can gain by lowering indoor temperature. Test period three (▲) was executed with an average indoor temperature of 0.2 °C higher than the one of the benchmark data, meaning that the 2.3% savings are likely to be contributed to the controller.

Having established that overall savings are possible under the current Danish price scheme, the next part investigates situations which are particularly favorable or unfavorable for the controller. Before reading on, keep in mind that *large savings can only originate from situations with large potential costs*. For the analysis Figs. 11, 13, 14, 15, Table 3 and 4 are used. Fig. 13 reveals that the largest share of consistent savings are generated between 0.7 and 4.0 °C. The large loss seen at 1.1 °C is the transition day between test period 2 and 3 where extra energy was needed to lift the average indoor temperature. The lower ambient temperature increases the demand for heat which increases the cost. However, as this is true for all buildings in the region not only the consumption dependent costs are driven up, so are the electricity prices. This is visible in the upper graph of Fig. 14, where the average daytime price is inversely correlated with the temperature. The result is that heat demand and price amplifies each other which increase the daily cost dramatically when the ambient temperature is below 5 °C.

Having established the factors driving up costs, we turn the attention to daily price variation which also impacts the potential for cost savings, see the lower graph in Fig. 14. Although, the results are more scattered than in the upper graph, three trends can be seen. First, the day/night price-ratio is more likely to be higher at high ambient temperatures. Second, at ratios above three, the controller is likely to save money, albeit these are mostly warm low cost days. Third, the most interesting trend is the range 0 to 5 °C, where the ratio often was above 2, securing significant percentage-vise savings.

At this point the price conditions for savings are established. Hence, we return focus to test periods 3 and 4 (▲ and ▲, respectively) and ask: *Is the potential for*

*savings larger than presented here?* The controller responded to the price signal by changing the daily heating pattern significantly, as seen in Fig. 17. Several things impact savings: model errors, forecasts errors, lack of controller robustness and more. This said, the loss of HP efficiency, mentioned in Section 6.3, stands out as a major plausible limiter. The efficiency loss originates not only from the higher loads but also due to the dynamic operations. The loss from dynamic operations puts load shifting at a disadvantage. When the supervisory controller calculates the heating plan it also considers the continuous approach featured by the benchmark controller but discards it as inefficient compared to the night heating approach. This happens because the controller relies on the HP efficiency model, which does not inform that the default controller—the one from the manufacturer—can operate the HP more efficiently. This can be used as a critique of the presently implemented heat controller, yet, it can also be posed as a question to why the manufacturers of domestic HP's do not let them be controlled according to a heat reference as an alternative to the ambient temperature heating curve.

A weakness has been noticed in the MPCs reliance on forecasts. The procedure has issues dealing with sunny days, even though the predictive nature should ensure superiority of the MPC. Fig. 13 clearly reveals that days with significant loses tend to have high sun intensity. We expect this to be due a combination of several factors which coalesce with unfortunate outcomes. The electricity prices invites the controller to boost heating between 00:00 and 06:00. If the model and forecasts were perfect the heat would be boosted accurately. However, in practice an overdose event is likely if a thick cloud cover is wrongfully predicted. The cloud cover data from the weather service has several times been unreliable even at time-of-use. This effect can be mitigated by corrections via the live PV data. Further, a robust control approach which restrains night boosting slightly should be applied.

## 8 Discussion

Having shown a savings potential through price responsive load shifting, the following topics deserve attention: the step from simulation to reality, potential performance improvements, control of the HP, heat scheduling using an average indoor temperature and minimizing operation costs rather than discomfort or indirect $CO_2$-emissions.

A large amount of papers assume perfect forecasting when conducting simulation studies of MPC with the consequence that results reflect upper performance boundaries. This is avoided in a real implementation. Nevertheless, the problem then shifts to estimating the true cost reduction or saving rate. Fig. 12 shows the extent of the challenge since the saving rate has not converged after 10-12 days. Even after 55 days this is not fully the case. The reason is the high volatility in daily savings and losses which are in the range ±€3. The implications are that short-term studies (of the order of days) are at risk of reporting saving rates which diverge severely from the true rate. If the so called "File Drawer Effect" (Failing to publish negative results) is at play, the bias might be towards too high savings potential. The strategy applied here is to rely on benchmark data collected from the prior heating season. However, even with a full season of data, there are holes in the coverage, meaning that there are experiment days without counterparts in the benchmark dataset. Ideally, the sensing equipment needs to be installed several seasons before the experimental controller is applied in order to have a reliable dataset.

The main focus areas for improved performance are HP control and modelling. The performance of the MPC was degraded by problems listed below.

- A side effect of using the compressor block function is that the HP attempts to heat the DHW using the electric heating rod, which has a power output of 10 kW. This is far from ideal, since just a few minutes in this state is costly. **Suggested solution**: block the compressor for space heating only.
- When the HP defrosts, the measured heat flow reverses. Any controller regulating the heat output needs to be able to detect and handle such a situation. **Suggested solution**: put the control in standby mode.
- It is not possible to start the heat pump on demand, the only option is to release the compressor brake and wait. The waiting time is observed to be between 60 and 120 min. **Suggested solution**: adapt the block release for best start-up timing or introduce/use open HP controller standards
- In certain situations the heat pump shuts down before it should. It is assumed that a combination of high ambient temperature and low flow caused the internal controllers to shut it down. **Suggested solution**: use data to figure out what events cause a shut down.
- A low pass filter and other unknown internal states make control through ambient temperature overwrite particularly challenging. **Suggested solution**: use a heat pump with reference control for heat.

All of these effects could have been prevented if the HP had an interface for set-point control. The path forward for commercial heat pumps should be to provide an interface for reference control which would allow the HP to operate in a near-optimal state while being part of a coordinated and cooperative control scheme.

Using an averaged room temperature in the upper control level has proven to be completely viable with respect to comfort. Controlling this way does conflict with

the idea that each room should be controlled strictly after individual references, but it is our experience that large temperature differences within the thick shell of a low energy house are difficult to obtain in any case.

Given that prices are the result of market mechanisms rather than purely physical processes, it is exceedingly difficult to forecast future prices. This controller can become more efficient if the daily price-volatility increases, on the other hand, lower prices can make the controller superfluous. This said, low prices are good for the consumer, so one might think of the controller as an insurance against long periods of high, volatile prices.

Lastly, a look at some economic aspects with respect to the current price situation and controller performance. If the heating season lasts 4 months ($\approx$ 120 days), an average cost reduction of €1 per day would translate into €1200 over a 10 year period.Although it is hard to predict, this could be a reasonable price for the controller. The MPC yielded a reduction of €0.28 per day, meaning that it would take 36 years to save €1200 under current price conditions. It has to be noted that this case involves a low energy house, and this calculation is not meant to be extrapolated to less energy efficient houses.

The analysis of the savings potential for the MPC controller would be incomplete if the effect of the relatively large evening peak price is ignored. The daily recurrence of the evening peak tariff begs the question: *What is the saving rate from simply blocking the HP in the evening peak period?* Using the method from section 4.6, the benchmark controller has used an extra 60.0 kW h electricity in the timespan 17:00-21:00 translating to an extra cost of €34.9 over the test period compared to the MPC approach. Postponing the electricity consumption to the hours following the evening peak would cost €16.1, based on the average price between 21:00 and 01:00, resulting in an overall reduction of €18.8. This is 69% of the estimated savings provided by the MPC. Two things have to be noted, the peak block saving assumes a COP of 4.2, which can only be achieved at moderate heating loads, and the cost reduction of the experiment is calculated based on all comfort levels.

## 9 Conclusion

During this study an implementation oriented, price-responsive MPC controller has been tested on a commercial HP, over the course of four months in the winter 2022-2023. The results show that load shifting can reduce heating costs by at least 2.3%, only by activating the heat capacity of the building structure and without reducing the indoor temperature. The production patterns have been shifted to support the grid through increased consumption at night and by shutting the HP down in the evening peak. Further, it has been established that under the current danish price scheme the evening peak is the decisive cost factor, and about 69% of the savings provided by the MPC can be obtained just by blocking the HP in the evening peak. Full or partial shutdown in the evening peakshould immediately be broadly implemented. This rule creates correlated consumption patterns, which might become problematic for the grid later. In case the grid operators wish to use more coordinated approach controllers of the type presented here are needed, but, at the moment the cost reduction obtained from price responsiveness cannot cover the costs of acquiring such capabilities, so more financial incentive needs to be provided.

The ambient temperature overwrite applied to control the heat flow of the HP has proven to be a functional but inefficient way to make the it smart grid-ready. A dedicated input for reference control as a standard is to be desired if advanced control of HPs should be the norm.

Several publications have suggested that the upper layer, in a hierarchical control structure can be controlled using a building model having only one heating zone without degrading indoor comfort. We can report that the results presented here support this idea. Although, it has to be mentioned that the highly insulated shell of the house might me a large contributor.

Future work is to automate the process of gathering quality data from the sensors and apply an update the models for building, HP and PV regularly. The next natural step for the MPC is to upgrade the HP retrofit to include control of domestic hot water production which, at this moment, is a randomly occurring process, often taking place in the evening peak.

## Credit author statement

**Simon Thorsteinsson:** Conceptualization, Methodology, Software, Formal analysis, Investigation, Data Curation, Writing - Original Draft, Visualization **Alex Kalaee:** Conceptualization, Writing - Review & Editing **Pierre Vogler-Finck:** Conceptualization, Writing - Review & Editing **Henrik Stærmose:** Resources, Conceptualization, Writing - Review & Editing, Funding acquisition **Ivan Katic:** Conceptualization, Writing - Review & Editing, Project administration, Funding acquisition **Jan Bendtsen:** Conceptualization, Resources, Writing - Review & Editing, Supervision, Funding acquisition.

## Declaration of Competing Interest

The authors have no competing interests to declare.

**Acknowledgements**

The authors would like to express their sincere gratitude to the family for risking money and comfort by letting us carry out this experiment on their house. This work is funded the Danish Energy Agency through the EUDP project OPSYS 2.0 (Case num.: 64018-0581).

**References**

[1] BR18. URL https://bygningsreglementet.dk/Historisk/BR18_Version1/Ovrige-bestemmelser/25/Krav/473_484.

[2] Prisændringer. URL https://cerius.dk/priser-og-tariffer/prisaendringer/.

[3] YR.no weather API, 2022. URL https://api.met.no/weatherapi/locationforecast/2.0/documentation.

[4] V. Amato, M. D. Knudsen, and S. Petersen. Dual-zone economic model predictive control of residential space heating for demand response using a single heat meter. *Energy and Buildings*, 281:112759, February 2023. ISSN 0378-7788. doi: 10.1016/j.enbuild.2022.112759. URL https://www.sciencedirect.com/science/article/pii/S0378778822009306.

[5] Joel A E Andersson, Joris Gillis, Greg Horn, James B Rawlings, and Moritz Diehl. CasADi – A software framework for nonlinear optimization and optimal control. *Mathematical Programming Computation*, 11(1):1–36, 2019. doi: 10.1007/s12532-018-0139-4.

[6] Steffen Bechtel, Sasan Rafii-Tabrizi, Frank Scholzen, Jean-Régis Hadji-Minaglou, and Stefan Maas. Influence of thermal energy storage and heat pump parametrization for demand-side-management in a nearly-zero-energy-building using model predictive control. *Energy and Buildings*, 226:110364, November 2020. ISSN 0378-7788. doi: 10.1016/j.enbuild.2020.110364. URL https://www.sciencedirect.com/science/article/pii/S0378778820313086.

[7] Alberto Bemporad and Manfred Morari. Control of systems integrating logic, dynamics, and constraints. *Automatica*, 35(3):407–427, March 1999. ISSN 0005-1098. doi: 10.1016/S0005-1098(98)00178-2. URL https://www.sciencedirect.com/science/article/pii/S0005109898001782.

[8] Danish Energy Agency. Data, tabeller, statistikker og kort Energistatistik 2019. Technical report, Danish Energy Agency. URL https://ens.dk/sites/ens.dk/files/Statistik/energistatistik2019_dk-webtilg.pdf. ISSN: 0906-4699 year: 2019.

[9] Danish Utility Regulator. DANSK ENERGIS TARIFERINGSMODEL 3.0. Decision, Forsyningstilsynet. URL https://forsyningstilsynet.dk/media/10807/tilkendegivelse-tarifmodel-3-0.pdf.

[10] Roel De Coninck and Lieve Helsen. Practical implementation and evaluation of model predictive control for an office building in Brussels. *Energy and Buildings*, 111:290–298, January 2016. ISSN 0378-7788. doi: 10.1016/j.enbuild.2015.11.014. URL https://www.sciencedirect.com/science/article/pii/S0378778815303790.

[11] Ján Drgoňa, Javier Arroyo, Iago Cupeiro Figueroa, David Blum, Krzysztof Arendt, Donghun Kim, Enric Perarnau Ollé, Juraj Oravec, Michael Wetter, Draguna L. Vrabie, and Lieve Helsen. All you need to know about model predictive control for buildings. *Annual Reviews in Control*, 50:190–232, January 2020. ISSN 1367-5788. doi: 10.1016/j.arcontrol.2020.09.001. URL https://www.sciencedirect.com/science/article/pii/S1367578820300584.

[12] Trent Hilliard, Lukas Swan, and Zheng Qin. Experimental implementation of whole building MPC with zone based thermal comfort adjustments. *Building and Environment*, 125:326–338, November 2017. ISSN 0360-1323. doi: 10.1016/j.buildenv.2017.09.003. URL https://www.sciencedirect.com/science/article/pii/S0360132317304110.

[13] Maomao Hu, Fu Xiao, John Bagterp Jørgensen, and Rongling Li. Price-responsive model predictive control of floor heating systems for demand response using building thermal mass. *Applied Thermal Engineering*, 153:316–329, May 2019. ISSN 1359-4311. doi: 10.1016/j.applthermaleng.2019.02.107. URL http://www.sciencedirect.com/science/article/pii/S1359431118361921.

[14] Nicolas J. Kelly, Paul G. Tuohy, and Adam D. Hawkes. Performance assessment of tariff-based air source heat pump load shifting in a UK detached dwelling featuring phase change-enhanced buffering. *Applied Thermal Engineering*, 71(2):809–820, October 2014. ISSN 1359-4311. doi: 10.1016/j.applthermaleng.2013.12.019. URL https://www.sciencedirect.com/science/article/pii/S135943111300896X.

[15] M. Killian, M. Zauner, and M. Kozek. Comprehensive smart home energy management system using mixed-integer quadratic-programming. *Applied Energy*, 222:662–672, July 2018. ISSN 0306-2619. doi: 10.1016/j.apenergy.2018.03.179. URL https://www.sciencedirect.com/science/article/pii/S0306261918305282.

[16] Sebastian Kuboth, Florian Heberle, Andreas König-Haagen, and Dieter Brüggemann. Economic model predictive control of combined thermal and electric residential building energy systems. *Applied Energy*, 240:372–385, April 2019. ISSN 0306-2619. doi: 10.1016/j.apenergy.2019.01.097. URL http://www.sciencedirect.com/science/article/pii/S0306261919300996.

[17] Zachary Lee, Kartikay Gupta, Kevin J. Kircher,

and K. Max Zhang. Mixed-integer model predictive control of variable-speed heat pumps. *Energy and Buildings*, 198:75–83, September 2019. ISSN 0378-7788. doi: 10.1016/j.enbuild.2019.05.060. URL https://www.sciencedirect.com/science/article/pii/S0378778819302609.

[18] Yannik Löhr and Martin Mönnigmann. MPC for heating systems with minimum up-and down-time requirements. *IFAC-PapersOnLine*, 54(6):206–211, January 2021. ISSN 2405-8963. doi: 10.1016/j.ifacol.2021.08.546. URL https://www.sciencedirect.com/science/article/pii/S2405896321013215.

[19] Laura Maier, Marius Schönegge, Sarah Henn, Dominik Hering, and Dirk Müller. Assessing mixed-integer-based heat pump modeling approaches for model predictive control applications in buildings. *Applied Energy*, 326:119894, November 2022. ISSN 0306-2619. doi: 10.1016/j.apenergy.2022.119894. URL https://www.sciencedirect.com/science/article/pii/S0306261922011576.

[20] Barbara Mayer, Michaela Killian, and Martin Kozek. Management of hybrid energy supply systems in buildings using mixed-integer model predictive control. *Energy Conversion and Management*, 98:470–483, July 2015. ISSN 0196-8904. doi: 10.1016/j.enconman.2015.02.076. URL https://www.sciencedirect.com/science/article/pii/S0196890415001971.

[21] F. L. Müller and B. Jansen. Large-scale demonstration of precise demand response provided by residential heat pumps. *Applied Energy*, 239:836–845, April 2019. ISSN 0306-2619. doi: 10.1016/j.apenergy.2019.01.202. URL https://www.sciencedirect.com/science/article/pii/S0306261919302156.

[22] Alessandra Parisio, Evangelos Rikos, and Luigi Glielmo. A Model Predictive Control Approach to Microgrid Operation Optimization. *IEEE Transactions on Control Systems Technology*, 22(5):1813–1827, September 2014. ISSN 1063-6536, 1558-0865. doi: 10.1109/TCST.2013.2295737. URL http://ieeexplore.ieee.org/document/6705582/.

[23] T.S. Pedersen, P. Andersen, and K. M. Nielsen. Central control of heat pumps for smart grid purposes tested on single family houses. In *2013 10th IEEE INTERNATIONAL CONFERENCE ON NETWORKING, SENSING AND CONTROL (ICNSC)*, pages 118–123, April 2013. doi: 10.1109/ICNSC.2013.6548722.

[24] Pietro Belotti, Pierre Bonami, John J. Forrest, Lazlo Ladanyi, Carl Laird, Jon Lee, Francois Margot, and Andreas Waechter. Bonmin. URL https://www.coin-or.org/Bonmin/.

[25] P.R. Shukla, J. Skea, R. Slade, A. Al Khourdajie, R. van Diemen, D. McCollum,, M. Pathak, S. Some, P. Vyas, R. Fradera, M. Belkacemi, A. Hasija, G. Lisboa, S. Luz, J. Malley, and (eds.). Summary for Policymakers. In: Climate Change 2022: Mitigation of Climate Change. Contribution of Working Group III to the Sixth Assessment Report of the Intergovernmental Panel on Climate Change. *Cambridge University Press, Cambridge, UK and New York, NY, USA*. doi: 10.1017/9781009157926.001.

[26] Statistics Denmark. Boligbestanden, 2021. URL https://www.dst.dk/da/Statistik/emner/borgere/boligforhold/boligbestanden.

[27] David Sturzenegger, Dimitrios Gyalistras, Manfred Morari, and Roy S. Smith. Model Predictive Climate Control of a Swiss Office Building: Implementation, Results, and Cost–Benefit Analysis. *IEEE Transactions on Control Systems Technology*, 24 (1):1–12, January 2016. ISSN 1558-0865. doi: 10.1109/TCST.2015.2415411. Conference Name: IEEE Transactions on Control Systems Technology.

[28] José Sánchez Ramos, Mcarmen Pavón Moreno, Mcarmen Guerrero Delgado, Servando Álvarez Domínguez, and Luisa F. Cabeza. Potential of energy flexible buildings: Evaluation of DSM strategies using building thermal mass. *Energy and Buildings*, 203:109442, November 2019. ISSN 0378-7788. doi: 10.1016/j.enbuild.2019.109442. URL https://www.sciencedirect.com/science/article/pii/S0378778819317852.

[29] Thomas Novak. European heat pump market. *The REHVA European HVAC Journal*, 58(4):40–43, August 2021. URL https://www.rehva.eu/rehva-journal/chapter/european-heat-pump-market.

[30] Pierre J. C. Vogler-Finck, John Clauß, Laurent Georges, Igor Sartori, and Rafael Wisniewski. Inverse Model Identification of the Thermal Dynamics of a Norwegian Zero Emission House. In Dennis Johansson, Hans Bagge, and Åsa Wahlström, editors, *Cold Climate HVAC 2018*, Springer Proceedings in Energy, pages 533–543, Cham, 2019. Springer International Publishing. ISBN 978-3-030-00662-4. doi: 10.1007/978-3-030-00662-4_44.

[31] Roger Wilfried Wimmer. *Regelung einer Wärmepumpenanlage mit Model Predictive Control*. Doctoral Thesis, ETH Zurich, 2004. URL https://www.research-collection.ethz.ch/handle/20.500.11850/148463. Accepted: 2017-06-13T04:49:59Z ISBN: 9783906483061.

[32] Charalampos Ziras, Lisa Calearo, and Mattia Marinelli. The effect of net metering methods on prosumer energy settlements. *Sustainable Energy, Grids and Networks*, 27:100519, September 2021. ISSN 2352-4677. doi: 10.1016/j.segan.2021.100519. URL https://www.sciencedirect.com/science/article/pii/S2352467721000904.

## A Resident statements

The 11$^{th}$ Jan. 2023, the residents were sent a questionnaire about the experienced indoor climate comfort. Before reading the questionnaire, note that it was not

conducted anonymously and the text is translated from Danish. The questions and answers are as follows.

(1) *Have you experienced an increase in discomfort with respect to indoor climate when you compare with last heating season?*
**Answer:** I actually think that we have felt a better comfort than I remember from last year. There was an experience of discomfort in the beginning of the experiment, which we talked about, thereafter it has been quite comfortable.

(2) *When you have experienced discomfort, has it been too warm, too cold or do you experience both too warm and too cold periods?*
**Answer:** No, we don't have any periods with unpleasantly low temperatures. We have as always lower temperatures in the cinema/hobby-room, but that has been fine.

(3) *Is there any time of day where the discomfort most often occurs?*
**Answer:** No comment

(4) What have you noticed with respect to floor temperatures?
**Answer:** It has actually been pleasantly warm, and I don't think that we have experienced cold floors, which we typically experience at middle-high outdoor temperatures.

(5) Have you experienced that the radiation from the floors has been too high?
**Answer:** No

(6) Have you experienced that the radiation was too low? A feeling of being cold even though the room temperature was high.
**Answer:** No, as said, we have not experienced that for long.

# B Model fits

## *B.1 Heat pump efficiency model*

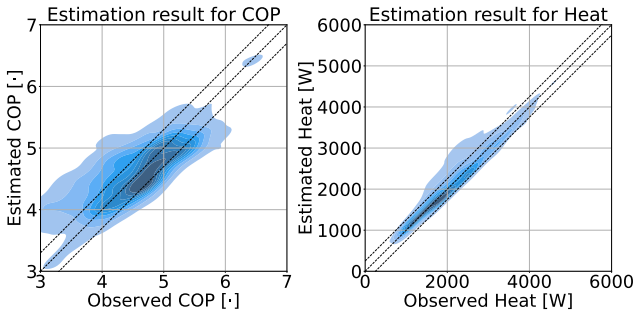


Fig. B.1. A diagram of the heat pump combined with the floor heating system.

Table B.1
Fitted parameters for heat pump efficiency model.

| date | $k_0$ | $c_0$ | $c_1$ | $c_2$ | $\bar{T}_F$ |
|---|---|---|---|---|---|
| 2022-11-05 | 125.256 | -25.348 | 414.026 | -62.854 | 26.63 |
| 2022-11-24 | -9288.9 | 2363.53 | 1325.13 | -210.53 | 50.00 |
| 2022-12-01 | -1880.2 | 273.2 | 694.6 | -101.28 | 50.00 |
| 2023-01-27 | -793.31 | 105.79 | 509.07 | -46.854 | 41.00 |

## *B.2 House model*

This section shows the first and last parameter fit for the house model described in Section 4.1.

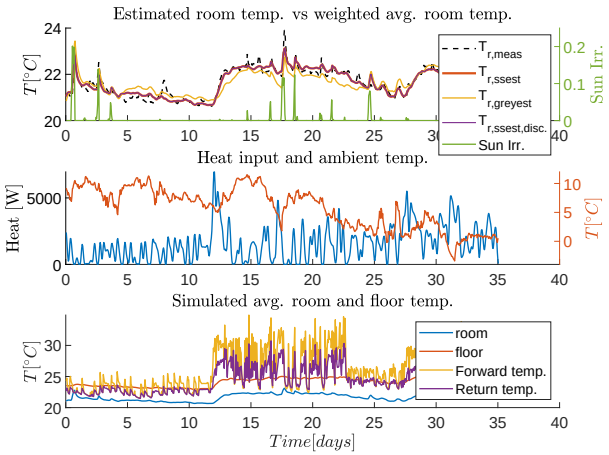


Fig. B.2. Fitted 2022-02-05 to the 35 prior days of data.

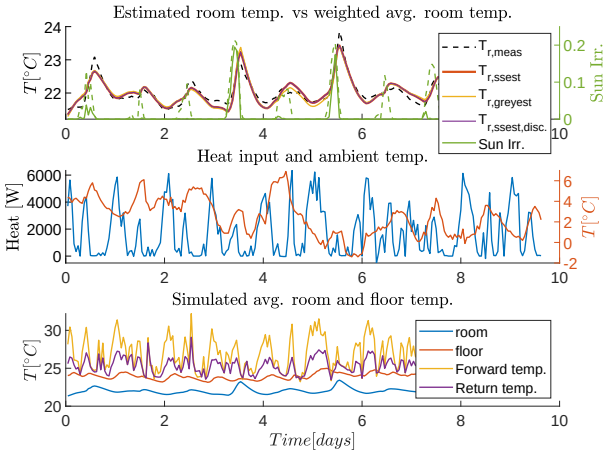


Fig. B.3. Fitted 2023-02-09 to the 10 prior days of data.

# Model predictive control of heat pump based on a regression model fitted to data measured in accordance to EHPA regulation

*Simon* Thorsteinsson[1*], *Søren Østergaard* Jensen[2] and *Jan Dimon* Bendtsen[1]

[1]Aalborg University, Department for Automation and Control, 9220 Aalborg Øst, Denmark
[2]Danish Energy Agency, Centre for Global Cooperation, 1577 Copenhagen, Denmark

**Abstract.** This paper presents a method for fitting a static regression model for the power consumption of a ground-sourced domestic heat pump, based on a low number of sample points extracted from a common measurement report developed in accordance to European Heat Pump Association (EHPA) regulation. Thereafter, we demonstrate how the coefficients can be updated with a *Recursive Least Squares* algorithm using only commonly accessible measurements. The regression model is designed to be used for control of a heat pump connected to an ON/OFF controlled floor heating system. The target of the method is especially systems where the flow in the floor heating circuits is unknown. The ability of the regression model to predict power consumption of the heat pump is evaluated using measurements obtained from a test-rig having the particular heat pump installed. The regression model is implemented as a module in a *Mixed Integer Non-linear Model Predictive Control* algorithm to illustrate the applicability of the model for control purposes. The promising results obtained from this investigation raise the question; should quality data be available in order to enable more advanced control of domestic heat pumps?

## 1 Introduction

The later years have seen a large increase in electric heat pumps becoming the main source of heat in single-family houses [1]. This electrification of the heat source creates an interesting bridge between space heating and electricity consumption. A connection, which is particularly interesting, if more energy assets (solar panels, energy storages, domestic wind turbines, etc.) are connected to the same system. Such energy assets are not independent, in the sense that the operational mode of one affect the others and vice versa.

In that light, there is a wish for harvesting the full potential of energy optimization for the combined system by coordinating these energy assets instead of letting them operate according to own objectives. Further, other external factors can be taken into account such as weather, resident behaviour, energy prices.

To optimize the operation with respect to energy savings, the controller must have knowledge about the system and environment and continuously collect measurements during operation in order to make optimal decisions regarding when, where and how much to heat.

Among other methods, such as *Neural Networks* (NN), *Machine Learning* (ML) and other *Artificial Intelligence* methods, *Model Predictive Control* (MPC) has been shown to be a solution to such a control problem. In [2] linear, linear time-varying and non-linear MPC are applied to control an air-to-water heat pump connected to radiant floor heating. The performance of the heat pump is modelled using a time dependent function. The authors in [3] controlled a solar assisted heat pump using MPC with the heat pump efficiency modelled using a piece-wise linear function.

In this work we focus on the model of a domestic ground-sourced heat pump as a component in an MPC control scheme. More specifically, the model is a static regression expression with linear coefficients. The method presented here is developed with three goals in mind. The inputs to the model are restricted to be control inputs and cheap to measure state variables. Second, only readily available data can be used for fitting the coefficients. Last, it is a requirement that the model takes part as module in a functioning MPC algorithm.

The reason for the restrictions on data and measurements is that MPC, as well as the other mentioned methods, in general suffers from high commissioning costs. It easily gets very expensive to either develop a model, which MPC relies on, or collect the necessary data for methods like ML and NN. Without extensive amounts of data ML and NN cannot identify the important connections between cause and effect in the system.

Until a solution is found most existing systems in single-family houses will likely either be regulated by ON/OFF- or PID-controllers.

We therefore ask whether it is possible to develop models and methods, which are cheap to obtain and perform acceptable.

To elaborate on the meaning of readily available data. It is common practice, for the manufacturer, to commission a measurement of the coefficient of

* Corresponding author: sith@es.aau.dk

performance (COP), seasonal coefficient of performance (SCOP) and other parameters according to the standards **DIN EN 14511** (COP) [4], **DIN EN 14825** (SCOP) [5], **DIN EN 16147** (Domestic hot water heat pumps) [6]. The data generated during these tests exists for most heat pumps, which means it holds the potential of becoming the foundation for a generalized method for obtaining the model fit.

The concept of fitting regression models to such standard measurements is not new, in [7] the authors, in similar fashion, fit regression models to catalogue data, provided by the manufactures, with a high degree of accuracy. In [8] different linear, non-linear regression and artificial neural networks models are compared. However, unlike the previous works, we aim specifically at using the model in MPC schemes.

The layout of the rest of the paper is; first, we describe the fit of the regression model. Thereafter, a *Recursive Least Squares* (RLS) algorithm is applied to update the coefficients using the measured input power of the heat pump.

To validate the heat pump model, we investigate the accuracy of the fit when compared to data obtained from a test-rig and implement the model into a *Mixed-Integer Non-linear* MPC example to prove that the model can be part of a solvable optimization problem.

In the end, we elaborate on the findings and potential issues. Further, we discuss the potential value of these measurement reports, being made according to requirements established by the European Heat Pump Association (EHPA), with respect to control, and ask whether such reports should be mandatory and publicly available.

## 2 Materials and Methods

In this section the system is presented, followed by the method for fitting and recursively updating the linear coefficients for the static regression model. At last the *Mixed Integer Non-linear Programming* (MINLP) *Model Predictive Control* (MPC) example is described.

### 2.1 Introduction to system

The system considered in this paper, seen in Figure 1, reflects a common installation found in many houses.

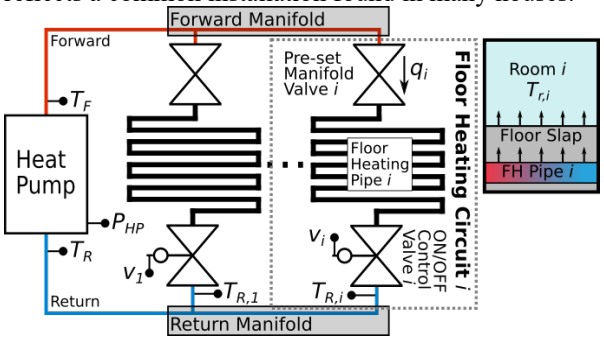


**Figure 1.** Overview diagram of system in scope [9].

The setup is a ground-sourced heat pump, which feeds $M$ floor heating circuits with hot water. Each floor heating circuit provides heat to its own separate room. The flow of each floor heating circuit is balanced using a pre-set manifold valve and is controlled by an ON/OFF control valve. The control valves in a floor heating manifold are often wax-motor driven, which means there is a delay between the control signal and the reaction of the valve. In this work, we assume the reaction to be instantaneous. Table 1 shows signals and measurements that are available during operation.

**Table 1.** The available measurements and signals.

| Symbol | Type | Description |
|---|---|---|
| $P_{HP}$ | Sensor | Electric power input to HP |
| $T_R$ | Sensor | Return temperature to HP |
| $T_{R,i}$ | Sensor | Return Temperature $i$ |
| $T_{r,i}$ | Sensor | Room Temperature $i$ |
| $T_F$ | Ctrl. signal | Forward Temp. from HP |
| $v_i$ | Ctrl. signal | Set-point of control valve $i$ |

The measurements have been limited to temperature and electric power, since they are measureable at low costs compared to e.g. measuring flow. There are $M+1$ control signals; the forward temperature from the heat pump $T_F$ and one valve state $v_i \in \{0,1\}$ for each of the $M$ circuits. The valve state 0 corresponds to *OFF* and 1 to *ON*. Note that the forward temperature is common for all open circuits, which means it is necessary to choose a forward temperature, which fits all open circuits.

### 2.2 Data

This study is based upon two main datasets, which are presented in the following two subsections. All data is freely available for download at [10].

#### *2.2.1 Standard test data*

The smaller dataset consist of 18 sample points extracted from the report containing the measurements obtained according to the standards EN14500, EN14825, EN16147. This data is from henceforward referred as the *standard test data*.

**Table 2.** Overview of *standard test data.*

| Symbol | Description | Unit |
|---|---|---|
| $Q_{HP}$ | Heat produced by HP | [W] |
| $P_{HP}$ | Electric power consumed by HP | [W] |
| $q$ | Mass flow | [kg/s] |
| $T_R$ | Return temperature to the HP | [˚C] |
| $T_F$ | Forward temperature from HP | [˚C] |
| $COP$ | Coefficient of performance | [·] |

#### *2.2.2 Test-rig data*

The larger dataset consist of time series data sampled each minute over a time period of 24 days. The data is obtained from a test rig where the heat pump delivers heat to a simulated house with four floor heating circuits. The simulation calculates the response of the house based on the forward temperature and water flow.

A cooling system cools the return water from each circuit to emulate the transfer of heat to the floor. This dataset is divided into two parts. The first part covers 10 days and plays the role as data measured during operation, and the second is used for validation. This is referred to as *fit test-rig data* and *validation test-rig data*. More information about the test-rig can be found at [11]. The *test-rig data* is freely available at [10].

**Table 3.** Overview of *test-rig data*

| Symbol | Description | Unit |
|---|---|---|
| $Q_{HP}$ | Heat produced by HP | [W] |
| $P_{HP}$ | Electric power consumed by HP | [W] |
| $q$ | Mass flow | [kg/s] |
| $T_R$ | Return temperature to the HP | [˚C] |
| $T_F$ | Forward temperature from HP | [˚C] |

## 2.3 Static Regression Model for estimation of power input to the heat pump

In this section, the method for obtaining the regression model for the estimated consumed electric power $\hat{P}_{HP}$ of the heat pump is described. The method consists of three main steps, a) use the *standard test data* to initially fit coefficients, b) replace the flow $q$ with an estimate based on the valve input vector $v$, and c) update the coefficients online using *Recursive Least Squares*.

### *2.3.1 Initial fit using standard test data*

To obtain an estimate for the heat pumps consumed electric power $\hat{P}_{HP}$, we formulate a multivariate quadratic polynomial

$$P_{HP} = c_0 + c_1 T_F + c_2 T_R + c_3 q + c_4 T_F^2 + c_5 T_R^2 + c_6 q^2 \quad (1)$$

Which takes the forward temperature $T_F$, return temperature $T_R$ and mass flow $q$ as inputs. Using the data described in Section 2.2.1 a system of linear equations are formulated in matrix form seen in (2).

$$\boldsymbol{P}_{HP} = \boldsymbol{A}\boldsymbol{c} \quad (2)$$

with $\boldsymbol{a}_i = [T_{F,i} \quad T_{R,i} \quad q_i \quad T_{F,i}^2 \quad T_{R,i}^2 \quad q_i^2]$ being the $i^{th}$ row in $\boldsymbol{A}$ and $\boldsymbol{c} = [c_0 \quad \cdots \quad c_6]^{\mathrm{T}}$ being the coefficients of (1) to solve for. This system of linear equations are overdetermined, so no exact solution exists. Instead, the coefficients in **c** are found by solving the *Least Squares* problem

$$\min_{c \in \mathbb{R}^6} \left\| \hat{\boldsymbol{P}}_{HP} - \boldsymbol{P}_{HP} \right\|_2 \quad (3)$$

having solution

$$\boldsymbol{c} = \boldsymbol{A}^{\dagger}\boldsymbol{P}_{HP} = (\boldsymbol{A}^{\mathrm{T}}\boldsymbol{A})^{-1}\boldsymbol{A}^{\mathrm{T}}\boldsymbol{P}_{HP} \quad (4)$$

with $\boldsymbol{A}^{\dagger}$ being the pseudo inverse of $\boldsymbol{A}$. The choice of variables is guided by two objectives. The first being physical relevance and the second is all but one are considered easy to measure. In this case we assume $T_F$, $T_R$ and $P_{HP}$ to be directly measured during operation leaving only the flow $q$ unmeasured.

### *2.3.2 Fitting valve input to estimated flow*

Since the flow is not measured it is replaced by an estimate based on the set of valve control signals defined as $v \in \{0,1\}^M$ where $M$ is the number of floor heating circuits. To obtain the estimate for the flow, $q$ is isolated in Eq. (1) as seen in Eq. (5).

$$\begin{aligned} \hat{q}_+ &= f_+(T_F, T_R, P_{HP}) \\ &= \frac{-b_{so} + \sqrt{b_{so}^2 - 4a_{so}c_{so}}}{2a} \\ \hat{q}_- &= f_-(T_F, T_R, P_{HP}) \\ &= \frac{-b_{so} - \sqrt{b_{so}^2 - 4a_{so}c_{so}}}{2a} \\ c_{so} &= c_0 - P_{HP} + c_1 T_F + c_2 T_R + c_4 T_F^2 + c_5 T_R^2 \\ b_{so} &= c_3 \\ a_{so} &= c_6 \end{aligned} \quad (5)$$

Solving the second order equation in Eq. (1) provides two solutions, so a choice has to be made whether to choose $\hat{q}_+$ or $\hat{q}_-$ for the estimate. The main criteria is that the values of $\hat{q}$ are positive, since a negative flow does not make physical sense in this context. If $c_3, c_6 > 0$, then the choice is always $\hat{q}_+$. This can be obtained by formulating Eq. (3) as a constrained optimization problem, with $c_3, c_6 \geq 0$. This is a linear programming problem, which most solvers can handle.

Since the flow largely is decided by the combination of open valves, a linear regression expression, seen in Eq. (6), is used.

$$\hat{q}_v = f_v(v) = k_1 v_1 + \cdots + k_M v_M = \boldsymbol{k}^T \boldsymbol{v} \quad (6)$$

This means that $\hat{q}_v$ can be interpreted as a sum of nominal estimates with $\hat{q}_{v,i} = k_i v_i$ being an estimate for the flow $q_i$. Again the coefficients in $\boldsymbol{k} = [k_1 \quad \ldots \quad k_M]^{\mathrm{T}}$ are found by minimizing the squared error between $\hat{q}_v$ and $\hat{q}$ using Eq. (3). The data needed to fit the coefficients in $\boldsymbol{k}$, is measured during operation. The expression for $\hat{q}_v$ in (6) is then inserted into Eq. (1) giving

$$\begin{aligned} \hat{P}_{HP} = f_{HP}(T_F, T_R, \boldsymbol{v}) &= c_0 + c_1 T_F + c_2 T_R \\ &+ c_3(\boldsymbol{k}^T \boldsymbol{v}) + c_4 T_F^2 + c_5 T_R^2 \\ &+ c_6(\boldsymbol{k}^T \boldsymbol{v})^2 \end{aligned} \quad (7)$$

The function $f_{HP}$ is now only a function of measured variables and inputs. Structural-wise the expression is in principle ready for use in a predictive control scheme applied to the system described in Section 2.1.

### *2.3.3 Recursive least squares update of linear coefficients*

Since $P_{HP}$ is measured during operation, it is possible to update the linear coefficients in $\boldsymbol{c}$, from Eq. (4), recursively as new data comes in. The algorithm applied here is a common *Recursive Least Squares* (RLS), which can be found in standard literature, for further reading [12] and [13]. The RLS algorithm is shown in (8)-(13). To initiate the RLS algorithm a set of initial coefficients $\hat{\boldsymbol{a}}_0$ and the constant $\delta$ must be chosen. As seen in (9), the coefficients from $\boldsymbol{c}$ is used. The constant

$\delta$ is a tweaking parameter, which if chosen low ($10^{-5}$) only changes the coefficients of $\hat{\boldsymbol{a}}^{(k)}$ slightly, and if chosen larger the coefficients might wander far from the initial values. In case all circuits are closed, the heat pump is turned off and the step of updating the coefficients is skipped.

$$\boldsymbol{P}_0 = \delta \mathbf{I},\ \boldsymbol{P}^{(k)} \in \mathbb{R}^{M\times M} \tag{8}$$

$$\hat{\boldsymbol{a}}_0 = [c_0\ \dots\ c_7]^{\mathrm{T}} \tag{9}$$

**CASE (Heat pump is ON)**

$$\hat{\boldsymbol{a}}^{(k)} = \hat{\boldsymbol{a}}^{(k-1)} + \boldsymbol{g}^{(k)}\left(y^{(k)} - \boldsymbol{x}^{(k)^T}\hat{\boldsymbol{a}}^{(k-1)}\right) \tag{10}$$

$$\boldsymbol{g}^{(k)} = \frac{\boldsymbol{P}^{(k-1)}\boldsymbol{x}^{(k)}}{1 + \boldsymbol{x}^{(k)^T}\boldsymbol{P}^{(k-1)}\boldsymbol{x}^{(k)}} \tag{11}$$

$$\boldsymbol{P}_k = \mathbf{P}_{k-1} - g_k \boldsymbol{x}_k^{\mathrm{T}}\boldsymbol{P}_{k-1} \tag{12}$$

**CASE (Heat pump is OFF)**

$$\hat{\boldsymbol{a}}^{(k)} = \hat{\boldsymbol{a}}^{(k-1)},\ \boldsymbol{g}^{(k)} = \boldsymbol{g}^{(k-1)},\ \boldsymbol{P}^{(k)} = \boldsymbol{P}^{(k-1)} \tag{13}$$

## 2.4 Validation

In this section, we present the MPC control problem, which has been implemented and simulated to prove that the derived expression can take part in a solvable *Mixed-Integer Non-linear Programming* (MINLP) optimization problem.

$$\min_u \left(\boldsymbol{c}_{HP}^T\boldsymbol{P}_{HP} + \sum_{i=1}^{M} c_{s,i}\left\|\boldsymbol{T}_{s,i} - \boldsymbol{T}_{r,i}\right\|_2^2\right)T \tag{14}$$

subject to (15)

$$i \in \{1,\dots,M\},\ k \in \{0\dots h_p - 1\} \tag{16}$$

$$\boldsymbol{c}_{HP} \in \mathbb{R}^{h_p}, c_{s,i} \in \mathbb{R}^{+} \tag{17}$$

$$\hat{\boldsymbol{x}}_i^{(k+1)} = F_x\left(\boldsymbol{x}_i^{(k)}, \boldsymbol{u}_i^{(k)}, \boldsymbol{d}^{(k)}\right) \tag{18}$$

$$\hat{\boldsymbol{x}}_i^{(0)} = \boldsymbol{x}_0 \tag{19}$$

$$v_i^{(k)} \in \{0,1\},\ \ \underline{T_F} \le T_F^{(k)} \le \overline{T_F} \tag{20}$$

$$\begin{aligned} f_x\left(\boldsymbol{x}_i^{(k)}, \boldsymbol{u}_i^{(k)}, \boldsymbol{d}^{(k)}\right) &= \mathbf{A}_i\boldsymbol{x}_i^{(k)} + \mathbf{B}_{x,i}T_w^{(k)}v_i^{(k)} \\ &+ \mathbf{B}_{u,i}T_F v_i^{(k)} + \mathbf{D}_i T_a^{(k)} \end{aligned} \tag{21}$$

$$\hat{P}_{HP}^{(k)} = f_{HP}(\boldsymbol{u}^{(k)}, T_R^{(k)}) \tag{22}$$

$$0 \le \hat{P}_{HP}^{(k)} \le \overline{P_{HP}}$$

$$\hat{T}_R^k = H(\boldsymbol{x}^{(k)}, \boldsymbol{u}^{(k)}) \tag{23}$$

$$H\left(\boldsymbol{x}^{(k)}, \boldsymbol{u}^{(k)}\right) = \frac{\sum_{i=1}^{M} k_{u,i}v_i^{(k)}(2T_{w,i}^{(k)} - T_F^{(k)})}{\boldsymbol{k}_u^{\mathrm{T}}\boldsymbol{u}^{(k)} + \varepsilon} \tag{24}$$

with vectors and matrices being

$$\boldsymbol{u}_i^k = [v_i \quad T_F]^{\mathrm{T}},\quad \boldsymbol{d}^{(k)} = T_a^{(k)} \tag{25}$$

$$\boldsymbol{x}_i^k = [T_{r,i}^{(k)} \quad T_{f,i}^{(k)} \quad T_{w,i}^{(k)}]^{\mathrm{T}} \tag{26}$$

$$\boldsymbol{P}_{HP} = \left[\hat{P}_{HP}^{(k)} \quad \dots \quad \hat{P}_{HP}^{(h_p)}\right]^{\mathrm{T}} \tag{27}$$

$$\boldsymbol{u}^{\boldsymbol{k}} = [v_1 \quad \dots \quad v_M \quad T_F]^{\mathrm{T}} \tag{28}$$

$$\boldsymbol{x}^{\boldsymbol{k}} = \left[(\boldsymbol{x}_1^{(k)})^{\mathrm{T}} \quad \dots \quad \left(\boldsymbol{x}_M^{(k)}\right)^{\mathrm{T}}\right]^{\mathrm{T}} \tag{29}$$

$$\mathbf{A}_i = \begin{bmatrix} -\alpha_{a,i} - \alpha_{f,i} & \alpha_{f,i} & 0 \\ \alpha_{f,i} & -\alpha_f - \alpha_w & \alpha_{w,i} \\ 0 & \alpha_{w,i} & -\alpha_{w,i} \end{bmatrix} \tag{30}$$

$$\mathbf{B}_{x,i} = \begin{bmatrix} 0 \\ 0 \\ -\frac{2\bar{q}c_w}{C_w} \end{bmatrix},\ \mathbf{B}_{u,i} = \begin{bmatrix} 0 \\ 0 \\ \frac{2\bar{q}c_w}{C_w} \end{bmatrix} \tag{31}$$

$$\mathbf{D}_i = \begin{bmatrix} u_{a,i} \\ 0 \\ 0 \end{bmatrix} \tag{32}$$

Superscript indicates the time period with $k \in \{0,\dots,h_p\}$ being the prediction window. In this example, the control and prediction horizon have the same length. The room number is indicated in subscript using $i$, with $M$ being the number of rooms.

The cost function is quadratic and punishes energy consumption by the heat pump and divergence from the reference temperature. The vectors $\boldsymbol{T}_{s,i}$ and $\boldsymbol{T}_{r,i}$ contain the room temperature reference and estimated room temperatures for room $i$ over the prediction window, respectively. The vector $\boldsymbol{c}_{HP}$ contains the cost weights for each sample and have the unit euro per watt-hour $[€/Wh]$. The discomfort penalty for room $i$ is $c_{s,i}$ with unit euro per kelvin squared hour $[€/(K^2h)]$. The sample time $\Delta T$ has unit hours $[h]$. The cost on temperature deviation is quadratic to punish both under and overheating of a room.

The function $F_x(\boldsymbol{x_i}, \boldsymbol{u_i}, \boldsymbol{d})$ is a 4th order Runge-Kutta [14] integration of the dynamics $\dot{\boldsymbol{x}}_i = f_x(\boldsymbol{x_i}, \boldsymbol{u_i}, \boldsymbol{d})$. The dynamics are implemented using multiple shooting [15].

The control signals in $\boldsymbol{u}$ are constrained according to (20), with the valve control signals being binary.

The model, seen in (21), reflects an RC-equivalent model, with two bilinear terms. The bi-linearity arises from the fact that both forward temperature and valve states are control inputs. The parameters $\alpha$ represent heat conductance $[W/K]$, $C_w$ is heat capacity $[J/K]$ and $c_w$ is specific heat capacity for water.

The estimated power consumption of the heat pump is $\hat{P}_{HP}^k$, which is derived in Sec. 2.3.

The return temperature $T_R^k$ is calculated using the output function $H(\boldsymbol{x}^k, \boldsymbol{u}^k)$. The output function is derived based on the energy balance in a mixing circuit seen in Eq. (33).

$$c_w q T_R = c_w q_1 T_{R,1} + \dots + c_w q_M T_{R,M} \Leftrightarrow \tag{33}$$

$$T_R = \frac{q_1 T_{R,1} + \dots + q_M T_{R,M}}{q} \tag{34}$$

Since we do not have a measure of $q$ or $q_i$ we replace it with the estimate $\hat{q}_v$ seen in (6) and the nominal estimates for each circuit $\hat{q}_{v,i}$. For Eq. (34) to make sense $\hat{q}_{v,i}$ has to be non-zero and positive.

$$T_R = \frac{k_1 v_1 T_{R,1} + \dots + k_M v_M T_{R,M}}{\boldsymbol{k}^T\boldsymbol{v}} \tag{35}$$

Further, the room model $f_x(\boldsymbol{x}_i^k, \boldsymbol{u}_i^k, \boldsymbol{d}^k)$ is fitted assuming the water temperature of room $i$, $T_{w,i}$, is the average of forward temperature $T_F$ and return temperature, $T_{R,i}$, as seen in Eq. (36).

$$T_{w,i} = \frac{T_{R,i} + T_F}{2} \tag{36}$$

Isolating $T_{R,i}$ gives

$$T_{R,i} = 2T_{w,i} - T_F \tag{37}$$

which gives the result

$$\hat{T}_R = \sum_{i=1}^{M} \frac{k_i^T v_i (2T_{w,i} - T_F)}{\boldsymbol{k}^T \boldsymbol{v} + \epsilon} \tag{38}$$

A small constant $\epsilon$ is added to avoid divison by zero.

# 3 Results

## 3.1 Regression results

The overall result regarding the regression is that the initial regression fit performs acceptable without further update of the parameters. This said, we show that an improvement is obtained by updating the coefficients recursively.

### *3.1.1 Regression from standard test data*

The result of for the initial regression expression fitted to the *standard test data* is presented in Figure 2.

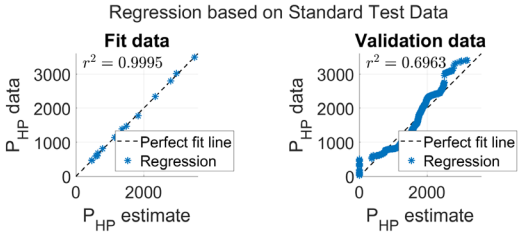


**Figure 2.** (Left) shows the regression result compared with original data used for the fit, (Right) shows the result compared with the *validation data* from test-rig.

As seen in the left sub-figure the $r^2$ value is close to one, indicating that no more information can be extracted from the 18 samples. The picture changes when the model is compared to the *validation data* where the inaccuracies get clearer with $r^2 \approx 70\%$.

The fitted expression with numerical values is

$$\begin{aligned}\hat{P}_{HP} = 2128.381 &- 98.954T_F - 60.415T_R \\ &+ 916.960q + 2.809T_F^2 \\ &+ 0.0992T_R^2 + 7533.07q^2\end{aligned} \tag{39}$$

**Table 4.** Root mean square error (RMSE) using different combinations of data and regression model. The model used is indicated with equation reference.

| Data | Eq. (1) | Eq. (7) |
|---|---|---|
| Standard test data | $RMSE = 26$ | |
| Test-rig validation/fit data | $RSME = 472$ | $RMSE = 506$ |

Notice that mass flow $q$ and forward temperature $T_F$ increase the cost and return temperature $T_R$ decreases it. This makes good sense, since a high return temperature means that less energy has to be induced to reach the requested forward temperature.

### *3.1.2 Results for linear regression of the flow*

This section contains the results for the linear regression model of the flow seen in Eq. (6) and the isolated flow estimate $\hat{q}_+$ seen in (5). To obtain a series of data points for $\hat{q}_+$ measurements of $T_F$, $T_R$ and $P_{HP}$ from the first 10 days of the *test-rig data* is used.

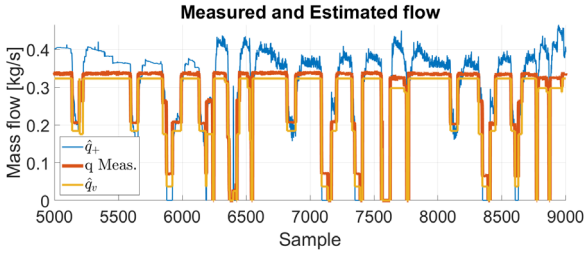


**Figure 3**. Shows the estimated flow obtained by isolating the flow $q$ in the regression model obtained from the standard test data and thereafter fitting a new regression model based on the valve input.

As can be seen in Figure 3 the estimate $\hat{q}_+$ is catching the trend, but it does overestimate at large values when compared to the flow measurements obtained from the test-rig. Interesting enough, the results improve when the linear regression model for $\hat{q}_v$, based on the control valve input signals, is used. This indicates that the initial assumption that the flow is a sum of nominal flows from each circuit is correct. Since $\hat{q}_+$ is calculated by solving a second order equation complex roots can appear. This was experienced in this particular investigation. The complex roots were few and handled by using the real part only.

### *3.1.3 Results for recursive least squares update of the coefficients*

The results from the RLS update of the coefficients in the regression model (7) show that it is possible to improve the estimate of the power input by use of online measurements. The graphs in Figure 4 compare the performance between RLC, for the cases $\delta = 10^{-5}$ and $\delta = 10^{6}$, and the original fit from (7).

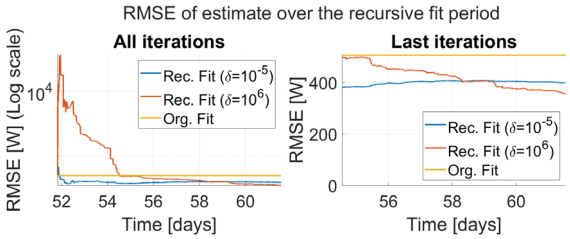


**Figure 4.** (left) Shows how the root mean squared error (RMSE) of the estimate of $P_{HP}$ compared with the *validation data* set progresses for all iterations. (right) shows the last iterations, after the initial settling period.

The RMSE reduces from the original value of 506[W], obtained using the regression model from (7), to approx. 400[W] for $\delta = 10^{-5}$ and 360[W] for $\delta = 10^{6}$ when compared to the *validation data*. To provide an overview on how such an improvement looks the time series results are presented in Figure 5.

The results showed a high value ($\delta = 10^{6}$) caused a significant improvement to the estimation as seen on the absolute cumulative error in Figure 5. The total energy consumption of the heat pump over the validation period, seen in Figure 5, is approx. 70 kWh, which gives the following relative accuracy errors seen in Table 5 with relative accuracy error $e_r$ defined in Eq. (40).

$$e_r = \frac{|\hat{x} - x|}{x} \tag{40}$$

Where $\hat{x}$ is the estimate and $x$ the measured value.

**Table 5**. Relative accuracy error for the consumption est.

| Fit from Eq. (7) | RLS ($10^{6}$) | RLS ($10^{-5}$) |
|---|---|---|
| 21.2 % | **16.9 %** | 20.5% |

The cost of choosing $\delta$ large is a very poor estimate in the initial period, seen in Figure 4.

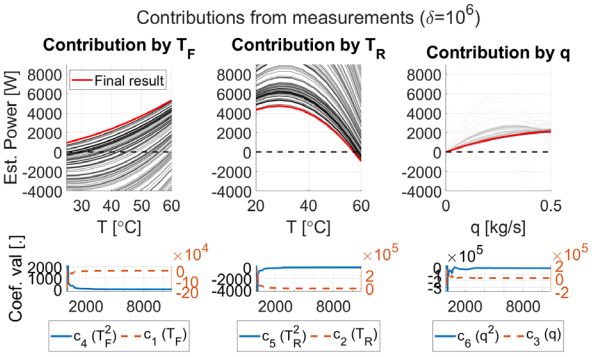


**Figure 5.** The upper row shows the contribution from each of the measuremnts swept over their operating area. The fan of lines represent their value as the RLS algorithm progresses. The red line is the final result. The lower line of figures shows the actual value of the coefficients as they progress for each iteration.

It took 2 days before the estimates improved compared to the initial fit. Further, the values of the coefficients were highly volatile before converging as seen in Figure 6. In contrast with $\delta = 10^{-5}$ the coefficients were more steady, but the improvement in estimate was insignificant when compare to the *validation data*.

The curves in the upper row of Figure 6 and Figure 7 show the individual contribution from each measurement to the full expression. The curves are generated by setting every measurement except one to zero, then making a sweep over the remaining. One curve is made for each set of coefficients as they develop over time. The lighter lines are early solutions while the darker are later solutions. The red line is the final, curve. This is done to give an idea of how the components of the function develops as the RLS algorithm progresses.

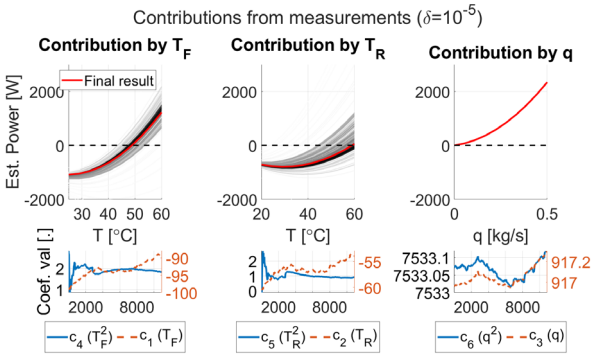


**Figure 7.** Shows change in coefficients for $\delta = 10^{-5}$.

The main conclusion is that both choices of $\delta$ have advantages and disadvantages. If faster settling time and low coefficient volatility is priority then $\delta$ should be chosen low. If the accuracy of the estimate is of highest priority, then a high value could be chosen.

## 3.2 Results for MPC validation example

The results from the simulation of the model predictive control (MPC) algorithm containing the heat pump model, described in Section 2.4, is presented here. Since the focus is on solvability, several simplifications have been made. First, the model used for simulation is the same as the model described in the optimization

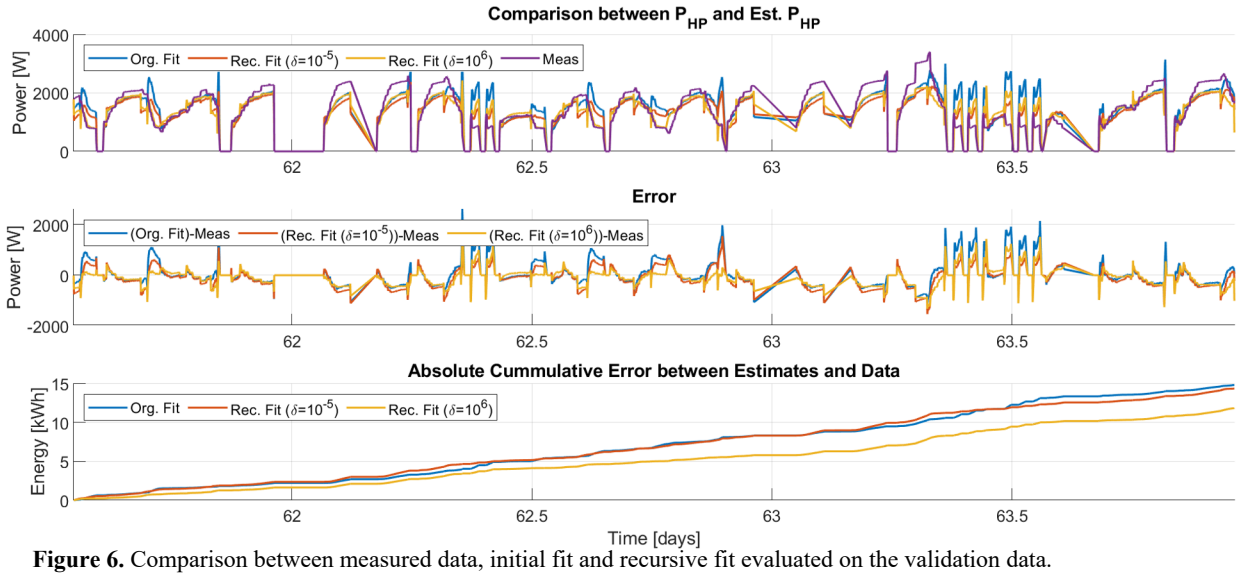


**Figure 6.** Comparison between measured data, initial fit and recursive fit evaluated on the validation data.

problem leaving out any model uncertainties. Additionally, it is assumed that future values, such as ambient temperature are known, fundamentally making it deterministic MPC. This said the optimization problem is solvable on a standard laptop (Lenovo T490s) as seen in Figure 8, which shows the progress of the states over the simulation window for each of the four rooms. The optimization problem is implemented in MATLAB using CasADi [16] for formulation and BONMIN as solver. The constraints in the optimization problem are relaxed using slack variables, when necessary, to maintain feasibility during simulation. The code is available in the public repository [10].

This particular example presented in Figure 8 and Figure 9 is solved using a sample time of 15 minutes and a prediction horizon of 8 samples corresponding to a length of 2 hours. This is relatively short, considering the time constants of a building. The deciding factor for the length of the prediction horizon is the complexity of the problem. The complexity of a *Mixed-Integer Programming problem* increases very fast with the length of the window. In this case, a prediction horizon of 10 samples occasionally took 30 min. to solve, which is problematic when the sample time is 15 min. Further, this issue only increases when more rooms are added to the problem, calling for another approach. A work-around is to use continuous variables in the range [0,1] and round to the closest integer. In this case solving time is seconds for windows of approx. 6 hours.

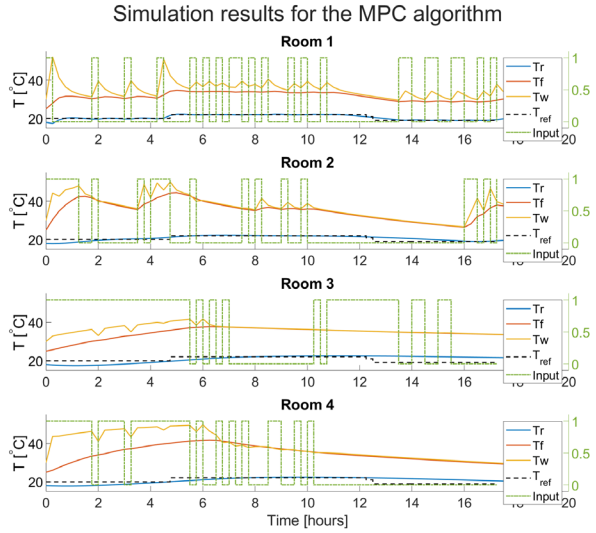


**Figure 8.** Shows the states and the valve control signals as they develop throughout the simulation. The states are room temperature $T_r$, floor temperature $T_f$ and an averaged water temperature in the pipe $T_w$. The input is the binary opening degree of the control valves.

The main conclusion from Figure 8 is that the controller is able to bring the room temperature to the reference using the discrete control inputs, which proves that the heat pump model can take part in a larger control problem.

Figure 9 presents the results, which are directly related to the regression model of the heat pump. The three plots in Figure 9 show the estimate for the consumption $\hat{P}_{HP}$ and the three inputs forward temperature $T_F$, return temperature $T_R$ and combined flow $q$ in the floor heating circuit. Using common sense, the following situations led to high power consumptions. A large flow, means a larger mass needs to be heated, a large difference between return and forward temperature also naturally demands more energy. Further, a high forward temperature lowers the *Carnot Coefficient of Performance* ($COP_{Carnot}$) due to the increased difference between cold (brine temperature) and warm (forward temperature) reservoir.

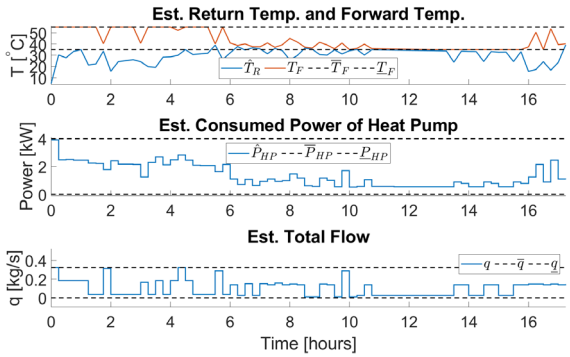


**Figure 9.** (Upper) Shows the input forward temperature $T_F$ and the estimated return temperature $T_R$. (Middle) Shows the estimated power consumption of the heat pump. (Lower) shows the estimated flow to and from the heat pump.

Some of these patterns are visible in the results. In the first six hours the difference $T_F - T_R$ is large combined with a high forward temperature which result in a high energy consumption, even though the flow is low. In the hours between 7 and 13, the consumption is lower, mainly due to the small difference between forward and return temperature. In the last period from hour 13 and onwards, the power consumption increases again due the combination of flow combined with rising forward temperature. It is an important conclusion that the power consumption increases with the forward temperature, since this effect reflects the drop in $COP_{Carnot}$. Note that the return temperature is estimated, and the expression seen in (38) is directly dependent on forward temperature. This might cause the value to be volatile, and highly affect the estimate for the power consumption, therefor and improvement in this estimate should lead to better estimates for the power consumption.

## 4 Conclusion

In this paper, a quadratic regression model estimating the power consumption of a heat pump connected to ON/OFF controlled floor heating is presented. The data and measurements, used for fitting the coefficients, are chosen based on degree of availability in such an installation.

The data is extracted from a report containing common manufacture-commissioned tests intended to measure the COP under controlled conditions. The validation and recursive update is performed using the data obtained from the test-rig. Both data sets are made available for the purpose of scrutiny and further work.

The regression model is integrated into a *Mixed -Integer Non-linear* MPC problem which is proven solvable by example. In the spirit of this text, one has to emphasise that the MPC only could be solved with a window length up till 2 hours, on a standard laptop, and calculation time for an iteration could take as long as 30 minutes. This is troubling, since the model consists of only four rooms and with the type of time constants in play a window length of minimum 6 hours is much more beneficial.

The results indicate that there is enough information contained in the few data points from the *standard test data* to establish a cost relation between control inputs to the heat pump and the power consumption. This relation is important since an actual price can be attached to the power consumption enabling the use of *Economic MPC (EMPC)*.

Since the data from the standard test seems to hold value in other contexts than for calculating COP and SCOP, the authors propose these test become mandatory and publicly available. One could imagine an online database containing operational data for all commercial models.

Because both the *Recursive Least Squares* (RLS) method and MPC are repetitive algorithms, it does not take much imagination to consider running the recursive algorithm parallel with the MPC algorithm. This approach might cause the optimization problem to become infeasible, due unexpected changes in the estimate of the heat pump power. Since this claim stays untested, we will not comment on it further.

The next logical step is to test the method against a heat pump, which is installed in a real house. Further, it is interesting to investigate whether a similar expression, using outside temperature, can be obtained for an air-to-water heat pump. At last, an investigation of a more meaningful formulation of a model predictive controller, using the heat pump model is in its place.

## References

[1] European Heat Pump Association, “ehpa - hp sales,” european heat pump association, 1 January 2017. [Online]. Available: http://stats.ehpa.org/hp_sales/story_sales/. [Accessed 8 Januar 2021].

[2] S. Rastegarpour, S. Gros and L. Ferrarini, “MPC approaches for modulating air-to-water heat pumps in radiant-floor buildings,” *Control Engineering Practice,* vol. vol. 95, p. p. 104209, 2020.

[3] H. Weeratunge, G. Narsilio, J. d. Hoog, S. Dunstall and S. Halgamuge, “Model predictive control for a solar assisted ground source heat pump system,” *Energy,* vol. vol. 152, p. pp. 974–984, 2018.

[4] DIN Deutsches Institut für Normung e. V, “Beuth, DIN EN 14511-2:2019-07,” Beauth, 7 January 2021. [Online]. Available: https://www.beuth.de/en/standard/din-en-14511-2/298537580. [Accessed 7 January 2021].

[5] DIN Deutsches Institut für Normung e. V., “Beuth, DIN EN 14825:2019-07,” Beuth Publishing DIN, 7 January 2021. [Online]. Available: https://www.beuth.de/de/norm/din-en-16147/254893177. [Accessed 7 January 2021].

[6] DIN Deutsches Institut für Normung e. V., “Beuth, DIN EN 16147:2017-08,” Beuth Publishing DIN, 7 January 2021. [Online]. Available: https://www.beuth.de/en/standard/din-en-16147/254893177. [Accessed 7 January 2021].

[7] F. Simon, J. Ordoñez, T. Reddy, A. Girard and T. Muneer, “Developing multiple regression models from the manufacturer's ground-source heat pump catalogue data,” *Renewable Energy,* vol. 95, pp. 413-421, 2016.

[8] X. Xu, J. Liu, Y. Wang, J. Xu and J. Bao, “Performance evaluation of ground source heat pump using linear and nonlinear regressions and artificial neural networks,” *Applied Thermal Engineering,* vol. 180, p. 115914, 2020.

[9] S. Thorsteinsson, *Heat pump connected to floor heating,* Aalborg: zenodo, 2021. DOI: 10.5281/zenodo.4445311

[10] S. Thorsteinsson, “gitlab,” gitlab, 16 January 2021. [Online]. Available: https://gitlab.com/Thorsteinsson/cold-climate-hvac-2021.git. [Accessed 16 January 2021].

[11] R. C. S. Ø. Jensen, T. Green, K. Vinther, T. Minko, J. Bendtsen, J. Pålsson, K. Prölls, L. Li and P. Dermont, “teknologisk.dk,” Dansk Teknologist Institut, September 2017. [Online]. Available: https://www.teknologisk.dk/optimering-af-gulvvarme-og-varmepumpesystemer/39663. [Accessed 12 January 2017].

[12] P. C. Young, Recursive Estimation and Time-Series Analysis, 2nd ed., Berlin Heidelberg: Springer-Verlag Berlin Heidelberg 2011, 2011, pp. 30-34.

[13] R. Qi, G. Tao and B. Jiang, Fuzzy System Identification and Adaptive Control, Cham: Springer Nature Switzerland AG, 2019.

[14] J. C. Butcher, Numerical Methods for Ordinary Differential Equations, West Sussex: Wiley, 2016.

[15] C. Kirches, Fast Numerical Methods for Mixed-Integer Nonlinear Model-Predictive Control, Heidelberg: Springer, 2010.

[16] J. A. E. Andersson, J. Gillis, G. Horn, J. B. Rawlings and M. Diehl, “CasADi - A software framework for nonlinear optimization and optimal control,” *Mathematical Programming Computation,* vol. 11, pp. 1-36, 2019.

# Intelligent energistyring i husstande

**Elpriserne er steget til himmels, og det skulle give grobund for udbredelsen af IoT. Løsningerne bliver dog ikke implementeret i tilstrækkeligt højt tempo. EUDP-projektet Opsys 2.0, som er beskrevet i denne artikel, handler netop om intelligent energistyring i husstande**

Af Simon Thorsteinsson, Aalborg Universitet, Ivan Katic, Teknologisk Institut, Henrik L. Stærmose, Neogrid, Brian Nielsen, Bosch og Søren Dueholm, Wavin

Det er næppe gået nogen elforbrugeres opmærksomhed forbi, at udgifterne til el nærmest er eksploderet, hvad enten man som bygningsejer har elbaseret varme eller ej. Dels er spotprisen på el i gennemsnit steget betydeligt, dels ser man nu store fluktuationer inden for døgnet, alt efter om der er vind og sol nok til at dække behovet. I tillæg hertil har visse netselskaber varslet store stigninger for nettariffen, med over 2 kr./kWh i kogespidsen. Grundet disse voldsomme ændringer er egenproduktion af sol-el igen blevet økonomisk interessant, og det samme er tidsmæssig styring af forbruget og energilagring.

Det vil sige, at vi efter megen snak om fortræffelighederne ved IoT og smart grid nu er i en situation, hvor det i høj grad kan betale sig at styre bygningers elforbrug på en intelligent måde. Dette ses i form af et hastigt stigende udbud af markedsførte "smart home"-løsninger, som dog oftest kun omfatter producentens egne apparattyper. Derfor bliver det ikke implementeret i bestående byggeri i det tempo, man kunne ønske. I denne artikel ser vi på nogle af de erfaringer, der er indsamlet i EUDP-projektet Opsys 2.0, som netop omhandler intelligent energistyring i husstande.

## Opsys 2.0-projektet

Projektet blev påbegyndt af en bred partnerkreds med det formål at udvikle og demonstrere en styring til de mange husstande, der har solceller og som i stigende grad også får varmepumpe og eventuelt en batteripakke koblet til.

Målet er at kunne styre en varmepumpe og et solcellebatteri på den økonomisk mest fordelagtige måde i en husholdning, hvor der også er forbrug til alle mulige andre apparater med varierende forbrugsmønster. Det gælder derfor om, at styringen kan gætte rigtigt på, hvad forbruget og egenproduktionen vil være i det kommende tidsinterval, så den kan træffe de rigtige dispositioner. Elprisen er kendt 11-35 timer frem via Nordpool, så denne kan indlæses som en simpel tabel. I modsætning hertil er de andre variable (vejr og forbrug) ikke 100 procent kendt på forhånd, men vi kan have en antagelse om dem.

Den største forbruger er i reglen varmepumpen, hvis elbehov varierer i takt med udetemperaturen og bygningens behov for varme og varmt vand. Imidlertid er koblingen fra el til varme meget "løs", således at en afbrydelse af varmepumpen ikke har øjeblikkelig konsekvens for husets komforttemperatur, og start af varmepumpen udløser kun en langsom temperaturstigning. Den skal blot levere den nødvendige energimængde over et læn-

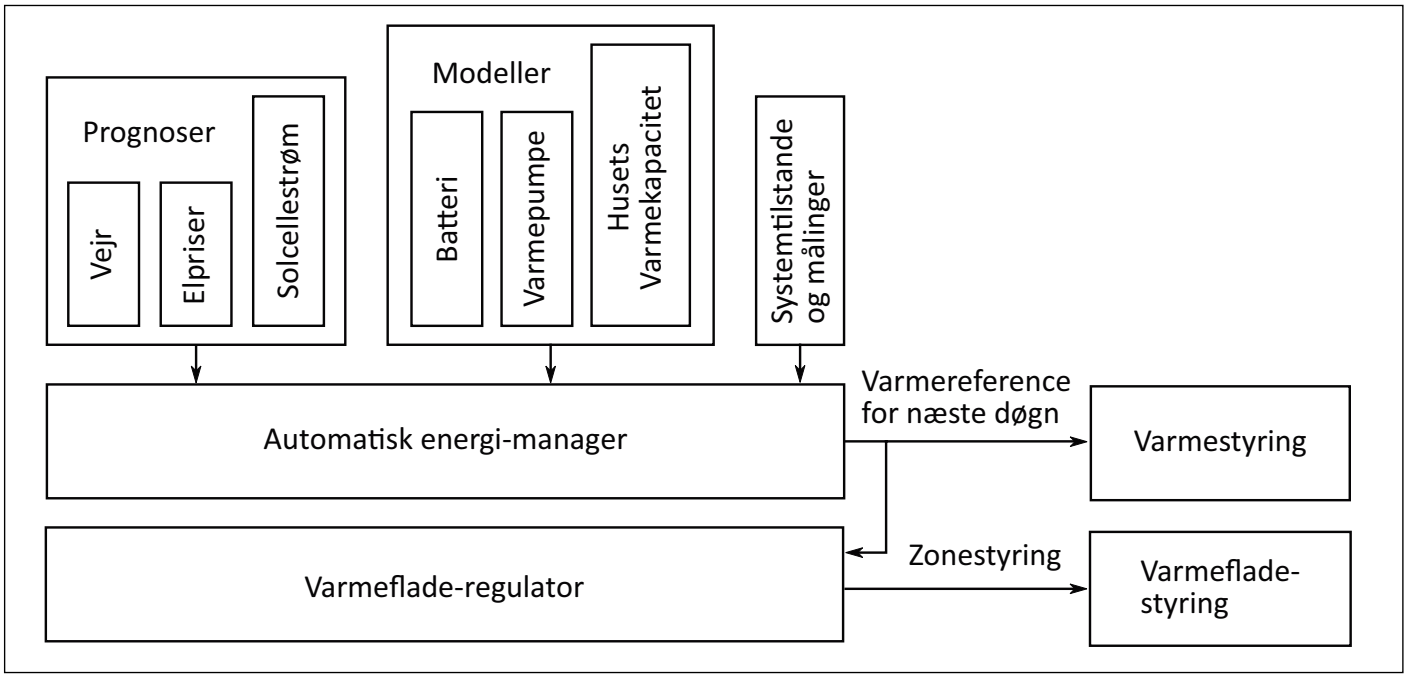


Den overordnede opbygning af styresystemet. I det konkrete hus der måles på, er varmestyring = overstyring af varmepumpens varmekurve og varmefladestyring = overstyring af gulvvarmeventiler.

▷ *Fortsat*

gere tidsforløb, for at huset hverken bliver koldt eller varmt.
Det er netop princippet i den udviklede styring; at den arbejder med et energibudget, der skal opfyldes per rullende døgn og ikke med en simpel termostat. Det nødvendige energiinput bliver beregnet hver time i en avanceret model, der især tager hensyn til udetemperatur og solindfald, samt øvrigt elforbrug, som jo afsættes internt som varme. Energien bliver så vidt muligt leveret, når strømmen er billigst - det vil sige, når den enten er egenproduceret og bruges direkte, eller når der er lav elpris og lav nettarif.
Ved lavpris vil systemet derfor søge at afsætte en øget varmemængde inden for budgettet - naturligvis med en øvre tilladt komforttemperatur. For at det kan lade sig gøre at tvinge varmepumpen til at afgive mere energi end dens egen styring tilsiger, bliver den fodret med en fiktiv udetemperatur, som snyder den til at køre op i fremløbstemperatur og dermed varme huset mere op.
I et traditionelt varmeanlæg vil termostater/telestater dog hurtigt begrænse flowet i takt med, at rumtemperaturen stiger og så slutter festen. For at udnytte husets termiske masse til varmelagring er det derfor nødvendigt, at termostaterne tvinges til at åbne under et opvarmningsforløb. I Opsys 2.0 sker det ved, at den centrale styring (Neogrid) sender et signal til gulvvarmestyringen (Wavin), så der på den måde er koordination mellem varmeproducerende og varmeaftagende enhed. Først når der er afgivet så meget energi, at budgettet er opfyldt, bliver opvarmningen afbrudt. Omvendt bliver opvarmningen forceret i det tilfælde, at varmepumpen ikke er gået i gang på grund af høj elpris, og kvoten ikke er leveret til tidsfristen. Regnestykket bliver relativt kompliceret, fordi virkningsgraden for varmepumpen varierer en del alt efter driftsforhold. For eksempel falder varmepumpens COP ved forceret drift, men det kan stadig godt betale sig at køre på den måde ved tilstrækkelig lav elpris. Ultimativt kan en elpatron komme i spil, hvis der for en stund er næsten gratis strøm.

## Praktiske erfaringer

Systemet har siden efteråret 2020 været installeret i et privat hus i Kalundborg. Huset er et tungt lavenergihus med gulvvarme i betongulve og forholdsvis store vinduer. Solen har derfor stor indvirkning på rumtemperaturen og dermed på, hvilken opvarmningsstrategi der er den rigtige. De tunge gulve gør det muligt at afbryde varmeforsyningen i lange perioder, uden at der sker mærkbare fald i rumtemperaturen. Den oprindelige gulvvarmestyring blev udskiftet med et system fra Wavin, som kan kommunikere direkte med den overordnede Neogrid-styring.

Der blev opsat bimålere på varmepumpe og solcelleanlæg for at kunne måle energibidrag herfra. Desuden blev der opsat varmemålere på gulvvarmen og det varme vand samt en række temperaturfølere. Alle principper med hensyn til overstyring er blevet eftervist, og nu måles der i varmesæsonen 2022/23, hvor systemet skal køre autonomt og registrere data. Sideløbende hermed er der på Teknologisk Institut arbejdet på en laboratorieopstilling til kontrollerede forsøg med nye styringsteknologier i forbindelse med varmepumper. Der er fire varmevekslere på aftagersiden, som skal emulere gulvvarmekredse og der er opstillet en brinetank med elpatron til at emulere jordvarme.
Ved hjælp af et CTS-anlæg kan anlægget styres ud fra simulerede vejr- og forbrugsdata. På elsiden kan man simulere et solcelleanlæg med batteri, som sammen med målt elforbrug til varmepumpen giver en balance på elsiden. På varmesiden måles energi til rumvarme og til varmt vand, som kan aftappes efter en fast behovsprofil.
Opstillingen skal nu testes med gentagne forløb af samme vejrdata - for eksempel en uge med sommerdrift, en med vinterdrift og en for overgangsperioden. Ved at bruge samme betingelser i gentagne kørsler kan de forskellige styringsstrategier blive holdt op mod hinanden.
Det nye bygningsreglement kommer til at stille krav om dokumentation af den ind- ▷

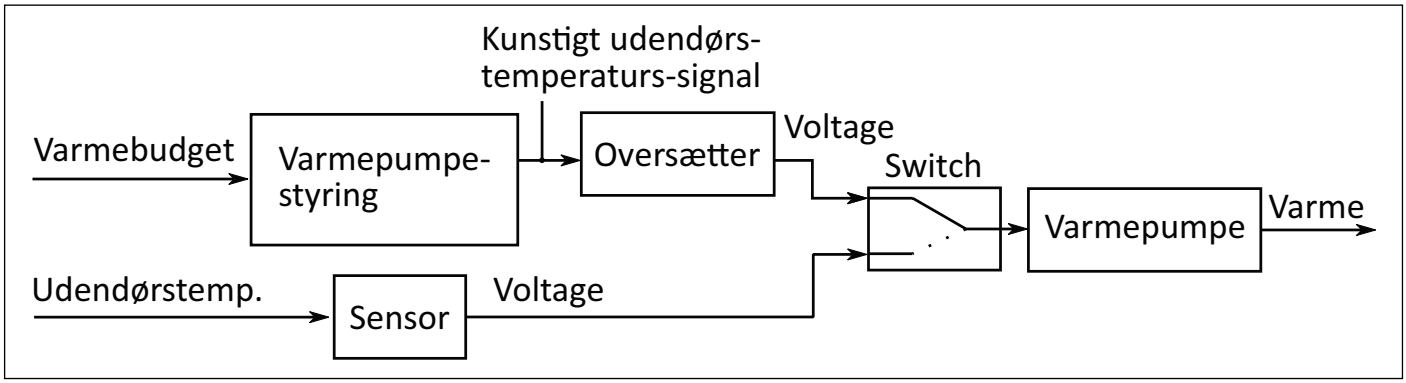


Signalet fra den udendørs temperatursensor til varmepumpens interne styring kan udskiftes med et kunstigt spændingssignal via et relæ.

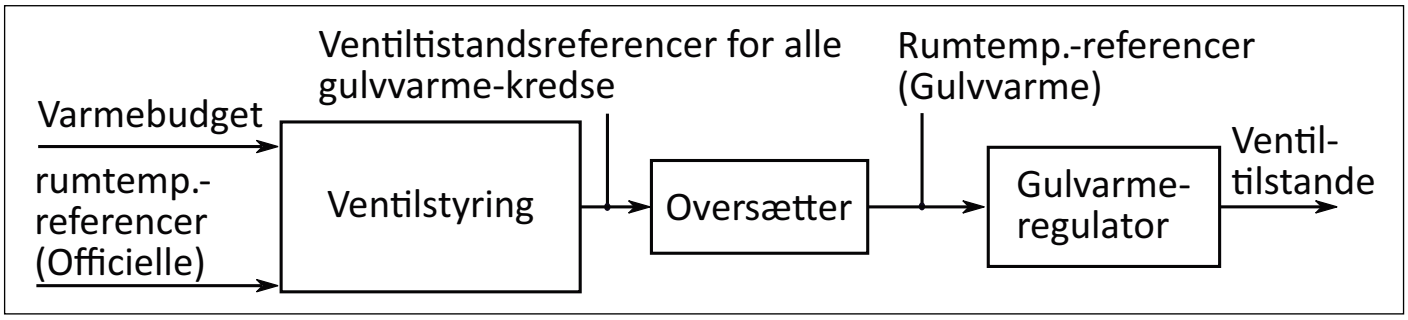


Gulvvarmestyringens egne data udlæses via en oversætter, som fortæller, hvad hvert enkelt rums temperatur er, og hvilken temperatur der ønskes. Setpunkter kan herefter manipuleres med nye gulvvarmereferencer. OBS! Praktiske begrænsninger: Pas på med for høj fremløbstemperarur til trægulve samt med varmtvandstemperaturen, hvis der ikke er skoldningssikring.

▷ *Fortsat*

lejrede $CO_2$-belastning fra byggematerialer og man kan derfor allerede se, at det lette træbyggeri vinder frem på bekostning af beton og murværk. Det vil give nye reguleringsmæssige udfordringer, når der ikke er meget termisk kapacitet i materialerne, hvilket også vil kunne undersøges i testriggen.

## Hvordan kommer vi (branchen) videre?

Vi har i det foregående beskrevet, hvordan vejrkompenserede varmepumper kan levere energifleksibilitet via manipulation med udendørstemperaturføleren. Det virker besværligt at styre ad den vej, og det er det også. Vi har denne metode, da der ikke på nuværende tidspunkt eksisterer et mere generelt input, hvorved varmepumperne kan styres. Havde det eksisteret, havde vi anvendt dette i stedet. Det er vigtigt, at der bliver udviklet simple retrofitløsninger, da de varmepumper som sælges i dag, ellers ikke kan opnå deres fulde potentiale i forhold til at understøtte elnettet.

Vi foreslår en enkel løsning, hvor varmepumpen kan køres i to modes: sameksistens og samarbejde. Sameksistens er den driftsform, som oftest ses i dag, hvor varmepumpen løser sin opgave relativt uafhængigt og uvidende om, hvad de andre systemer i bygningen som evt. solceller, batteripakker osv. foretager sig. Samarbejde er den tilstand, hvor varmepumpen er villig til at udveksle information med andre energiaktiver i systemet for at opnå et mere optimalt mål end dem, som de enkelte komponenter kan formulere alene. Eksempler herpå: Varmepumpen kører efter maksimum effektivitet (COP), varmedistributionssystemet styrer efter maksimal temperaturkomfort og pumperne efter et tredje mål. Vi skal væk fra det sted, hvor enhver komponent kun sigter efter egne mål og derhen, hvor der styres efter optimalt el- og varmeforbrug defineret af de pågældende energiaktiver,

### Opsys 2.0

Opsys 2.0 bygger videre på resultaterne fra EUDP-projektet Opsys. AAU og Neogrid har stået for styringens software og hardware, Wavin har stået for gulvvarmestyring og Bosch for support vedrørende varmepumpen. Teknologisk Institut er projektleder. Projektets hjemmeside: www.teknologisk.dk/40581.


**Opsys teststand på Teknologisk Institut. Første fag fra venstre indeholder varme- og kølebuffer. Midterste fag er gulvvarme-manifold og fire vekslere, som hver repræsenterer en gulvvarme-streng. Sidste fag er jordvarmepumpen (Bosch) og jordvarme buffertank til sidst.**

som er til rådighed, så slutkunden opnår den ønskede komfort, samtidig med at omkostningerne til varme minimeres. Langt de fleste varmepumper har allerede en app tilknyttet - dvs. at varmepumpen kan kommunikere til en cloud-løsning, hvorfra andre teoretisk set kan få adgang. Det sker bare ikke, da disse løsninger oftest er proprietære. Argumenterne imod at stille denne mulighed til rådighed er, at udefrakommende styring risikerer at skade komponenten og at virksomhederne ser det som en konkurrencefordel at holde API'en lukket.

For at imødegå det første problem, foreslås herfra, at styresignaler er referencer, altså et forslag til styringen, hvor komponenten bibeholder en vetoret. Eksempel: varmepumpen tager en ekstern reference til varmeproduktionen, men følger kun referencen, hvis det er mekanisk forsvarligt.

For at imødegå det andet argument bør man overveje, om lukkethed med hensyn til API'en leder mod en "winners-take-all" tilstand, hvor kun de producenter, som kan levere totalløsninger, der dækker værdikæden fra sensorer til styring, designet for hele bygninger eller områder, løber med ordren. På den lange bane bør vi sigte mod standardisering, ikke kun af kommunikationsprotokoller, men også af den information som skal udveksles mellem systemer. Men på den korte bane ville det være et stort skridt, hvis der blev åbnet op for, at en 3. part kan få adgang til at aflæse interne målere og for at justere styresignaler til varme og varmtvandsproduktion.